INFORMATION TO USERS

This manuscript has been reproduced from the microfilm master. UMI films the text directly from the original or copy submitted. Thus, some thesis and dissertation copies are in typewriter face, while others may be from any type of computer printer.

The quality of this reproduction is dependent upon the quality of the copy submitted. Broken or indistinct print, colored or poor quality illustrations and photographs, print bleedthrough, substandard margins, and improper alignment can adversely affect reproduction.

In the unlikely event that the author did not send UMI a complete manuscript and there are missing pages, these will be noted. Also, if unauthorized copyright material had to be removed, a note will indicate the deletion.

Oversize materials (e.g., maps, drawings, charts) are reproduced by sectioning the original, beginning at the upper left-hand corner and continuing from left to right in equal sections with small overlaps. Each original is also photographed in one exposure and is included in reduced form at the back of the book.

Photographs included in the original manuscript have been reproduced xerographically in this copy. Higher quality 6" x 9" black and white photographic prints are available for any photographs or illustrations appearing in this copy for an additional charge. Contact UMI directly to order.

UMI

University Microfilms International
A Bell & Howell Information Company
300 North Zeeb Road, Ann Arbor, MI 48106-1346 USA
313/761-4700 800/521-0600

Reproduced with permission of the copyright owner. Further reproduction prohibited without permission.

Order Number 9316040

The influence of pore fluids on shear strength and stress-strain behavior of granular soils

Ratnaweera, Prasanna, Ph.D.

New Jersey Institute of Technology, 1992

U·M·I
300 N. Zeeb Rd.
Ann Arbor, MI 48106

THE INFLUENCE OF PORE FLUIDS ON SHEAR STRENGTH AND STRESS-STRAIN BEHAVIOR OF GRANULAR SOILS

by
Prasanna Ratnaweera

A Dissertation
Submitted to the Faculty of
New Jersey Institute of Technology
in Partial Fulfillment of the Requirements for the Degree of
Doctor of Philosophy
Department of Civil and Environmental Engineering
October, 1992

APPROVAL PAGE

The Influence of Pore Fluids on Shear Strength and Stress-Strain Behavior of Granular Soils

by

Prasanna Ratnaweera

______________________ 06/22/92

Dr. Namunu J. Meegoda, Dissertation Adviser
Associate Professor of Civil and Environmental Engineering, NJIT
Date

______________________ 07/22/92

Dr. Raj P. Khera, Committee Member
Professor of Civil and Environmental Engineering, NJIT
Date

______________________ 06/29/92

Dr. Dorairaja Raghu, Committee Member
Professor of Civil and Environmental Engineering, NJIT
Date

______________________ 06/22/92

Dr. Methi Wecharatana, Committee Member
Associate Professor of Civil and Environmental Engineering, NJIT
Date

______________________ 06/22/92

Dr. Bruce Bukiet, Committee Member
Associate Professor of Mathematics, NJIT
Date

ABSTRACT

The Influence of Pore Fluids On Shear Strength and Stress-Strain Behavior of Granular Soils

by

Prasanna Ratnaweera

When a dry granular soil is subjected to an external load, the stresses are transferred through mineral to mineral contacts. The shear strength of such a soil is governed by its contact properties. Presence of a thin layer of fluid between mineral to mineral contacts in a saturated soil will alter its contact properties. Therefore any change in the physical properties of pore fluid can logically be reasoned to influence the deformation characteristics of granular soils.

To investigate the influence of pore fluid viscosity on shear strength and stress-strain behavior of a soil, a series of consolidated drained triaxial tests were performed on a silty sand. The samples were prepared with four different pore fluids of varying viscosities and tested subjected to different consolidation pressures. Tests were performed with the aid of an automated triaxial testing apparatus.

Since the stress-strain behavior of this silty sand can not be normalized, the variation of residual shear strength with critical void ratio was used for the analysis of results. When residual shear strength values were plotted against its critical void ratios, a family of curves that could be identified by their pore fluid viscosities were obtained. For a given critical void ratio, as pore fluid viscosity increased the residual shear strength was found to decrease.

To provide a mechanistic explanation to the changes in the strength characteristics due to pore fluid viscosity, a microscopic model was used to study the changes in the contact properties at particle level. The microscopic numerical model TRUBAL, based on the DEM was used in this research to simulate the me-

chanical behavior of a granular soil subjected to a triaxial stress condition. Since this numerical model was developed to simulate the behavior of a dry granular assembly of spheres, it was modified to incorporate the effects of pore fluid viscosity by using Reynolds equation for hydrodynamic lubrication. The modified TRUBAL program was used to simulate deformation characteristics of saturated granular soils.

The modified program was then used in a qualitative study to simulate stress-strain behavior of a granular assembly having different pore-fluid viscosities, subjected to consolidated drained triaxial test conditions. Numerical simulations showed a similar trend as observed in the physical tests.

BIOGRAPHICAL SKETCH

Author: Prasanna Ratnaweera

Degree: Doctor of Philosophy

Date: October, 1992

Undergraduate and Graduate Education:

- Doctor of Philosophy in Civil Engineering, New Jersey Institute of Technology, Newark, New Jersey, 1992
- Master of Science in Civil Engineering, New Jersey Institute of Technology, Newark, New Jersey, 1988
- Bachelor of Science in Civil Engineering, University of Moratuwa, Sri Lanka, 1985

Major: Geotechnical Engineering

Presentations and Publications:

Meegoda, N. J., P. Ratnaweera, 1992. ''Identification and Classification of Contaminated Soils.'' Mediterranean Geo-Environmental Conference, Cesme, Turkey.

Ratnaweera, P., and N. J. Meegoda. 1991. ''Microscopic Modeling of Shear Strength of Contaminated Soils.'' Mechanics Computing in 1990's and Beyond , ASCE 8th Engineering Mechanics Speciality Conference, Columbus, Ohio, Proceedings, (Ed. by H. Adeli and R. L. Sierakowski) Vol. 2, pp. 1199-1203.

Ratnaweera, P., and N. J. Meegoda. 1991. ''Comparison of a Microscopic Model and a Macroscopic Model Predictions on the Stress-Strain behavior of a Soil.'' Mechanics Computing in 1990's and Beyond, ASCE 8th Engineering

Mechanics Speciality Conference, Columbus, Ohio, Proceedings, (Ed. by H. Adeli and R. L. Sierakowski) Vol. 2, pp. 1204-1208.

Meegoda, N. J., and P. Ratnaweera. 1987. "A New Method to Characterize Contaminated Soils." Superfund '87, Proceedings of the 8th National Conference, Nov. 16-18, Washington, D. C., pp. 385-389.

Meegoda, N. J., and P. Ratnaweera. 1987. "Field Prediction of Transmissivity of Fractured Rock." EOS Transactions, American Geophysical Union, Vol. 68, No. 16, 301-304.

Peiris, T. A., P. Ratnaweera, A. M. Rodrigo. 1985. "Performance of Road Pavements in Sri Lanka, with respect to formation of Potholes." Civil Engineering Faculty Conference, University of Moratuwa, Sri Lanka.

This thesis is dedicated to my parents

ACKNOWLEDGEMENT

It is a pleasure to be able to express in print the appreciation of constant advise and guidance of my advisor, Dr. Namunu Meegoda, at each step of this research and writing of the thesis. Thanks are also due to members of my advisory committee for their invaluable advice and suggestions.

I am greatly indebted to my wife Poorna, for her suggestions and constructive criticisms in preparing this manuscript and mainly for being patient and understanding during the past few years. My thanks also go to our son Rivi for being patient with me in my selfish venture.

I extend my gratitude to my friends Kuo-neng Chang and David Washington for their support and help.

Last but not the least, I should mention with gratitude the faithful support received from TESLA@NJIT.EDU. At a time when other computers had abandoned me, she stood by me day and night as my friend and colleague.

TABLE OF CONTENTS

Page

APPENDICES

Page

LIST OF FIGURES

LIST OF ABBREVIATIONS

C	Global damping constant proportional to mass.
C^*	Global damping constant proportional to moment of inertia.
d	Distance between surfaces at a distance x from point 1.
d_1	Distance between surfaces at point 1.
d_2	Distance between surfaces at point 2.
$\bar{d}_2$	Distance between surfaces at the point where maximum pressure is developed.
D	Distance between the centers of spheres (a) and (b).
$\hat{c}_i$	Unit vector in local $\hat{c}$ direction; subscript i=1,2,3 in global co-ordinates.
e_{cv}	Critical void ratio.
F	Frictional force.
$F_{(a)}$	Resultant force at contact m for particle (a).
F_j^c	Force at contact c of particle p.
F_n	Force in the normal direction at the point of contact.
F_s	Force in the tangential direction at the point of contact.
g	Gain specified in servo mechanism.
h	Height of the fluid column at co-ordinates (x,y).
h_o	Inter-particle spacing measured along the line joining two sphere centers.
i,j	Co-ordinate of a grid point (j,i).
$I_{(a)}$	Moment of inertia of sphere (a).
$I_{(b)}$	Moment of inertia of sphere (b).
k	Radius of gyration.
k_n	Normal stiffness.
k_s	Tangential stiffness.

m	Number of elements in the Finite Difference grid in x direction, mass of a sphere, number of contacts on particle p.
$m_{(a)}$	Mass of sphre (a).
$m_{(b)}$	Mass of sphre (b).
$M_{(a)}$	Resultant moment at contact m for particle (a).
n	Number of elements in the Finite Difference grid in y direction.
n_i^c	Unit normal vector at contact c.
$\dot{n}_i$	Normal component of the relative velocity $\dot{X}_i$.
N	Number of particles in volume V; Normal force at point of contact.
$\vec{OA}$	Position vector of A with respect to O.
$\vec{OB'}$	Position vector of B with respect to O′.
p	Pressure.
p_i	Force vector.
p'_o	Effective consolidation stress.
p_{max}	Maximum pressure.
p',q	Arms extending from a node point in the j direction.
P	External force applied.
$P_{(a)}$	Contact point on sphere (a).
$P_{(b)}$	Contact point on sphere (b).
q_i	Rate of flow, as signified by subscript i in x,y,z directions.
q_{res}	Residual shear strength.
q_{peak}	Peak shear strength.
r,s	Arms extending from a node point in the i direction.
r_o	Average radius of radii R_1 and R_2.
R	Radius of the projected area.
$R_{(a)}$	Radius of sphere (a).

$R_{(b)}$	Radius of sphere (b).
R_i^p	Position vector at point of contact C.
R^p	Radius of particle p.
R_1	Radius of sphere (1).
R_2	Radius of sphere (2).
$\dot{s}_i$	Tangential component of the relative velocity $\dot{X}_i$.
$\hat{s}_i$	Unit vector in local y direction; subscript i=1,2,3 in global co-ordinates.
S	Surface area of assembly.
SO_{reqd}	Required mean stress.
SO_{meas}	Measured mean stress.
S_{xy}	Lateral mean stress.
S_{xyreqd}	Required lateral mean stress.
S_{xymeas}	Measured lateral mean stress.
t_{cr}	Critical time step.
t_N	Time at N th step.
$\hat{t}_i$	Unit vector in local x direction; subscript i=1,2,3 in global co-ordinates.
u_i	Local velocity in the x direction; subscript i=1 for velocity at h=0, subscript i=2 for velocity at h=h.
T	Tangential force at point of contact.
U	Relative velocity in the x direction.
u_1	Velocity at point A in local x direction.
u_2	Velocity at point B in local y direction.
U_i	Velocity at the center in the local x direction; subscript i for sphere 1 and 2.
U_r	Relative linear velocity of the two spheres in the local x direction.
V	Volume of a granular assembly; volume of a soil element.

v_{cv}	Specific volume at critical void ratio.
v_c	Specific volume after consolidation.
v_i	Local velocity in the y direction; subscript i=1 for velocity at h=0, subscript i=2 for velocity at h=h.
v_o	Linear velocity vector at the center of sphere (1).
$v_{o'}$	Linear velocity vector at the center of sphere (2).
v_A	Velocity vector at point A.
v_B	Velocity vector at point B.
v_1	Velocity at point A in local x direction.
v_2	Velocity at point B in local y direction.
V_i	Velocity at the center in the local y direction; subscript i for sphere 1 and 2.
V_O	Velocity vector at O.
$V_{O'}$	Velocity vector at O′.
V^p	Volume of particle p.
V_r	Relative linear velocity of the two spheres in the local y direction.
w_i	Local velocity in the z direction; subscript i=1 for velocity at h=0, subscript i=2 for velocity at h=h.
w_1	Velocity at point A in local z direction.
w_2	Velocity at point B in local z direction.
W_i	Velocity in the local z direction; subscript i denoting for sphere 1 and 2.
W_r	Relative linear velocity of the two spheres in the local z direction.
x,y,z	Distance measured in the local x, y, z directions.
x_i	Global co-ordinates of center of sphere (a); subscript i=1,2,3.
x_i^c	Position vector of contact c.
x_i^p	Position vector of centroid, particle p.

$\dot{x}_i$	Velocity of sphere (a); subscript i=1,2,3 in global co-ordinate directions.
$\ddot{x}_i$	Acceleration of sphere (a); subscript i=1,2,3 in global co-ordinate directions.
$\dot{X}_i$	Relative velocity between the contact points $P_{(a)}$ and $P_{(b)}$.
y_i	Global co-ordinates of cetner of sphere (b); subscript i=1,2,3.
$\dot{y}_i$	Velocity of sphere (b); subscript i=1,2,3 in global co-ordinate directions.
$\ddot{y}_i$	Acceleration of sphere (b); subscript i=1,2,3 in global co-ordinate directions.
δt	Incremental time (t_{N+1}-t_N).
ΔF_n	Incremental normal force.
ΔF_s	Incremental tangential force.
Δn	Incremental relative normal displacement.
Δs	Incremental relative tangential displacement.
ϵ_q	Shear Strain.
ϵ_v	Volumetric Strain.
ϵ_1	Vertical Strain.
$\dot{\epsilon}_i$	Strain rate in i direction where i=x,y and z.
η	Coefficient of viscosity.
$\dot{\theta}_{(a)}$	Angular velocity vector of sphere (a).
$\ddot{\theta}_{(a)}$	Angular acceleration vector of sphere (a).
$\dot{\theta}_{ij}$	Angular velocity of spehre j in i direction; subscript i=x,y,z and j=1,2.
$\dot{\theta}_{ir}$	Relative angular velocity of the two spheres in local i direction, subscripts i for x, y, z directions.
$\dot{\theta}_{O}$	Angular velocity vector at the center of spher (1).
$\dot{\theta}_{O'}$	Angular velocity vector at the center of spher (2).
μ	Coefficient of static friction.

μ_{mic}	Coefficient of friction between two surfaces at a contact.
τ	Shear stress.
σ_{ii}	Stress in the global i direction, subscript i=x,y,z.
σ_{ij}	Stress tensor.
$\bar{\sigma}_{\mathrm{ij}}$	Average stress tensor of a macro element.
$\sigma_{\mathrm{ij}}^{\mathrm{p}}$	Average stress tensor of particle p.
φ_{cv}	Angle of internal friction at critical void ratio.
φ_{max}	Angle of internal friction at peak strength.
φ_{mic}	Angle of inter-particle friction.
φ_1	Angle subtended at the center of sphere O by inter sphere height h.
φ_2	Angle subtended at the center of spher O' by inter sphere height h.
φ_{μ}	Angle of friction due to frictional resistance.

CHAPTER 1

THE INFLUENCE OF PORE FLUIDS ON STRESS-STRAIN BEHAVIOR OF GRANULAR SOILS

1.1 Introduction

It is evident that during the past few decades, the industrial and economic growth has introduced a large variety as well as a large quantity of chemicals to the world's eco-system. Human activities which were unregulated at that time have given rise to contamination of our precious groundwater system, soil and the environment as a whole. High concentrations of organic chemicals, pesticides, petrochemical products, and numerous industrial solvents have been observed in the areas of chemical and petroleum spills and unregulated landfills. Soil contamination observed in the vicinities of chemical storage facilities and hazardous material disposal sites cannot be overlooked.

Contaminant chemicals are either adsorbed by the soil particles or held between soil particles as miscible or immiscible liquids. With the passage of time the adsorbed chemicals disperse within the soil matrix causing extensive soil contamination. Percolating surface water and groundwater movements actively participate in propagating this contamination. Thus the resulting contamination of soil will not be confined to the immediate locality of the source of pollution, but will be spread unrestricted, perhaps irreparably.

Prolonged contamination can partially or fully replace the pore fluid of soil with contaminant chemicals and thereby change the viscous characteristics of pore fluid. However, researchers in the field of geotechnical engineering do not have a fundamental understanding of deformation characteristics of soils with chemicals (pore fluids) of different viscosities. Therefore, a fundamental investigation to evaluate the influence of pore fluid viscosity on the stress-strain behavior of soil would be useful to the Geotechnical engineering profession.

1.2 Soil Structure

The soil matrix consists of solid, liquid and gaseous phases. These three phases of the soil matrix are not present as a continuum as described in solid mechanics, but rather as a heterogeneous mixture of all three phases. Although this model quantifies the amounts of the three phases present in a soil element, it does not describe the actual soil structure. The solid phase consists of soil particles of solid material. Common solid particles in soils are fairly inert solids (sands), reactive non-clay minerals (limestone, metal ores), clay minerals and organic matter.

In geotechnical engineering practice, the structure of a soil is taken to mean the geometric arrangement of the particles or mineral grains (*i.e.* soil fabric) as well as the inter-particle forces. In granular soils, the inter-particle forces are very small, so both the fabric and the structure of gravels, sands, and to some extent silts are the same (Holtz and Kovacs, 1981).

Photomicrographs of natural sand and silt particles indicate that particles are mineral aggregates having different shapes. They could be rounded, sub-rounded, elongated, or angular depending on the degree of weathering. In granular soils water has very little effect on the structure since the grains are non porous inert particles. The surfaces of granular particles being less active exhibit low water retention and negligible adsorption. They tend to form a ''single grain structure'' with a loose or dense packing as a result of settling in a soil-fluid suspension or being deposited by air.

1.3 Shear Strength and Stress-Strain Behavior of Soils

In a dry soil, the shear strength is developed at mineral to mineral contacts. In a saturated soil a thin layer of fluid exists between two mineral contacts. Therefore, the shear strength of a saturated soil depends on the properties of the pore fluid as well as those of the minerals.

When a soil is subjected to a change in stress, the excess load is taken by the soil matrix and the pore fluid. At the points of contact, the contact forces may have normal as well as tangential components. An increase in the normal force causes particles (or particle clusters in the case of clay soils) to deform while the tangential component may cause slippage. In the case of clay soils, when a load is applied on the soil matrix, the clay particles and/or particle clusters may elastically bend or relax previously bent ones. For granular soils, this mechanism may occur but to a lesser extent. When the applied load causes a sufficiently large change in effective stress within the soil matrix, slippage and rotation may occur causing plastic deformation.

The factors influencing the stress-strain behavior and shear strength of granular materials include the effective stress, frictional and strength properties of the individual grains, particle shape, and void ratio/relative density. It is recognized that the soil fabric (structure) also influences soil behavior, although a practical method of quantifying this factor is not currently available.

For granular soils, the predominant effect contributing to changes in particle arrangement is the mobilized friction. Therefore, unlike clay soils, at low effective consolidation stresses, granular soils do not display a unique specific volume-effective consolidation stress relationship. Hence normalizing of shear strength is not possible for granular soils.

Attempts to normalize the drained stress-strain behavior of granular materials have been met with limited success. Sladen and Oswell (1989) used the critical state concept to normalize the undrained behavior of very loose sands in triaxial compression. Application of critical state concept to the drained stress-strain behavior of granular materials has been much less successful in achieving a normalizing relation.

Casagrande (1936) related the angle of friction $\phi_{\max}$ to Coulomb's theory. Beyond the peak strength, 'cohesionless soils' show changes in volume during shearing, and when the residual shear strength is reached shearing will occur at a constant volume where the corresponding 'angle of friction' is denoted by ϕ_{cv}.

He also observed that the loose sand reaches its maximum strength at the residual friction angle, φ_{cv} without passing a peak. Roscoe, et al. (1958) proved that assemblies of particles attain a final single porosity for a given normal pressure the value of which may depend on particle shape and grading.

Many researchers have observed the significance of volume change on the behavior of granular material. The peak strength of a soil comprises of three components: (a) strength mobilized by frictional resistance; (b) strength developed by energy required to rearrange and reorient soil particles: and (c) strength developed by energy required to cause expansion or dilatation of the material. Taylor (1948) attempted to identify separately, the strength components due to 'friction' from that due to expansion in the shear box. This idea was later extended by Bishop (1954) and Rowe (1962, 1971). They attempted to account for the difference in peak and residual strengths as an effect of volume change behavior.

Although it has long been recognized that the true angle of friction φ_{μ} is less than the angle of friction corrected for dilatation, many researchers have attempted to relate φ_{μ} to the residual friction. When a granular soil reaches the critical state, the friction angle, φ_{cv} corresponding to the residual strength will depend on the strength mobilized by frictional resistance for a given confined pressure. Caquot (1934) derived the following expression:

$$\tan\varphi_{cv} = \frac{1}{2}\pi\tan\varphi_{\mu} \tag{1.1}$$

while Bishop (1954) presented the empirical relationship:

$$\sin\varphi_{cv} = \frac{15\tan\varphi_{\mu}}{10 + 3\tan\varphi_{\mu}} \tag{1.2}$$

relating the residual angle of friction, φ_{cv} and the true angle of friction φ_{μ}.

1.3.1 Influence of Pore Fluid

In saturated granular soils, the magnitude of elastic and plastic responses to an external stress depend on the shape and surface characteristics of the minerals and the physical properties of the pore fluid. When subjected to an external force, the increase in load is taken by the pore fluid increasing the prevailing hydrostatic pressure. This increases the forces acting at mineral to pore fluid contacts. Under drained conditions, the pore water pressure in excess of the hydrostatic pressure will dissipate causing an increase in the load taken by the mineral to mineral contacts. Under undrained conditions, excess pore water pressure will build up to take the load thus reducing the load taken at mineral to mineral contacts. Although the shearing mechanism is not clearly identified (Scott, 1963), it is associated with instantaneous elastic and plastic deformations occurring simultaneously between particles and/or particle clusters.

Soil moisture also plays an important role in compaction. Proctor (1933) explained the role of pore fluid in compaction using the difference in friction angles between the dry and wet samples of the same soil due to viscosity of the pore fluid. Horn and Deere (1962) stated that as the surface moisture increases, the frictional resistance that can be developed between surfaces of minerals with layered lattice (such as micas) decreases, whereas the reverse is true for massive structured minerals (granular materials such as quartz). However, conventional drained triaxial tests done on dry and saturated granular soils indicate that with the introduction of water, the shear strength is reduced (Lee et al., 1967).

1.3.2 Effects of Chemicals

The solid phase of a granular soil is relatively inactive than the combined solid-fluid phase. Therefore, when a granular soil is contaminated, the contaminant chemicals will be held in the pore fluid. Since the strength of a saturated granular soil depends on properties of both the minerals and the pore fluids, the changes in the physical properties of pore fluid can change the strength characteristics.

Thus any changes in the strength characteristics of a granular soil can be logically reasoned to be related to the changes in the contact properties at points of contact of mineral grains in the presence of a pore fluid. Therefore, to provide a mechanistic explanation to the changes in strength characteristics due to chemical contamination, changes in the contact properties have to be studied at particle level. The constitutive laws for soils cannot be used to study this phenomenon since these laws are derived based on experimental results to model a macro-element of soil where soil is treated as a continua rather than a discrete array of individual grains and pore fluid in contact. Therefore, to study the actual mechanism responsible for this behavior, it is imperative that a microscopic model be used.

1.4 Microscopic Modeling of Granular Soils

Numerical methods of modeling has been in use in the field of geotechnical engineering for over three decades now. Numerical models can either be macroscopic or microscopic. The macroscopic models such as the Cam-Clay model and the Cap model etc., are rationally formulated based on the experimental results obtained from material codes of behavior. In macroscopic models, the actual mechanisms, which are not exactly understood, are disguised behind the name of macroscopic internal variables. The advantage of such formulations is the ability to interpret experimental data into straight forward mathematical relations which may be used to predict behavior of soil under similar conditions. In macroscopic models, the behavior of a macro element is extended using a Finite Element Method to model the laboratory simulations and field boundary value problems.

On the other hand, the microscopic models such as TRUBAL (Cundall and Strack, 1984), based on the Distinct Element Method (DEM), study the behavior of micro-elements such as individual soil grains which consist of a few particles and their ambient space. The microscopic models provide a better insight into the fundamental mechanisms responsible for actual soil responses. The disadvantage of the microscopic models is the difficulty to bring over from the micro level to the real macro level without many simplifying assumptions. Although the earliest models were inspired by and used in rock mechanic related studies (Cundall, 1971), today there is a drive to develop, improve and use numerical models extensively in soil mechanics. Though they are not as popular as their macroscopic counterparts numerous mathematical models have been presented in the last two decades, to model granular soils. They are being used with large numbers of particles using super computers so that the simplifying assumptions can be avoided.

The success in predicting the observed behavior using a microscopic model depends on how well the physically observed quantities can be expressed using fundamental concepts. On the other hand for macroscopic models one would not encounter this problem since the macroscopic model parameters are obtained from experimental data. The ultimate goal of both methods however is to produce a constitutive model for granular material that can account for the changes in the fabric which occur during deformation.

Although it is often treated as a continuum, soil like most other physical systems, is discontinuous at some level. It is rewarding to model such continuums as discrete assemblies of material at microscopic level, because as the microscopic mechanisms are understood, more knowledge about the macroscopic behavior can be gained. Being composed of solid particles, pore fluid and air, soil can be modeled as a discrete granular assembly.

The strength of a granular assembly is the ability of its solid phase to sustain a load without excessive deformation. At points of contact, the contact forces have normal and tangential components. An increase in the normal force causes particles to deform, while the tangential component causes rigid body movement (translation and rotation). When a load is applied to the soil matrix, particles may elastically deform or release the previous deformations. When the applied load causes a sufficiently large change in effective stress within the soil matrix, translation and rotation occur causing plastic deformations. Microscopic models simulate these interactions occurring at the contact points. Therefore they provide a better insight into the fundamental mechanisms responsible for the observed behavior of a soil.

However in the field of soil mechanics, microscopic modeling has so far been used purely for qualitative studies. Exact one on one modeling of the soil fabric, has not been achieved by the models developed so far. Most of the models that have been developed, based on DEM and other numerical schemes, use not more than 4 particle sizes in element test type analysis and up to eight particle sizes in boundary value analysis (Dobry and Ng, 1989). The total number of particles used and the shapes also have been limited. As such an exact image, representing soil fabric in every detail cannot be generated by these models and therefore the results cannot be directly quantitatively compared with macroscopic models or experimental results.

1.5 Literature Survey

The shear strength of granular soils depends entirely on mechanical effects. Therefore, any changes observed in the shear strength should be associated with changes in contact properties. Any changes in the physical properties of pore fluid can bring about changes in the pore fluid to mineral contact properties.

Meegoda (1989) carried out direct shear tests on a silt contaminated with glycerol/water solutions of different proportions to investigate whether pore fluid viscosity has any influence on shear strength of granular soils. Results of this study indicated that the residual angle of internal friction decreased with the increase of coefficient of static viscosity of pore fluid.

Evgin and Das (1992) studied the stress-strain behavior of loose and dense sands when saturated with water and with oil. Significant changes in the angle of friction were observed for both sands, when oil was used as the pore fluid. The volumetric strain versus vertical strain curve was also found to change, with the change in pore fluid, for both sands. When oil was used as pore fluid, the volumetric strain was found to be more compressive than it was with water.

These results do consolidate the view that the viscosity of pore fluid is an important factor governing the shear strength and stress strain behavior of granular soils. However, the exact mechanism which causes this strength reduction associated with the increase in pore fluid viscosity has hitherto not been explained. Since the strength of a granular soil is governed by the mineral to mineral contacts and mineral to mineral contacts in the presence of pore fluids, the observed changes should invariably be associated with these particle contacts. Therefore, it is imperative that the soil structure be studied at a microscopic level to understand the actual mechanism behind this macroscopic behavior.

Many attempts have been made by previous researchers to explain macroscopic behavior of granular assemblies using microscopic models. Microscopic modeling of granular media has shown that the microscopic friction angle (which is based on the Mohr-Coulomb failure criteria) is a key factor controlling the macroscopic behavior. Therefore it is reasonable to believe that it is the lubricating effect at microscopic level due to the viscosity of the pore fluid that is responsible for the observed macroscopic behavior.

Mathematical modeling of sand as a granular assembly was introduced by Mogami (1965). In 1971, the Distinct Element (Discreet Element) method was introduced by Cundall, mainly to model the behavior of rock elements. Soon after its introduction, it was being used to model granular assemblies with considerable success. Numerical codes have been developed to model two dimensional assemblies of discs (Cundall, 1978) as well as three dimensional assemblies of spheres (Strack and Cundall, 1984) using the DEM. Independent to Cundall, Hakuno and Hirao (1973) conducted a simulation of a dry granular assembly of circular particles to study the static deformation of sand.

The Distinct Element Method is a numerical procedure for simulating behavior of a system of discrete, interacting bodies. It is developed based on the assumption that each individual element abides by the Newton's Laws of motion and the force-displacement relationship at points of contact. The interaction of the particles is viewed as a transient system for a given time increment with states of equilibrium developing whenever the internal forces are balanced.

Since its introduction, the microscopic modeling of granular assemblies have been studied and used in many applications by many researchers. Numerous models with many similarities, but developed not entirely on these principles have been published (Ting et al. (1989), Hakuno and Tarumi (1988)). Application of DEM for microscopic modeling is also very wide spread in the geotechnical field today. DEM simulations can be categorized in to two groups, as element tests or boundary value problems. In element test type simulations, boundary effects are eliminated or reduced, to study the constitutive behavior. When a system is evaluated as a boundary value problem, the entire system is modeled with a desired number of particles and the particle behavior when subjected to specified boundary conditions, is studied. This has numerous limitations, because of large numbers of particles that are needed to model a system. For the same reason 3-D problems are either avoided or reduced to 2-D cases for ease in computations.

Microscopic models based on the DEM have been used to study the constitutive behavior of a macro-element (Cundall and Strack, 1979a, 1983). This would also enable the models to be used as a research tool in developing more representative constitutive laws for soils. The success achieved in predicting the stress-strain behavior of a macro element, has enhanced the use of the DEM in modeling physical experiments.

Cundall and Strack (1979b) used the 2-D DEM model to compare the force vector plots obtained from the computer program BALL with the corresponding plots obtained from a photo-elastic analysis. This quantitative analysis has been possible because the simulation has been carried out for an assembly of photo-elastic discs and not a natural granular soil. Cundall (1988) compared the results of a numerical simulation with results of a physical experiment performed on a dense sphere assembly in 3-D. Petrakis et al. (1989) simulated small and large strain responses of a sand under dynamic loading using a 2D non-linear DEM model.

Ting et al. (1989) used the computer program DISC, which is a 2-D DEM source code (Corkum and Ting, 1986) to simulate laboratory 1-D compression tests, direct simple shear and triaxial tests, and laboratory simulations of deep and shallow footings with a granular assembly of discs. These results indicated that the 2-D DEM model could simulate non-linear, stress history-dependent soil behavior when individual particle rotations are inhibited. This is, in fact, quite logical since the irregular shaped soil particles would not rotate as much as would an assembly of discs. They had attempted to use the scaling laws in Geotechnical Centrifuge modeling to decide on a computationally practical size for the granular assembly.

Ratnaweera and Meegoda (1991a) compared the predicted behavior of a soil under different stress paths using 3-D DEM microscopic model, TRUBAL with the Bounding Surface macroscopic model, EVALVP (Kaliakin and Herrmann, 1989) in order to check the ability of TRUBAL to model soil behavior. Since an exact one to one representation of a macroscopic element of soil, using a microscopic model was not possible, a conventional drained triaxial test was simulated using both models and the macroscopic model parameters were adjusted so as to be compatible with the microscopic model simulations (Table A.1, Figure A.1). This microscopic model and the macroscopic model were then used to simulate the stress-strain behavior of a soil in a plane strain triaxial test. The results of the two models were comparable (Figure A.2). However when the two models with the same model parameters were used to simulate a constant pressure triaxial test, the volume change behavior for both models were found to be incompatible (Figure A.3). This study showed that selection of microscopic model parameters and the laws of contact between two soil grains play an important role in predicting the macroscopic behavior of a soil using microscopic models.

Ratnaweera and Meegoda (1991b) modeled the undrained triaxial behavior by deforming a in 3-D granular assembly along an undrained stress path while maintaining zero volumetric change.

The past research work in DEM simulations also includes many boundary value type simulations. Actual physical tests such as bearing capacity tests, geostatic stresses in bin of particles, stresses in infinite slopes, lateral earth pressure tests (Ting et al, 1989) and dynamic loading conditions such as vibration due to driving of piles (Uemera and Hakuno, 1987) have been simulated qualitatively with considerable success. Hakuno and Tarumi (1988), and Iwashita and Hakuno (1988) used the DEM model to predict soil response to seismic loading patterns. The 2-D DEM model developed by Cundall has been used to model ground surface settlements during construction of a tunnel (Kiyama et al, 1982) and behavior of grain particles in a silo (Kiyama and Fujimura, 1983).

Izutsu et al. (1986) conducted a granular assembly simulation taking in to account the pore water pressure but without including relative displacements. Hakuno and Tarumi (1988) modeled soil liquefaction as a boundary value problem using a disc assembly, taking in to account the changes in pore water pressure of micro pore volumes.

Although applications of DEM to model granular material have taken to a wide range and is been numerous, these analysis have only been qualitative that one on one direct simulation of actual physical tests is still an impossibility.

1.6 Objectives

The primary objective of this research is to investigate the influence of pore fluid viscosity on deformation characteristics of granular soils. A two fold approach is taken to achieve this objective. First an experimental study was carried out with silty sand samples and Glycerol/Water solutions with different viscosities to study the effects of pore fluid viscosity on deformation characteristics of granular soils.

The effect of pore fluid viscosity on soil behavior was then studied at a microscopic level, to provide a mechanistic explanation to this phenomenon. A microscopic mathematical model, TRUBAL (Cundall and Strack, 1984), based on Distinct Element Method, was modified to include the effects due to pore fluid viscosity and was used in a qualitative study to verify the results of the physical tests. Simulations of drained triaxial tests were carried out for granular assemblies of spheres with pore fluids of different viscosities.

CHAPTER 2
METHODOLOGY AND TEST PROGRAM

2.1 Methodology

At low effective consolidation stresses granular soils do not display a unique relationship between specific volume and effective consolidation stress. Therefore, shear strength of granular soils cannot be normalized. Although at very high effective consolidation stresses shear strength of granular soils can be normalized (Vesic and Clough, 1968), high stresses cannot be used since they would crush soil particles. As such it will not reflect the frictional component of the shear strength correctly, because the strength mobilized in crushing particles will also be included in the shear strength.

The other alternative would be to start all tests with the same initial specific volume and test at the same effective consolidation pressure. But it is not possible to prepare all the samples with different pore fluids to have the same initial specific volume since pore fluids with different viscosities have different drainage properties.

Since it was not practically possible to normalize the results, as an alternative, variation of the residual shear strength with the critical void ratio was analyzed. As discussed in the Article 1.3, when a granular soil reaches its critical void ratio, the frictional resistance of the soil predominates its shear strength. Since the frictional resistance of soil is evolved at particle contacts, effects of pore fluid composition, if any, will be indicated by changes in the residual shear strength. The changes in critical void ratio will also be indicative of effects of pore fluid composition since it involves particle movements which change the configuration of the soil matrix.

Soil samples with four different pore fluid viscosities were used in this study. Samples were prepared by mixing the prepared pore fluid with the dry soil instead of leaching out prepared samples with the selected pore fluids. This process was adopted mainly to ensure that the pore fluid was distributed uniformly within the

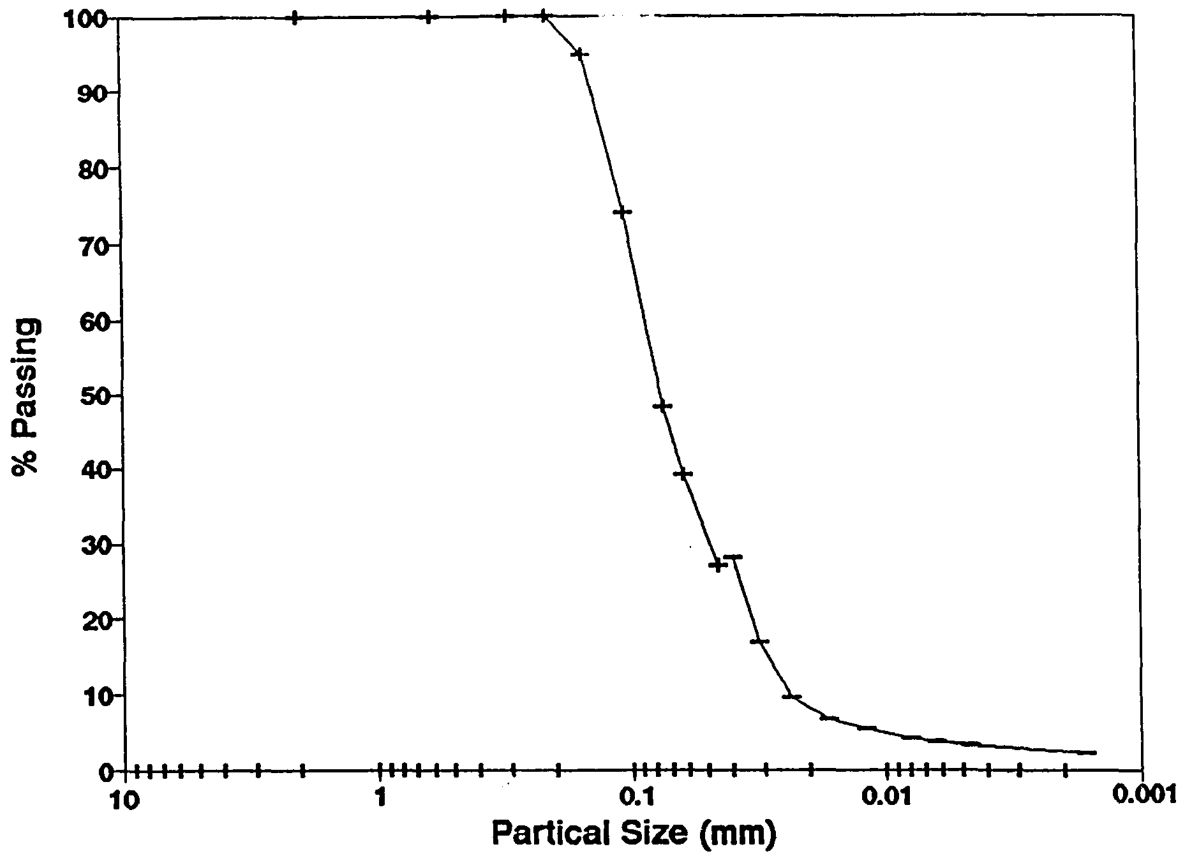

Figure 2.1 Particle Size Distribution Curve for the Silty Sand

soil sample. An added advantage of this process was the short sample preparation time compared with the leaching process.

2.2 Material

2.2.1 Soil

For the entire test program the same soil, a silty sand was used. To classify and identify the soil, a particle size distribution test, and Atterberg limit tests were carried out. The sample was tested for specific gravity conforming to the ASTM D854. The specific gravity was found to be 2.71.

Wet sieving of the soil revealed that more than 50% of the soil retained on No. 200 sieve (0.075 mm) making it a coarse grained soil. To obtain the particle size distribution for the total range of grain sizes, results of the wet sieve analysis and a hydrometer analysis for the part passing No. 200 sieve, were combined.

The distribution curve obtained (Figure 2.1) showed that the soil is a uniformly graded soil, 100% of it passing No. 40 sieve (0.42mm).

Portion of the soil passing through No. 40 sieve (0.42 mm) was used for the Atterberg limit tests. The Unified Soil Classification system indicated that this soil although fine enough, (48% passing No. 200 sieve and 100% passing No. 40 sieve) is granular. The plastic limit could not be established since it was not possible to be rolled to a thickness of three millimeters. Crumbling started at about 5 mm thickness. When the liquid limit test was carried out, the soil flowed easily and did not stick to the bowl. Even at the lowest possible water content, the soil slipped on the surface of the cup and the grove closed after about 5 blows. From these test results the soil was concluded to be a silty sand.

2.2.2 Pore Fluid

The only two fluids that were used in combination, as pore fluid for the soil samples were water and glycerol. The water was deionized and deaired. Glycerol was selected as the contaminant because it is completely miscible in water and has a high viscosity of 1490 centipoise, which would permit producing different pore fluids with a good distribution of viscosities. The pore fluid compositions were selected from a past research carried out by Meegoda (1989). The viscosities of these pore fluids, as measured by Rajapakse (1989) are given in Table B.1

2.3 Test Program

Soil samples with the following compositions (Table B.1) viz,

1) Water.
2) 16.54% glycerol/water solution.
3) 28.39% glycerol/water solution.
4) 44.22% glycerol/water solution.

were used in the test program. The samples with water as pore fluid were tested under effective consolidation pressures of 50 kPa, 75 kPa, and 125 kPa. All the other samples were tested under effective consolidation pressures of 50 kPa, 100 kPa and 125 kPa.

2.4 Triaxial Test

2.4.1 Triaxial Testing Apparatus

An automated triaxial testing apparatus (Soil Engineering Equipment Co., CA) was used for the test program. This computer controlled system provides a uniform and accurate procedure far superior to manual or semi-automated systems (Li et al., 1988).

The triaxial testing apparatus was equipped with a force transducer (to measure the deviatoric load), an LVDT (to measure axial deformation), three pressure transducers (to measure the cell pressure, pore pressure and the volume change) and two internal transducers which were used to check and perform operational directives. Pressures were applied by compressed air. This was preferred over the Bishop's apparatus because of quick and easy operational ability and safety.

However the presence of the air/water interface tends to dissolve air in water causing unsteady behavior during the test.

The triaxial cell which was specially designed for the automated set up had all the features included in a conventional triaxial cell. The chamber pressure and the back pressure were transferred to water at an air/water interface.

2.4.2 Sample Preparation

The required amount of soil was mixed with deaired de-ionized water to make a soil slurry. This soil slurry was further deaired while being mixed in an air tight container under vacuum.

It was then poured into a cylindrical triaxial sample mold. Throughout the preparation, the sample was kept saturated. Before the slurry was poured into the mould, the porous stones were deaired and saturated, the rubber membrane was checked for possible leakages and placed on the membrane holder, and the filter papers for base and top were saturated.

The soil used for the test, being a silty sand retained water well and could be easily mixed into a homogeneous slurry, and poured in to the mold, without any segregation. However as an extra measure against possible segregation, the slurry was poured in to the mold in 5 layers.

A vacuum was applied to remove the excess fluid from the sample while sample densification. Throughout this process the effective stress of the sample was kept below the effective consolidation stress. The vacuum was stopped at the appearance of a dry patch on the top surface. Then the cap, the o-rings and the water line were connected, and the mold removed.

2.4.3 Test Procedure

The triaxial test was performed conforming to the standard test method for consolidated drained triaxial compression tests.

The drainage lines filled with liquid were connected to the sample and the fluid was permeated from the bottom, until the sample was completely saturated. To ensure that no air bubbles are trapped within, a vacuum not exceeding the effective consolidation pressure was applied at the top, throughout the permeation. This was continued until no more air bubbles were observed in the top drainage line. When the sample was saturated, the mold was removed and a minimum of three height measurements (120° apart) and three diameter measurements at quarter points of height were made. The vacuum was continuously applied to the sample to ensure that it would not collapse or deform under its weight, when the mold was removed.

The triaxial cell was then assembled, rod (which applies the deviatoric load) and LVDT placed and volume measuring chamber filled with deaired water. A bladder accumulator was connected to the bottom drain and the volume measuring device. After the vacuum was stopped, sample was allowed to equilibrate for an hour. Then the cell was filled with water, top cover of the cell positioned and the rod was attached to the top of the sample.

Once the soil sample was mounted on the triaxial cell, the piston rod was clamped in order to avoid any accidental loads while setting up the system. The cell chamber and the volume change measuring chamber were filled with deaired water. In the cell chamber, the air/water interface was maintained approximately at one inch below the top of the chamber. The volume change measuring chamber was filled up to one quarter of its full capacity. The triaxial cell was then positioned below the loading frame with the force transducer coupled to the setup.

Before the pressure source was connected, the force transducer, cell pressure transducer and the differential transducer measuring the effective stress were set to zero. The LVDT was positioned to read -3.20 volts approximately and the calibration for the transducer measuring the volume change was checked by adjusting the voltage gain within the operational range of 0 - 5 volts. The strain controlled tests were run by applying deviatoric stress using the oil actuator. An oil actuator gives a slower response enabling a strain controlled test. Then the pressure source was connected to the system and the computer program was activated.

The sample was allowed to consolidate under this pressure until the sample showed no pressure build up. At this stage the back pressure was applied in steps of 10 kPa while the cell pressure was being automatically increased simultaneously. Before increasing the back pressure any further the pore pressure was observed for any changes. When the back pressure had reached 200 kPa, the pore pressure parameter 'B' was checked and was found to be between 0.96-0.98. Then the sample was consolidated under the required effective consolidation stress. At the end of the consolidation, pore pressure was checked to see if it had completely dissipated. The sample was then sheared at a strain rate of 0.005% per minute until failure.

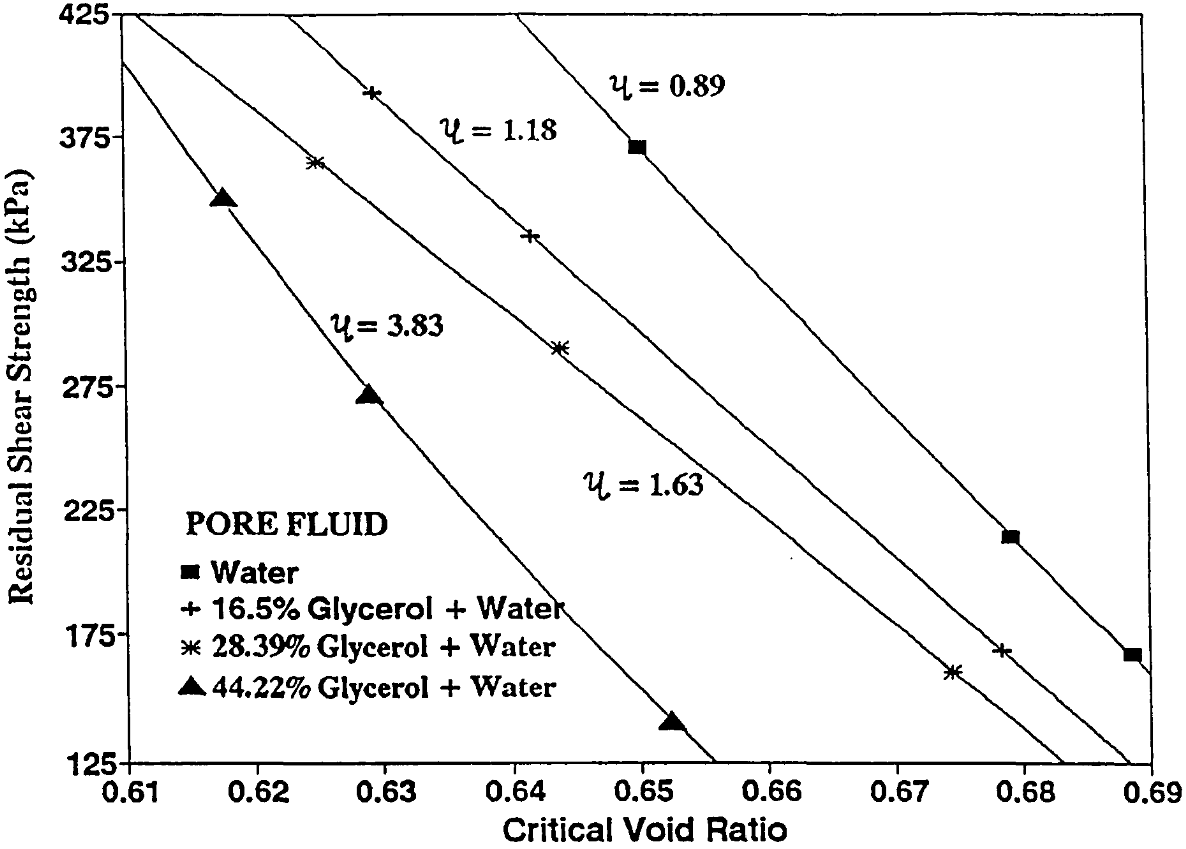

Figure 3.1 Variation of Residual Shear Strength with Critical Void Ratio for Different Pore Fluid Viscosities

CHAPTER 3

EXPERIMENTAL RESULTS AND DISCUSSION

Drained Triaxial tests were carried out for soil samples with four different pore fluids tested under three different effective consolidation pressures. The results of these tests are given in Table B.2. A direct comparison of these results is not possible since stress-strain behavior of this soil cannot be normalized. However, a comparison is possible, when the variation of residual shear strength is plotted against the critical void ratio (Figure 3.1) as discussed in the Article 2.1.

The plot of residual shear strength against critical void ratio gives a family of curves identifiable by the pore fluid viscosities. The residual shear strength show a curvilinear relationship with the critical void ratio. The regression lines drawn through data points of each pore fluid type seem almost parallel to each other.

This graph also shows that when a soil fails at any critical void ratio, the corresponding residual strength is higher for a soil with lower pore fluid viscosity. For any given residual shear strength, the corresponding critical void ratio is higher for soils with lower pore fluid viscosities.

Quite evidently, the pore fluid viscosity plays an important role in determining the shear strength of a granular soil. Therefore it is imperative that this factor be recognized and included in the strength parameters of granular soils.

It is apparent that when a soil is contaminated by chemicals, and the viscosity of the resulting pore fluid differs from that of water, the residual shear strength will not be the same as for an uncontaminated soil. The line of 0.89 centipoise viscosity, on the graph represent the characteristics of a soil with water as pore fluid while the other three lines represent the characteristics of the same soil with different pore fluid viscosities. At any critical void ratio, each soil would develop different residual shear strengths, soils with higher pore fluid viscosities developing lower strength.

Similarly, any shear strength on the plot would correspond to different critical

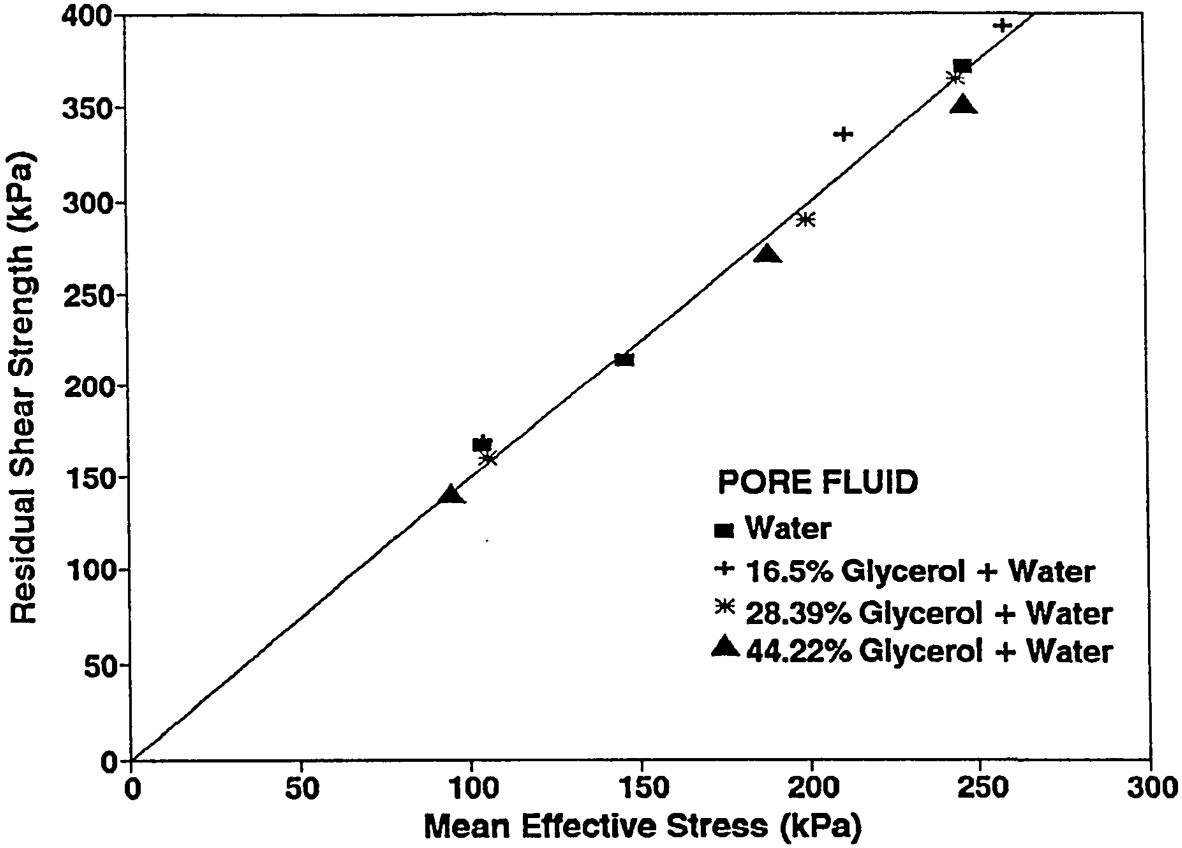

Figure 3.2 Variation of Residual Shear Strength with Mean Effectvie Stess for Different Pore Fluid Viscosities

void ratios for soils with different pore fluid viscosities. Thus a soil with a higher pore fluid viscosity has to be more densely packed than a soil with water as the pore fluid, to develop the same shear strength. This means that if a soil, even though very densely packed, is contaminated later by a fluid with higher viscosity, the strength properties will be affected and the soil may fail unexpectedly.

As seen in the graph, the residual shear strength corresponding to any critical void ratio is higher for a soil with lower pore fluid viscosity than for a soil with a higher pore fluid viscosity. Apparently as the pore fluid viscosity is increased, the shear strength of that soil decreases. However, with the low shear strain rate used in this investigation, the observed changes in the stress-strain behavior was not associated with a reduction in the angle of internal friction, ϕ_{cv} which delineates the frictional strength characteristics of the macro-element (Figure 3.2). The average angle of internal friction φ_{cv} for silty sand was found to be 36.7°.

These observations lead to the hypothesis that the mechanism behind the reduction of shear strength is a local phenomenon. Since the shear strength of a saturated granular soil depends on the characteristics of mineral to mineral contacts in the presence of pore fluids, for a drained soil sample this phenomenon in fact should occur at particle contact points. Furthermore, the very low rates of strain adopted for the tests, would allow dissipation of any pore fluid pressures that may be generated locally.

Figure 3.3 shows the variations of deviatoric stress with shear strain and volumetric strain with shear strain, for four silty sand samples which have different pore fluid viscosities but approximately similar critical void ratios (0.65). These graphs correspond to the four data points on Figure 3.1 with a critical void ratio close to 0.65.

Obviously the exact mechanism responsible for the observations made in the physical experiments can be understood only through an investigation at microscopic level, which would monitor the interaction and movement of soil grains subjected to the conditions imposed by the physical experiments. In an

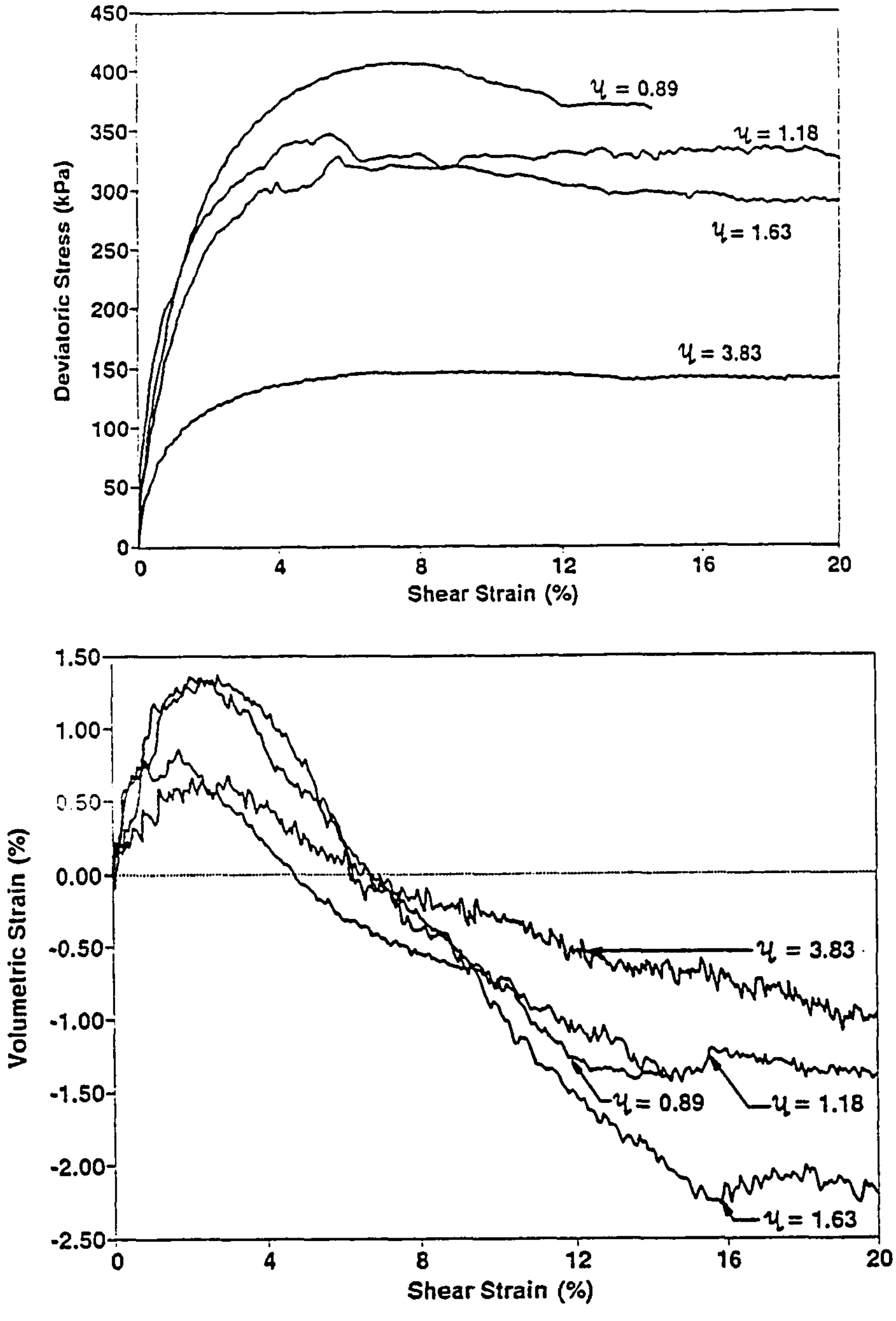

Figure 3.3 Stress-Strain Behavior Corresponding to a Critical Void Ratio of 0.65

effort to study this phenomenon at a microscopic level and provide a mechanistic explanation it was decided to use a numerical model and conduct a series of numerical simulations.

CHAPTER 4

MICROSCOPIC MODELING OF VISCOUS EFFECTS OF SOILS

4.1 The Distinct Element Method

The distinct element method was introduced as a particular discrete element scheme that uses deformable contacts and explicit solutions of the original equations of motion (Cundall and Strack, 1983). Several other numerical simulation schemes have been presented since then, but identified to be different in character or basic assumptions. Following the study of many such methods, Cundall and Hart (1989) proposed that the name discrete element method should apply to numerical schemes only if it (a) allows finite displacement and rotation of discrete bodies including complete detachment; and (b) recognizes new contacts as the calculation proceeds.

The DEM is based on the assumption that each individual element satisfies Newton's laws of motion. The interaction of particles is viewed as a transient system for a given time increment with stable equilibrium developing whenever the internal forces are balanced.

The stress tensor of an average macro-element is statistically computed from forces acting on all the elements for each time step. Therefore, the corresponding deformation at a particular stress state can be obtained by tracking the displacements at equilibrium. The concept of the average stress tensor adopted here, was proposed by Hill (1964). The average stress tensor σ_{ij} for a spherical particle of radius R_p, generated within cartesian co-ordinate axes x_1, x_2 and x_3 can be defined as:

$$\bar{\sigma}_{ij} = \frac{1}{V} \int_{V} \sigma_{ij} dV \tag{4.1}$$

The integral becomes a summation for a particulate material because it exist only within the particles:

$$\sigma_{ij} = \frac{1}{V} \sum_{p=1}^{N} \sigma_{ij}^{p} V^{p} \tag{4.2}$$

In the same way the average stress tensor within any particle *p* is defined as:

$$\sigma_{ij}^{p} = \frac{1}{V^{p}} \int_{V^{p}} \sigma_{ij} dV^{p} \tag{4.3}$$

Application of Gauss divergence theorem to (4.3), gives:

$$\sigma_{ij}^{p} = \frac{1}{V^{p}} \int_{s} x_i p_j ds \tag{4.4}$$

where p_j is the pressure acting on particle p. Since the surface forces are discrete the above can be expressed as a sum

$$\sigma_{ij}^{p} = \frac{1}{V^{p}} \sum_{c=1}^{m} x_i^c F_j^c \tag{4.5}$$

The combination of (4.2) and (4.5) yields

$$\sigma_{ij}^{p} = \frac{1}{V} \sum_{p=1}^{N} \sum_{c=1}^{m} x_i^c F_j^c \tag{4.6}$$

For discs and spheres, $x_i^c = x_i^p + R_i^p n_i^c$ and since for equilibrium

$$\sum_{c=1}^{m} x_i^p F_j^c = x_i^p \sum_{c=1}^{m} F_j^c = 0$$

the average stress tensor of a macro-element can be expressed in terms of its radius and forces, normal and tangential acting on it, as follows:

$$\sigma_{ij} = \frac{1}{V} \sum_{p=1}^{N} R^{p} \sum_{c=1}^{m} n_i^c F_j^c \tag{4.7}$$

The important aspects in the formulation of DEM models are the representation of contacts, representation of solid material and the method of detecting and revising the set of contacts.

The very existence of contacts define the discontinuity of a system. There are two approaches in the mathematical formulation for representing contacts. In soft contact approach a finite normal stiffness is taken to exist at a contact while in the hard contact approach, interpenetration at the point of contact does not exist. In soft contact approach, what really happens is surface deformation, rather than interpenetration and the displacement is accounted for by elastic distortion around the circular flat area of contact. Hard contact approach assumes that no interpenetration of the two bodies that come into contact occurs but shear movement can occur. The collisions are assumed to be brief and to produce instantaneous exchanges of momentum.

Solid material may be modeled as rigid or deformable. In the cases where deformation is due to movements in discontinuities, particles may be assumed to be rigid. However, when the deformability of solid material cannot be neglected, it could be introduced either by dividing the body into internal and/or boundary elements and increasing the degrees of freedom or by superposition of several mode shapes (Cundall and Hart, 1989).

Before mechanical calculations are done, for the whole system of discrete bodies, pairs of bodies that can interact and the type of such interaction should be identified. This procedure has to be followed at each time step.

A discontinuous system can be modeled by DEM in two distinct ways, as a boundary value problem or as an element test. In a boundary value problem the system as a whole is modeled using a finite number of elements and the response to boundary value conditions are obtained. This method has limitations due to the difficulties arising from the large number of particles that has to be used in order to get more accurate responses. This is the main limitation to the 3–D simulations of boundary value problems.

In an element test, a representative element is studied to measure the constitutive behavior of a discrete assembly. In order to achieve more realistic responses, the boundary effects should be reduced to a minimum or eliminated altogether.

For this purpose, the representative element is confined within a periodic space, which allows the particles to 'flow' through the element boundaries. The boundaries confining the periodic space are imaginary planes so that when the periodic element is distorted and the particles within move and reorient themselves, void spaces between particles and the bounding faces will not be created. New particles will be generated to fill the void spaces created by particle movements even if the newly generated particle may not be completely inside the element. The particles may lie across the boundary surface.

The success of the DEM as a microscopic constitutive model and its ability to model boundary value problems has inspired many researchers to use it to predict soil behavior in laboratory experiments and field conditions under static, dynamic, drained and undrained loading conditions.

4.2 Microscopic Model TRUBAL

The microscopic numerical model TRUBAL based on the DEM is capable of describing the mechanical behavior of an assembly of dry granular spherical particles. It uses an explicit numerical scheme in which the interactions of the particles are monitored at points of contact and the particle motions are modeled for each particle. In the Distinct Element Method, the equilibrium contact forces and displacements of a stressed assembly of spheres are found through a series of calculations which track the movements of individual particles.

In this constitutive model, every particle is imagined to be embedded in a uniform strain field, applied independent of any developed stresses, in the manner of a strain-controlled test. This is achieved by distorting the particle space under a uniform strain rate. The model calculates the effect of the applied strain-rate tensor on an average particle. The applied global strain rate defines the motion of the granular assembly. The assembly is strained in the prescribed direction in time steps selected to be a fraction of the critical time step t_{cr}, which is equal to $2\sqrt{m/k}$ where m and k are mass and radius of gyration of the particles, respectively.

For a given time step, the applied strain increment causes displacements at the centers of each sphere. Due to the prescribed motion, two spheres may form a contact point. At contact points, spheres could undergo rotation and translation, giving rise to linear and angular displacements, velocities and accelerations. Due to the relative movement of particles in contact, forces are set up at each point of contact to produce local deformations at those points. These local deformations are smaller than the global deformation of the granular assembly. For any sphere the linear and angular accelerations are determined by the resultants of the forces and moments acting on that sphere.

The calculations alternate between the application of Newton's second law of motion (Subroutine Motion) for the spheres and the force-displacement law (Subroutine Ford) for the contacts. The complete equation of motion for every particle is integrated numerically, using an explicit central difference formula to obtain the velocities and accelerations for the next time step. The strain rate applied to the macro elements defines the velocity for the system. The local velocity is vectorially added to the global velocity to determine the resultant velocity of each particle. Although Newton's laws of motion are used in the computations, this is not a continuously dynamic system but rather a system in a quasi-static state since the granular assembly is loaded at a rate slow enough for inertial effects to be neglected. The formulations for the application of force displacement law and Newton's law of motion in the program TRUBAL are given in Appendix C.1.

For microscopic simulation of granular soils, TRUBAL generates particles within a periodic space, because the periodic space eliminates or reduces the boundary effects. Since the actual soil element is located within the soil mass, away from boundaries, periodic space gives a closer simulation of the actual soil element, leading to more accurate responses. The periodic space may consist of one or several periodic elements. When strains are applied to the assembly of spheres, the periodic space is distorted at a given rate. Depending on magnitude and direction of the applied strain rate the periodic space will either shrink or expand. When the periodic space shrinks the spheres are brought close to each other establishing contacts. These contacts give rise to contact forces and moments which in turn results in rotations and translations of the spheres.

TRUBAL can successfully simulate compaction of a granular assembly to a desired effective consolidation stress. This is achieved by applying an isotropic strain to bring the mean effective stress close to the required effective consolidation stress and then by using a servo controlled strain rate. A lower coefficient of friction under the same confining stress will yield a low compacted void-ratio. A high confining stress for the same void-ratio can be achieved by defining a higher coefficient of friction.

TRUBAL also permits simulation of conventional drained triaxial tests by using a servo mechanism to hold the lateral stresses unchanged during shearing.

The user manual for TRUBAL version 1.51 (Cundall, 1989) is given in Appendix C.2.

4.3 Viscous Effects of Soil

The surface roughness can hinder the movement of a sliding body subjected to applied boundary forces by developing frictional resistance to the motion. A body resting on a surface, subjected to an external force P will be ready to slide if:

$$P \geq F \tag{4.8}$$

where F is the frictional force developed. At limiting equilibrium, the frictional force is directly proportional to the normal force, N. Therefore the above equation could be expressed as:

$$P \geq \mu N \tag{4.9}$$

where μ is the coefficient of friction for the two surfaces. When a film of lubricant

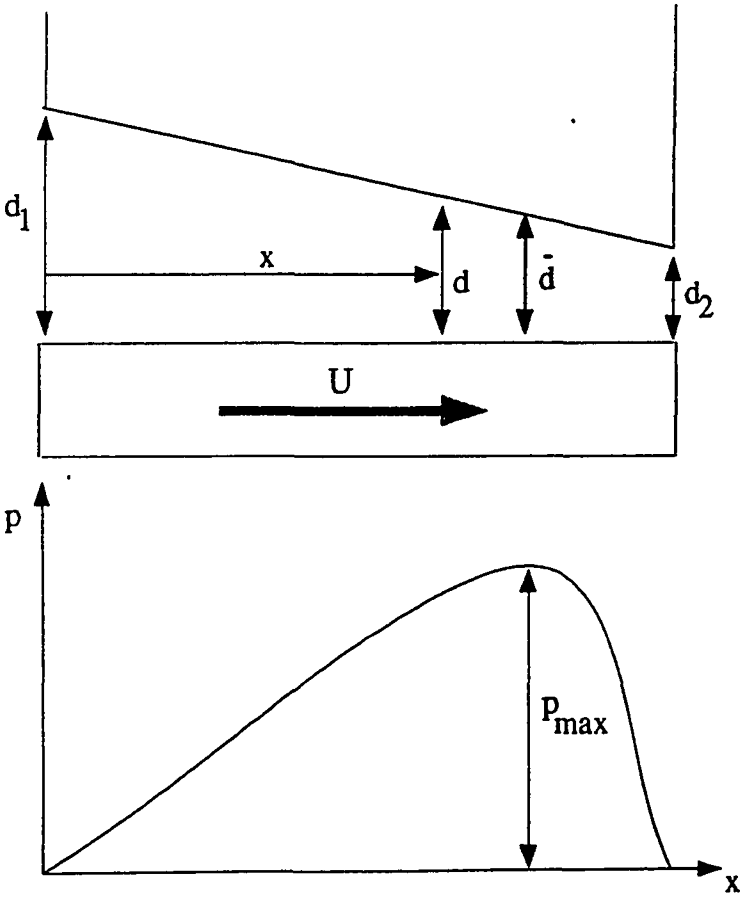

Figure 4.1 Pressure Generated at a Converging Fluid Wedge

is present between the two surfaces, it will carry a part of the normal force, causing a reduction in F and thereby allowing them to slide.

In situations where a lubricant is trapped within a convergent wedge, there is an increase in the 'local pore pressure' between the two surfaces. Figure 4.1 shows an oil wedge between two converging surfaces. The lower surface drags the oil film towards the converging gap. Since the space between the two surfaces reduces along the converging gap, the fluid is prevented from moving at the same velocity as the lower surface. This causes a pressure build up within the wedge, while the pressures at the two ends of the wedge are zero. With the increase in pressure within the wedge, the pressure gradients between the point of maximum pressure inside the gap and the edges of the wedge where the pressures are zero also increases. This pressure gradient accelerates the drainage, thereby reducing the pressure at the convergent end of the wedge (Cameron, 1976). Reynolds equation can be used to represent the pressure build up within the wedges.

Soil being a frictional material, the same concept can be used to explain the behavior of a soil with a pore fluid. Granular soil friction is derived at the particle contacts and the soil stress-strain behavior is determined from these grain contacts. During mechanical deformation, soil grains in contact will have linear and angular velocities. Due to these velocities, and the pore fluid (according to Reynolds equation) localized fluid pressures will be generated at the points of contact. Since these pressures are localized, they cannot be measured at the macroscopic level using pore pressure transducers. The localized pore pressures will reduce the intergranular stresses at the points of contact.

4.4 Quantification of Viscous Effects of Soil

Although fluid lubricants have been used for many centuries, the theory involved in hydro dynamic lubrication was not formulated until late in the 19th century when Reynolds published his treatise on the subject. Reynolds demonstrated that it is possible for a fluid to keep two solid surfaces separated and that when this

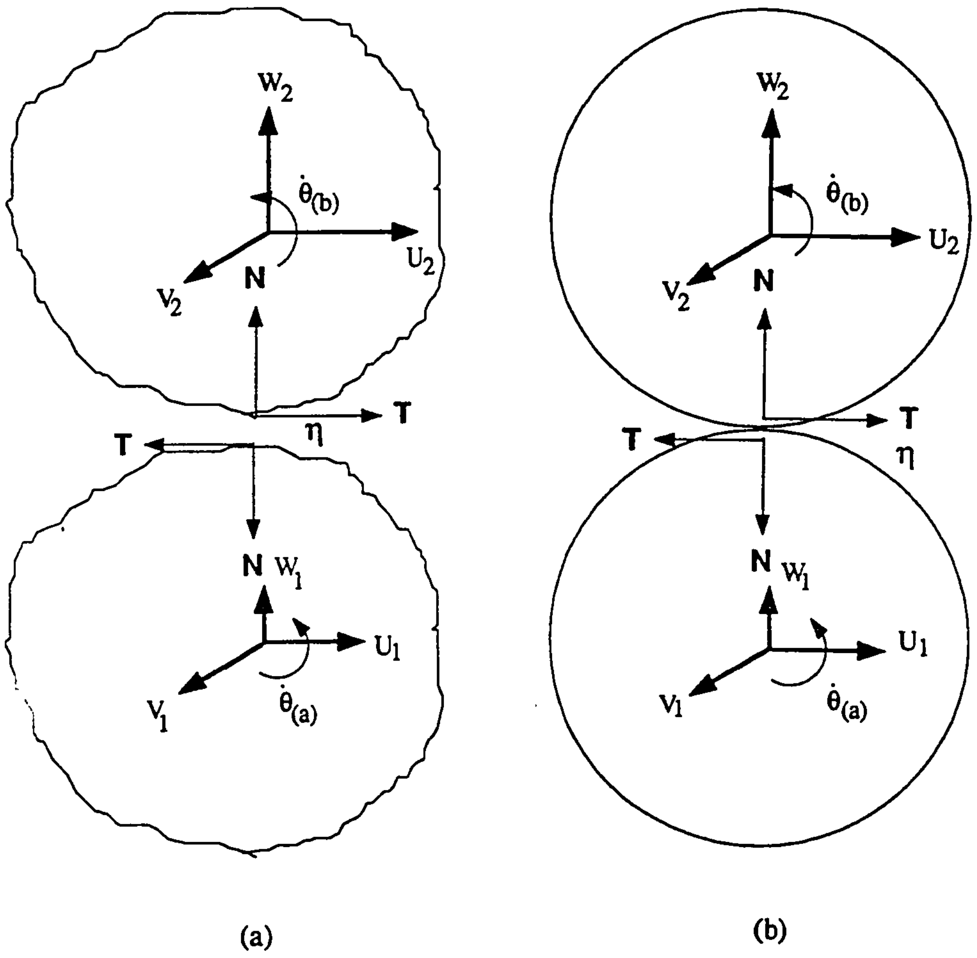

Figure 4.2 (a) Contact Forces and Velocities of Two Particles in Contact
(a) Actual Grains of Soil, (b) Idealized by Spheres

phenomenon occurs the frictional resistance developed between the surfaces is dependent on the viscosity of the fluid.

The presence of a lubricant between two spheres could be mathematically modeled using Reynolds equation for hydrodynamic lubrication:

$$\frac{\partial}{\partial x}\left(\frac{h^3}{\eta}\frac{\partial p}{\partial x}\right) + \frac{\partial}{\partial x}\left(\frac{h^3}{\eta}\frac{\partial p}{\partial y}\right) = 6\left\{\frac{\partial}{\partial x}(u_1 + u_2)h + \frac{\partial}{\partial y}(v_1 + v_2)h + 2(w_2 - w_1)\right\} \tag{4.10}$$

The derivation of this equation is given in Appendix C.3. Figure 4.2(a) shows two soil grains lubricated at the point of contact. When a load is applied to the soil, soil grains will undergo rotations and translations. The microscopic phenomena associated with lubrication can be modeled using two spheres with linear and angular motion as shown in figure 4.2(b).

Consider two spheres of radii R_1 and R_2, separated by a thin film of fluid as shown in Figure 4.3. Points A and B lie on the surfaces of the spheres 1 and 2 respectively, on a line parallel to the z axis. Equation (4.10) can be used to represent the pressure along line AB.

If the coordinates of the two points are given as:

$$A = \left(x, y, -\frac{x^2 + y^2}{2R_1}\right)$$

$$B = \left(x, y, h_o + \frac{x^2 + y^2}{2R_2}\right)$$

The linear velocities at A and B can be expressed as:

$$v_A = v_O + \dot{\theta}_O x O\vec{A} \tag{4.11}$$

$$v_B = v_{O'} + \dot{\theta}_{O'} x O\vec{B} \tag{4.12}$$

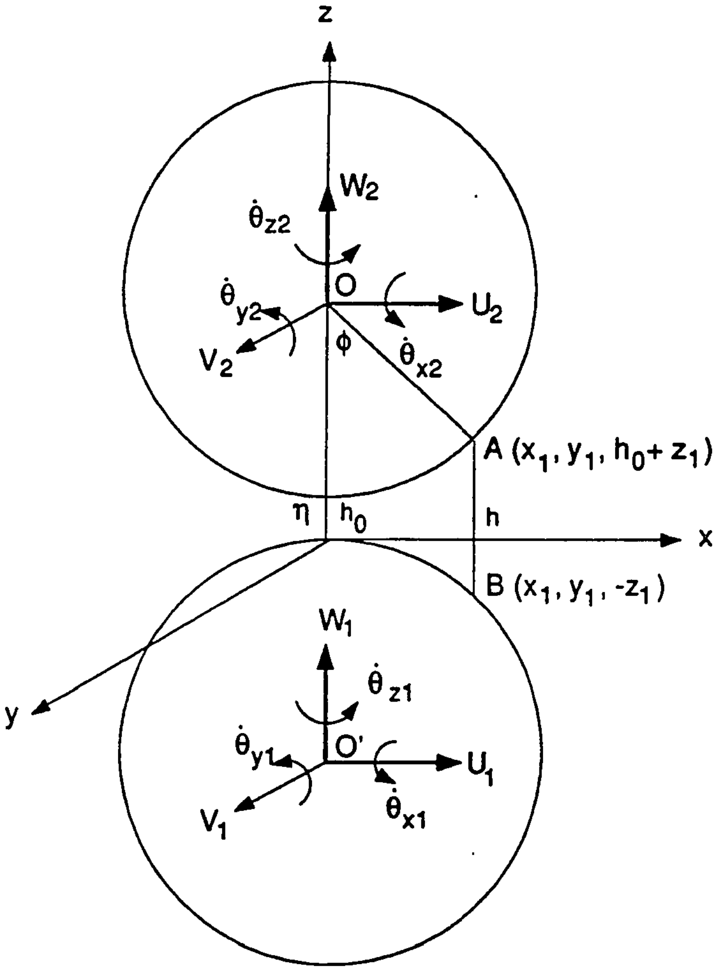

Figure 4.3 Dynamics of Two Spheres in Space, Separated by a Thin Film of Lubricant

where V_O and $\dot{\theta}_O$ are the linear and angular velocities at the center of the sphere 1 and V'_O and $\dot{\theta}_O'$ correspond to the same for sphere 2. $\vec{OA}$ and $\vec{OB}$ are the position vectors given by:

$$\vec{OA} = x\hat{t} + y\hat{s} + \left(R_1 - \frac{x^2 + y^2}{2R_1}\right)\hat{e} \tag{4.13}$$

$$\vec{OB} = x\hat{t} + y\hat{s} + \left(-R_2 + \frac{x^2 + y^2}{2R_2}\right)\hat{e} \tag{4.14}$$

Combining equations (4.11) through (4.14), the velocities at points A and B, can be expressed as:

$$v_A = U_1\hat{t} + V_1\hat{s} + W_1\hat{e} + \left(\dot{\theta}_{x1}\hat{t} + \dot{\theta}_{y1}\hat{s} + \dot{\theta}_{z1}\hat{e}\right)x\left[x\hat{t} + y\hat{s} + \left(R_1 - \frac{x^2 + y^2}{2R_1}\right)\hat{e}\right] \tag{4.15}$$

$$v_B = U_2\hat{t} + V_2\hat{s} + W_2\hat{e} + \left(\dot{\theta}_{x2}\hat{t} + \dot{\theta}_{y2}\hat{s} + \dot{\theta}_{z2}\hat{e}\right)x\left[x\hat{t} + y\hat{s} + \left(-R_2 + \frac{x^2 + y^2}{2R_2}\right)\hat{e}\right] \tag{4.16}$$

With further simplifications v_A and v_B can be expressed as:

$$v_A = u_1\hat{t} + v_1\hat{s} + w_1\hat{e} \tag{4.17}$$

$$v_B = u_2\hat{t} + v_2\hat{s} + w_2\hat{e} \tag{4.18}$$

where u_1, v_1, w_1 and u_2, v_2, w_2 are the coefficients of the unit vectors representing the local velocities in x, y, z directions, at points A and B respectively.

Thus

$$u_1 = U_1 + \dot{\theta}_{y1}\left[R_1 - \frac{x^2 + y^2}{2R_1}\right] - \dot{\theta}_{z1}y$$

$$v_1 = V_1 - \dot{\theta}_{x1}\left[R_1 - \frac{x^2 + y^2}{2R_1}\right] - \dot{\theta}_{z1}x$$

$$w_1 = W_1 + y\dot{\theta}_{x1} - x\dot{\theta}_{y1}$$

and

$$u_2 = U_2 + \dot{\theta}_{y2}\left[-R_2 + \frac{x^2 + y^2}{2R_2}\right] - \dot{\theta}_{z2}y$$

$$v_2 = V_2 - \dot{\theta}_{x2}\left[-R_2 + \frac{x^2 + y^2}{2R_2}\right] + \dot{\theta}_{z2}x$$

$$w_2 = W_2 + y\dot{\theta}_{x2} - x\dot{\theta}_{y2}$$

Introducing the velocities, each term in the Reynolds equation can be further simplified and generalized.

The actual inter-sphere spacing AB can be expressed as:

$$h = h_o + R_1(1 - \cos\varphi_1) + R_2(1 - \cos\varphi_2)$$

since

$$\sin\varphi_1 = \frac{\sqrt{x^2 + y^2}}{R_1}$$

$$\sin\varphi_2 = \frac{\sqrt{x^2 + y^2}}{R_2}$$

and for small angles of φ approximating $\cos\varphi = 1 - \varphi^2/2$, the distance AB can be approximated to

$$h = h_o + \frac{(x^2 + y^2)}{2}\left[\frac{1}{R_1} + \frac{1}{R_2}\right] \tag{4.19}$$

This approximation is commonly applied in partial differential equations in the field of hydro-dynamic lubrication (Cameron, 1976).

In this analysis, lubrication is considered to be effective only within a limited radius of $r_0/2$ where r_0 is defined as the average radius of the particles such that:

$$\frac{1}{r_o} = \frac{1}{R_1} + \frac{1}{R_2} \tag{4.20}$$

This limitation is reasonable enough since the lubricating effect diminishes along the radial distance from the point of contact and beyond $r_0/2$ reduces to minute values which do not have a significant contribution to the resultant, and also because the equation defining the lubricating surface (equation (4.19)) is only an approximation which defines the surface within 5% error limit only up to a radius of $r_0/2$.

The lubrication between two particles is taken to be effective only when the distance between their surfaces h_0 is less than 1.0 unit. The minimum distance between any two particles coming in contact is taken to be 0.1 units. There exist three distinct cases of lubrication between two spheres. (a) when the distance between the surfaces (measured along the center line) h_0 is within the upper limit 1.0 unit and lower limit of 0.1 units, lubrication between two spherical surfaces are considered. (b) when the particles come in close contact, due to the elastic nature of the particle surfaces, the surfaces in contact could be flattened, giving a plane circular area of contact. When the area of contact is of a radius less than $r_0/2$, the total lubricating surface will consist of a plane circular surface at the center and a spherical surface circumscribed by the radius $r_0/2$ at the outer edge, (c) when the area of contact is of a radius greater than $r_0/2$, the total lubricating surface will consist only of a plane surface circumscribed by radius $r_0/2$.

The terms on the LHS of equation (4.10) can be expressed as:

$$\frac{\partial}{\partial x}\left(\frac{h^3}{\eta}\frac{\partial p}{\partial x}\right) = \frac{h^3}{\eta}\frac{\partial^2 p}{\partial x^2} + \frac{3h^2 x}{\eta r_o}\frac{\partial p}{\partial x}$$

$$\frac{\partial}{\partial y}\left(\frac{h^3}{\eta}\frac{\partial p}{\partial y}\right) = \frac{h^3}{\eta}\frac{\partial^2 p}{\partial y^2} + \frac{3h^2 y}{\eta r_o}\frac{\partial p}{\partial y}$$

Substituting for the velocities u_1, v_1, w_1 and u_2, v_2, w_2 the terms on the RHS of equation (4.8) can be given by:

$$\frac{\partial}{\partial x}(u_1 + u_2)h = (u_1 + u_2)\frac{x}{r_o} + hx\left(\dot{\theta}_{y2}/R_2 - \dot{\theta}_{y1}/R_1\right)$$

$$\frac{\partial}{\partial x}(v_1 + v_2)h = (v_1 + v_2)\frac{y}{r_o} + hy\left(\dot{\theta}_{x1}/R_1 - \dot{\theta}_{x2}/R_2\right)$$

$$(w_2 + w_1) = (W_2 - W_1) + y\left(\dot{\theta}_{x2} - \dot{\theta}_{x1}\right) + x\left(-\dot{\theta}_{2y} + \dot{\theta}_{y1}\right)$$

Thus the Reynolds equation can be expressed as:

$$\frac{1}{\eta}\left[h^3\frac{\partial^2 p}{\partial x^2} + h^3\frac{\partial^2 p}{\partial y^2} + \frac{3h^2 x}{r_o}\frac{\partial p}{\partial x} + \frac{3h^2 y}{r_o}\frac{\partial p}{\partial y}\right] = 6hx\left(-\frac{\dot{\theta}_{y1}}{R_1} + \frac{\dot{\theta}_{y2}}{R_2}\right) + 6hy\left(-\frac{\dot{\theta}_{x1}}{R_1} + \frac{\dot{\theta}_{x2}}{R_2}\right) + 6\left\{(u_1 + u_2)\frac{x}{r_o} + (v_1 + v_2)\frac{y}{r_o} + 2(w_2 - w_1)\right\} \tag{4.21}$$

The above equation could be expressed in the form:

$$a_1\frac{\partial^2 p}{\partial x^2} + a_1\frac{\partial^2 p}{\partial y^2} + a_2\frac{\partial p}{\partial x} + a_3\frac{\partial p}{\partial y} + a_4 = 0 \tag{4.22}$$

where a_1, a_2, a_3 and a_4 are the coefficients of the partial differential equation. Thus for the case of two spheres in a viscous media separated by a thin film of fluid, the Reynolds equation can be written in terms of linear and angular velocities at the centers of the two spheres in x, y, z directions.

The pressures given by equation (4.10) could be positive or negative. The normal fluids cannot stand large and continuous negative pressures without cavitation. The sub-zero pressures predicted from equation (4.10) would inevitably cause the fluid to vaporize and become discontinuous. Thus in such cases, the equation (4.10) will not explain the actual physical phenomenon. Therefore, the negative pressures when exists are neglected and the pressure in that area is taken to be zero. The resulting pressure distribution pattern is also known as the half Sommerfeld condition (Cameron, 1976).

4.5 Modification of TRUBAL to Include Viscous Effects

4.5.1 Direct Computation Approach

The microscopic model TRUBAL has been developed to model dry granular soils, neglecting the presence of pore fluid. Therefore it does not model mineral to pore fluid to mineral contacts, but mineral to mineral contacts only. In order to study the behavior of soil matrix in the presence of pore fluids of different viscosities, this model was modified to include the mineral to pore fluid contacts. As discussed in Article 4.3, the presence of a pore fluid alters the existing contact forces. Additional forces are introduced at the contact points as a result of the pressure generated due to lubricating effect of pore fluid. Two method of introducing these forces to the original model TRUBAL are presented here.

The Reynolds equation, in the form of

$$a_1 \frac{\partial^2 p}{\partial x^2} + a_1 \frac{\partial^2 p}{\partial y^2} + a_2 \frac{\partial p}{\partial x} + a_3 \frac{\partial p}{\partial y} + a_4 = 0$$

expressed in terms of linear and angular velocities at the centers of the spheres, in x, y, z directions is used in program TRUBAL.

Subroutine FORD of TRUBAL formulates the force displacement relations for the spheres and it also has access to the linear and angular velocities and displacements at the centers of spheres, calculated by the program.

Therefore, using these velocities, as input data for the Reynolds equation, a modification is introduced to subroutine FORD to include viscous effects. These velocities are given in global co-ordinate system and must be converted to local coordinates before they are used as input data. Where, $\hat{t}$, $\hat{s}$, and $\hat{c}$ are the local co-ordinate directions and $\hat{i}$, $\hat{j}$, and $\hat{k}$ are the global coordinate directions, the conversion can be given as:

$$\hat{t} = t_1\hat{i} + t_2\hat{j} + t_3\hat{k}$$

$$\hat{s} = s_1\hat{i} + s_2\hat{j} + s_3\hat{k}$$

$$\hat{c} = c_1\hat{i} + c_2\hat{j} + c_3\hat{k}$$

For a quantitative analysis of the shear strength under different pore fluids, the local pore pressure should be included in each contact for each sphere and for each time step. With the incorporation of the above pore pressures, the program TRUBAL should be run until failure to obtain the shear strength of the granular medium. This can be done by (a) incorporating the finite difference formulation in TRUBAL which would compute the forces due to local pore pressures or (b) by constructing a data base which TRUBAL could access and read the force generated due to local pressures corresponding to the relative positions and motions of the two spheres at the point of contact.

The pressure distribution under the projected area of a particle is calculated by means of a finite difference method developed for curved boundary value problems (Carnahan and Luther, 1969). This requires the projected area to be enclosed in a square grid so that the partial differential equation governing the pressure within the projected area, can be discretized and solved to find the pressures acting at each node of the grid.

In order to select an optimum grid size, four different grid sizes; 10 x 10, 20 x 20, 40 x 40 and 60 x 60 were tried. The 10 x 10 grid size can give a solution with 5% error and with a 20 x 20 grid, this is found to reduce to a 1% with a maximum of 150 iterations. With the 40 x 40 grid, although the amount of data that is handled increases there was no marked decrease in the percentage error and with 60 x 60 grid the percentage error seemed to increase. Therefore, a 20 x 20 grid size was selected as optimum for the calculation.

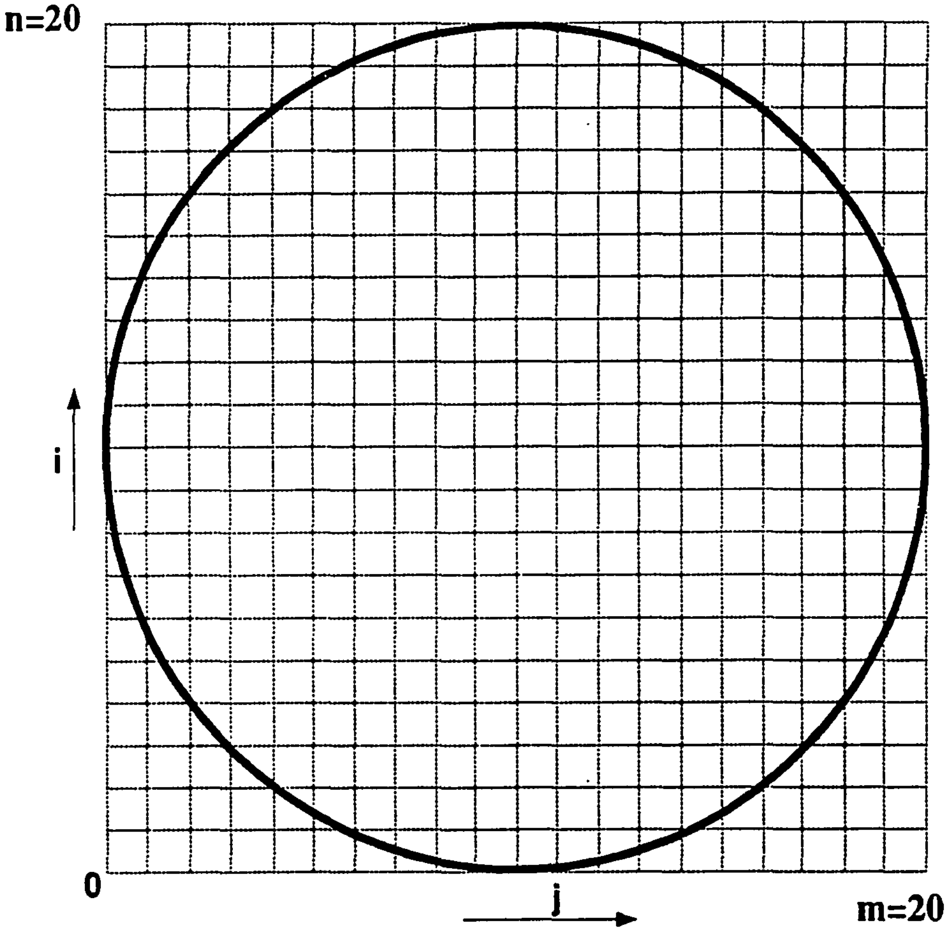

Figure 4.4 The Projected Area Enclosed within the Grid used for Finite Difference Formulation.

The projected area, circular in shape, is enclosed within a 20 x 20 grid (Figure 4.4). Each node of the grid is identified as either an interior point, an exterior point or a boundary point, depending on its location inside, outside or on the boundary of the circle. Beyond and on the circular boundary, the pressure generated due to lubrication is considered to be zero. Pressures developed at interior points are governed by equation (4.22).

Figure 4.5(a) shows a typical node point E surrounded by 4 other node points A, B, C and D. If point E is a point surrounded by 4 other interior points, the arms extending from E (p, q, r, and s) will be of equal length. However, a point close to the boundary will have unequal arms (r and s) close to the circular boundary. Figure 4.5(b) shows the different configurations possible for a boundary point or a point close to the boundary.

The partial differential equation (4.22) could be discretized as:

$$\frac{\partial^2 p}{\partial x^2} = \frac{2}{\Delta x^2}\left[\frac{p(i.j+1)}{q(s+q)} - \frac{p(i.j)}{sq} + \frac{p(i.j-1)}{s(s+q)}\right]$$

$$\frac{\partial^2 p}{\partial y^2} = \frac{2}{\Delta x^2}\left[\frac{p(i+1.j)}{p(p+r)} - \frac{p(i.j)}{pr} + \frac{p(i-1.j)}{r(p+r)}\right]$$

$$\frac{\partial p}{\partial x} = \frac{p(i.j+1) - p(i.j-1)}{\Delta x(s+q)}$$

$$\frac{\partial p}{\partial y} = \frac{p(i+1.j) - p(i-1.j)}{\Delta x(p+r)}$$

to yield:

$$\frac{2a_1}{\Delta x^2}\left[\frac{p(i.j+1)}{q(s+q)} - \frac{p(i.j)}{sq} + \frac{p(i.j-1)}{s(s+q)}\right] + \frac{2a_1}{\Delta x^2}\left[\frac{p(i+1.j)}{p(p+r)} - \frac{p(i.j)}{pr} + \frac{p(i-1.j)}{r(p+r)}\right] + \frac{a_2}{\Delta x}\frac{p(i.j+1) - p(i.j-1)}{(s+q)} + \frac{a_3}{\Delta x}\frac{p(i+1.j) - p(i-1.j)}{(p+r)} + a_4 = 0 \qquad (4.23)$$

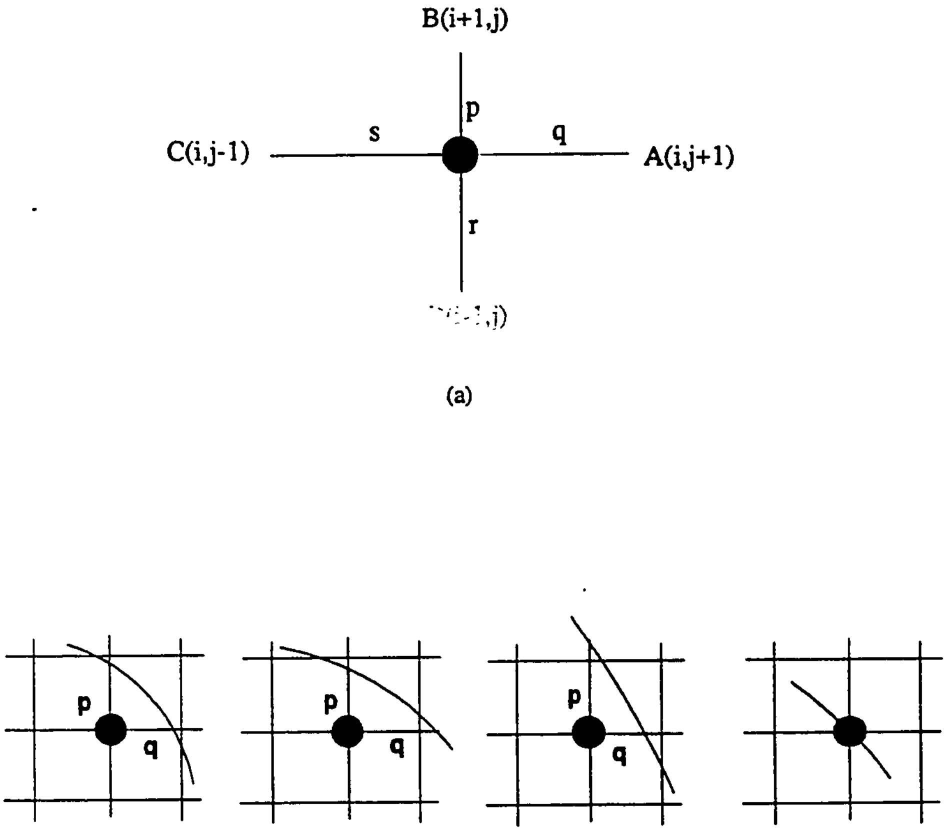

(a)

(b)

Figure 4.5 (a) General Configuration of an Interior Node (b) Four Possible Configurations for Corner Node.

The above equation can be re-written as follows, to give the pressure at any node point (i,j) in terms of the pressures at surrounding node points.

$$p(i,j) = a[p(i,j+1)] + b[p(i+1,j)] + c[p(i,j-1)] + d[p(i-1,j)] + e \tag{4.23}$$

where

$$a = \frac{sqpr}{pr+sq}\frac{\Delta x}{2a_1}\frac{1}{s+q}\left[\frac{2a_1}{q\Delta x} + a_2\right]$$

$$b = \frac{sqpr}{pr+sq}\frac{\Delta x}{2a_1}\frac{1}{p+r}\left[\frac{2a_1}{s\Delta x} + a_3\right]$$

$$c = \frac{sqpr}{pr+sq}\frac{\Delta x}{2a_1}\frac{1}{s+q}\left[\frac{2a_1}{s\Delta x} - a_2\right]$$

$$d = \frac{sqpr}{pr+sq}\frac{\Delta x}{2a_1}\frac{1}{p+r}\left[\frac{2a_1}{r\Delta x} - a_3\right]$$

$$e = \frac{sqpr}{pr+sq}\frac{\Delta x}{2a_1}\frac{1}{s+q}a_4$$

To solve equation (4.24), for each point (i,j), the Fortran source code LUB (Appendix C.4) adopts Gause-Siedel iteration. The iteration is carried out until the values for two consecutive iterations are within the tolerable error of 0.01 pressure units.

Validity of this method involving finite difference solutions was checked by analysing a simple one directional problem and comparing the results with those from the closed form solution for one directional Reynolds equation given as:

$$\frac{\partial}{\partial x}\left(\frac{h^3}{\eta}\frac{\partial p}{\partial x}\right) + \frac{\partial}{\partial x}\left(\frac{h^3}{\eta}\frac{\partial p}{\partial y}\right) = 6U\frac{\partial h}{\partial x} \tag{4.25}$$

For a sphere of radius R coming in to contact with a plane surface, separated by a distance h_o measured along the centre line drawn perpendicular to the plane surface, the pressure generated at any distance x from the center line along the plane surface, can be expressed as:

$$p = -2U\eta\frac{x}{h^2} \tag{4.26}$$

where η is the coefficient of viscosity, U is the linear relative velocity and h is the distance between the surfaces at any distance (x,y) (Cameron, 1976). Since the inter surface height h is given as $h = h_o + (x^2 + y^2)/2R$, at a distance x=R, the pressure p will not be zero.

In the finite difference method of solution however the pressure along the circular boundary is taken to be zero. Since this is not the boundary condition used in the closed form solution, the resulting pressure distribution from the finite difference method would not comparable with the closed form solution. Therefore the pressure at a distance x=R was found using the close form solution and used as a boundary condition for the finite difference method of solution to obtain the pressure distribution within the projected area. The results thus obtained were consistent with the results of the closed form solution.

Advantages of the an iterative method are: (a) computational problems related to matrix operations do not occur and (b) low computer memory requirements. However, the iterative procedure uses a higher CPU time making it virtually impossible to be run on a slower computer.

4.5.2 Incorporation of Mathematical Formulation Through a Database

When the numerical model is modified to include the viscous effects of the pore fluid, the reduction in normal contact force at contact points of particles, is found through a lengthy process of iteration and included in the program. This iteration is time consuming. Considering the number of iterations that has to be carried out to include all contact points, for all particles, for each cycle, this would take a higher CPU time. To avoid this, all the information sought from iterations are included in a data base and made available for the computations. Force generated due to lubricating effects of pore fluid at each contact point, described by relative velocity of particles coming in contact, inter particle spacing and viscosity of the pore fluid can be directly read off from a table.

This data base is presented as a four dimensional array consisting of four array variables, namely inter-particle height, h_o, linear relative velocity, w_r, and two relative angular velocities $\dot{\theta}_{xr}$ and $\dot{\theta}_{yr}$. Each element of the array described by the four variables represents the normal force due to the lubrication generated at that point of contact.

For any two particles coming into contact, the inter particle height is the distance between the two surfaces, measured along the line connecting the centers of the particles. When particles are idealized as spheres, inter-particle height is computed by subtracting two radii from the distance between the centers of the spheres. Therefore, when particles overlap at a point of contact, the inter-particle height takes a negative value. The linear relative velocity considered here is that in the direction of the line connecting the centers of the two spheres. The angular velocities are those in directions orthogonal to the line connecting the centers of the spheres.

Array elements are computed for all combinations of the four variables, for their normally expected domains. The inter particle height is expected to range between +0.25 to -1.0 units while linear relative velocity is expected to range from -0.05 to +0.03 units. The expected ranges for the two angular velocities lie between 0.0 to 0.02 units. Each of these ranges are divided into 11,16, 11 and 11 divisions respectively, giving a total of 21296 combinations.

Array elements are computed for each of these combinations and made available to the main program, so that the forces corresponding to the conditions described by the variables can be directly read off or interpolated.

In most cases when a direct reading is not possible, an interpolation is necessary. The process adopted for interpolation for this four dimensional array can be illustrated as follows:

If the variables describing the force F, are h_o, w_r, $\dot{\theta}_{xr}$ and $\dot{\theta}_{yr}$, find

h_a and h_b such that $h_a<h_o<h_b$

w_a and w_b such that $w_a<w_r<w_b$

$\dot{\theta}_{xa}$ and $\dot{\theta}_{xb}$ such that $\dot{\theta}_{xa} < \dot{\theta}_{xr} < \dot{\theta}_{xb}$

$\dot{\theta}_{ya}$ and $\dot{\theta}_{yb}$ such that $\dot{\theta}_{ya} < \dot{\theta}_{yr} < \dot{\theta}_{yb}$

These values give the lower and upper limits of the intervals containing the given values of variables h_o, w_r, $\dot{\theta}_{xr}$ and $\dot{\theta}_{yr}$. Select those closest to the given values to be h_1, w_1, $\dot{\theta}_{x1}$ and $\dot{\theta}_{y1}$ and the others to be h_2, w_2, $\dot{\theta}_{x2}$ and $\dot{\theta}_{y2}$. For an instant, if h_o is closer to h_a than to h_b then

$$h_1=h_a$$

$$h_2=h_b$$

If w_r is closer to w_b than to w_a then

$$w_1=w_b$$

$$w_2=w_a$$

Let F_1 be the force corresponding to the variables h_1, w_1, $\dot{\theta}_{x1}$ and $\dot{\theta}_{y1}$; let F_2 be the force corresponding to the variables h_2, w_2, $\dot{\theta}_{x2}$ and $\dot{\theta}_{y2}$; then

$$F = F_1 + \left[\frac{\partial F}{\partial h}(h_o - h_1) + \frac{\partial F}{\partial w}(w_r - w_1) + \frac{\partial F}{\partial \dot{\theta}_x}\left(\dot{\theta}_{xr} - \dot{\theta}_{x1}\right) + \frac{\partial F}{\partial \dot{\theta}_y}\left(\dot{\theta}_{yr} - \dot{\theta}_{y1}\right)\right] \tag{4.27}$$

where the corresponding partial derivatives are given as:

$$\frac{\partial F}{\partial h} = \frac{F\left(h_2.w_1.\dot{\theta}_{x1}.\dot{\theta}_{y1}\right) - F\left(h_1.w_1.\dot{\theta}_{x1}.\dot{\theta}_{y1}\right)}{h_2 - h_1}$$

$$\frac{\partial F}{\partial w} = \frac{F\left(h_1.w_2.\dot{\theta}_{x1}.\dot{\theta}_{y1}\right) - F\left(h_1.w_1.\dot{\theta}_{x1}.\dot{\theta}_{y1}\right)}{w_2 - w_1}$$

$$\frac{\partial F}{\partial \dot{\theta}_x} = \frac{F\left(h_1, w_1, \dot{\theta}_{x2}, \dot{\theta}_{y1}\right) - F\left(h_1, w_1, \dot{\theta}_{x1}, \dot{\theta}_{y1}\right)}{\dot{\theta}_{x2} - \dot{\theta}_{x1}}$$

$$\frac{\partial F}{\partial \dot{\theta}_y} = \frac{F\left(h_1, w_1, \dot{\theta}_{x1}, \dot{\theta}_{y2}\right) - F\left(h_1, w_1, \dot{\theta}_{x1}, \dot{\theta}_{y1}\right)}{\dot{\theta}_{y2} - \dot{\theta}_{y1}}$$

Solving equation (4.27), the force described by the variables h, w_r, $\dot{\theta}_{xr}$ and $\dot{\theta}_{yr}$ can be found. This however, is a method of approximation and the force calculated is only a fairly good estimate. More accuracy can be achieved if the intervals are made smaller, but this has limitations since it would result in a large array of data.

This database has been constructed for particles of radius 10 units and unit pore fluid viscosity. For other combinations a modification is introduced as follows:

$$F' = F\eta\left[2.60041\frac{(r_a + r_b)}{20} - 1.60041\right] \tag{4.28}$$

where η is the pore fluid viscosity, and r_a and r_b are the radii of the particles coming into contact.

Due to the limitations imposed by computer memory in storing and handling large numbers of data that would be generated by arrays of higher orders, only the variables that show substantial effects on the pressure development were selected, following an initial investigation. The parameters that did not show significant contributions to the pressure generation such as U_r, V_r and $\dot{\theta}_{zr}$ were neglected. Those parameters that showed direct linear relationships such as the coefficient of viscosity, η were incorporated in the calculation. Since the linear and angular velocities in x or y directions impose similar conditions, those in only one of the directions were considered for this study while the angular velocity in z direction was not considered at all as its motion does not create a confining fluid wedge between the surfaces, and therefore would not affect the pressure distribution in the projected area.

Relative velocities were used in lieu of absolute velocities of the particles, to avoid higher order arrays. Computer simulations show that for both linear and angular velocities, irrespective of the way they are represented, with absolute values or relative values, the resulting pressure distribution in the projected area is the same. However, this does not hold true when the two particles coming in to contact have linear velocities of same magnitude in x and y directions. The relative velocity for such a case would be zero suggesting that no pressure is generated. But if the absolute velocities are used, the Reynolds equation (equation 4.21) will show a pressure distribution. The latter is true if this is a global phenomenon, but for drained test conditions, where there is no influence from the surrounding fluid, pressure build up due to lubrication is purely a local phenomenon which depends on the relative velocity of the particles.

Although using larger arrays, the accuracy of the database method can be increased to some extent, at its best it is still an approximation to the iterative method of solution. Accuracy of this method can best be verified by comparing the results of a complete drained triaxial test simulated using the two methods. However, the amount of computer time required to run such a test to get an acceptably good response in the iterative method, makes it practically impossible. For a 300 sphere assembly, at the rate of 5 seconds per iteration for an average of 800 contacts per sample and at 250 cycles for each of the 100 data points on the stress strain curve, this would require nearly 1157 days of VAX8800 computer time. Therefore the forces calculated by the two methods were compared at arbitrarily selected points on the stress path. At selected points on the stress-strain curve, the inter-particle spacing and the velocities of the particles at these point were used in the two methods to calculate the forces due to lubrication. When compared, the lubrication pressures computed using the database method was found to deviate only 11% from those of the iterative method.

The forces observed at a contact point cannot however be used as a measure to compare the complete responses of the two methods, since the cumulative effect

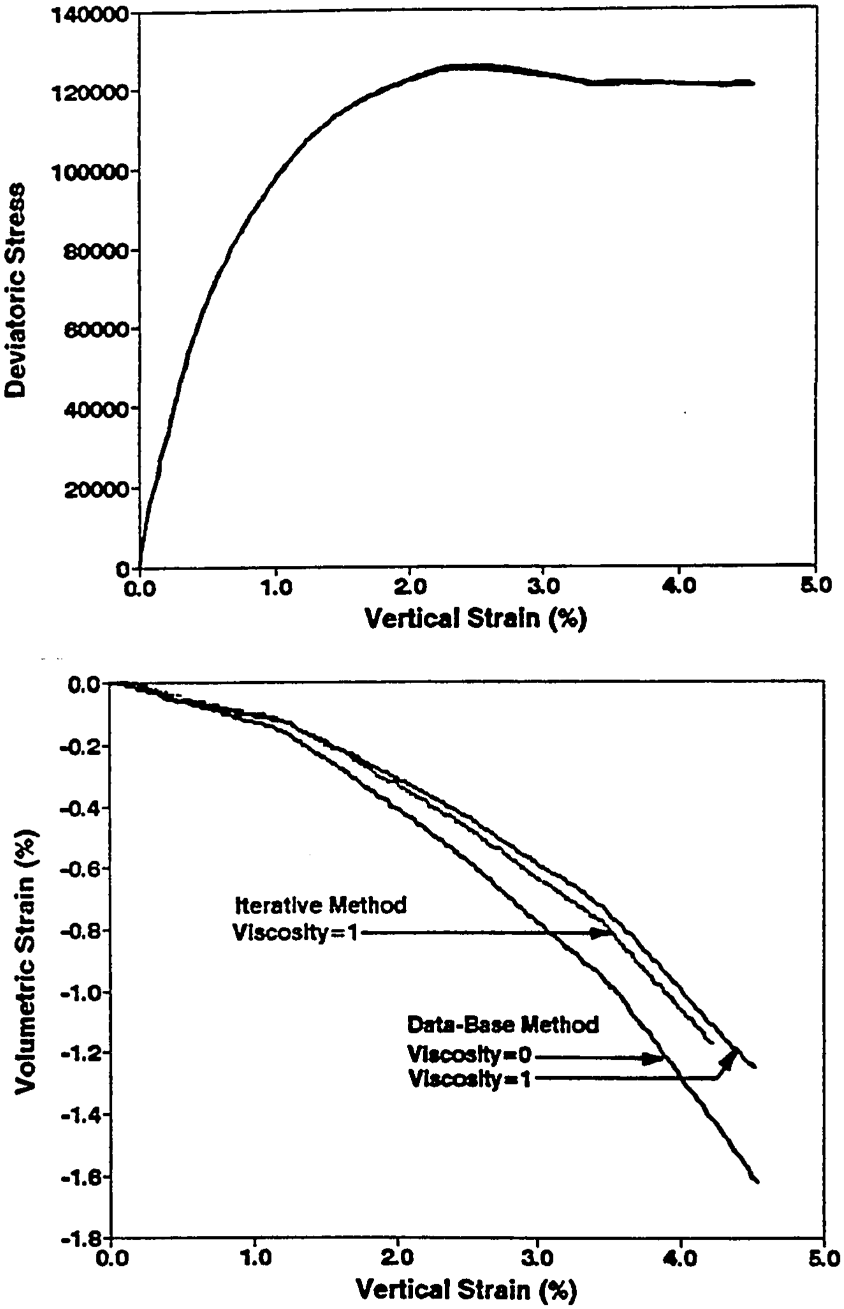

Figure 4.6 Comparison of the Response Obtained Using the Data-Base Method and the Iterative Method

may lead to different stress-strain responses. Therefore in an effort to compare the stress-strain behavior generated by the two methods, simulations were carried out using a single sized, 20 particle assembly. Since a drained triaxial test could not be successfully simulated using a 20 sphere assembly, simulations were carried out for a constant pressure test. The results of these simulations are given in Figure 4.6. The responses obtained from the iterative method and the database method for the sample with viscosity 1 Trubal Unit, were compared and found to be very close. A slight deviation was observed in the curves showing the variation of volumetric strain with vertical strain, but within a maximum of 10% of the results of the iterative method.

CHAPTER 5

MICROSCOPIC SIMULATIONS

5.1 General

Microscopic models based on DEM have been used by researchers to model natural soils other than granular assemblies of spheres and found to be considerably successful in predicting stress-strain behavior of soil subjected to both steady and cyclic loading conditions, but for small strains. Attempts to model large strain tests have met with limited success. At small strains, the movements of the particles are predominantly governed by the force-displacement laws, and using non-linear force-displacement laws for soils, the particle movements at micro level and therefore the response at macro level can be predicted with considerable success. At larger strains however predictions based on force-displacement laws cannot be successful since movements of particles are dominated by slippage at points of contact. Especially for large strain tests, selection of spheres to model irregular shaped soil grains become a major shortcoming since it overlooks the natural mechanisms such as particle interlocking associated with such irregular shaped grains.

Therefore, the large strain test simulations that have been carried out so far can be used only in a qualitative sense. Although quantitative simulations for small strain tests have been carried out successfully for granular assemblies such as glass beads, the simulations for large strain tests for soils have not been as successful in quantitative representations. Nevertheless researchers in the field of geotechnical engineering have attempted large strain test simulations of soils, even in qualitative studies, since for studies in this field, the complete behavior patterns of soil until failure is more important than response for small strains. The comparison of a microscopic model and a macroscopic model under different stress paths (Ratnaweera and Meegoda, 1991a) indicated the possibility of the use of such a model in a qualitative study.

5.2 Method of Simulation

The term 'microscopic simulation' as used in this section can be interpreted as numerical simulations of conventional triaxial tests using computers. The 3-D computer model TRUBAL, modified to include the viscous effects of pore fluid was used for the simulation.

Irrespective of the method used to introduce the forces generated due to the lubricating effect of pore fluid, as discussed in Article 4.4, the same procedure was adopted to simulate the triaxial tests. Similar to the conventional triaxial test procedure, samples were generated, consolidated to desired pressures and tested subjected to vertical and lateral stresses.

A computer simulation is described by three factors; the model variables, the soil parameters and the stress state. The model variables include the size and numbers of particles used. In this study only two particle sizes were used. The soil parameters comprise of normal stiffness, shear stiffness and coefficient of friction. The stress state is expressed by initial stress or porosity.

5.2.1 Sample Generation

Initially the required number of spheres are generated randomly, without overlapping, and held in a loose array within a large volumetric space. The stiffness coefficients for the spheres in the normal and tangential directions, k_n and k_s, described in the test parameters are introduced to the system and the sample is compacted by applying isotropic compressive strains. Before the sample is compacted, the coefficient of friction μ_{mic} is set to a value lower than the actual value to avoid interlocking of particles and allow free particle movements. This allows initial compaction to be carried out at a higher strain rate. As the compaction progresses, the periodic space shrinks and the particles are brought closer to each other.

At a point when the stress within the periodic space is close to the desired consolidation stress, the initial compaction is stopped and the velocities of the spheres are made zero. The latter part of the compaction, until the required stress is reached, is carried out by a servo control mechanism which simulates an isotropic consolidation. At this stage the coefficient of friction is replaced by the actual coefficient of friction. The servo mechanism which simulates an isotropic consolidation defines strain rate as:

$$\dot{\epsilon}_{ii} = g * (S0_{reqd} - S0_{meas}) \tag{5.1}$$

so that, with each cycle, the strain rate diminishes gradually until it is zero when the consolidation stress reaches the required consolidation stress. At this stage the system is in an almost static state. Here, $S0_{reqd}$ is the required consolidation stress, $S0_{meas}$ is the measured consolidation stress and g is a constant. The measured consolidation stress is defined as the average stress within the periodic space at any time step, expressed as:

$$S0_{meas} = (\sigma_{xx} + \sigma_{yy} + \sigma_{zz})/3 \tag{5.2}$$

where σ_{xx}, σ_{yy}, and σ_{zz} are the stresses in global x, y, z directions respectively.

The particle movements and the stresses within the periodic space are controlled and monitored by a loop in the computer program (Article 4.2) which includes the servo control mechanism. The sample is cycled through this loop until the effective consolidation stress is reached. At this point, as stipulated by the servo control mechanism, the consolidation stress will have reached the prescribed value and the consolidation process is ended. A typical input data file used for a 'sample compaction' simulation is given in Appendix C.6.

5.2.2 Triaxial Testing

The consolidated sample is then sheared, by applying a vertical load while maintaining the lateral pressure, as in any conventional triaxial test. At the onset of this process, the volume of the consolidated sample is measured. The vertical loading of the sample is simulated by applying a constant strain rate $\dot{\epsilon}_z$ in z direction. The lateral pressure is maintained steady at the initial consolidation stress S0 by means of yet another servo control mechanism. The lateral stress S_{xy} is defined by the servo mechanism as:

$$\dot{\epsilon}_{xy} = g * (S_{xyreqd} - S_{xymeas}) \tag{5.3}$$

so that any deviation from the required lateral pressure is corrected and a steady stress state is maintained. Here $S_{xy\,meas}$ is the average stress in global x and y directions such that

$$S_{xymeas} = (\sigma_{xx} + \sigma_{yy})/2 \tag{5.4}$$

where σ_{xx} and σ_{yy} are the normal stresses in the global x and y directions.

The vertical strain is applied at each time step at a constant rate, and particles move to new positions building up a new 'stress state', again to be given a new increment of strain. Throughout this cycle the lateral stress is maintained constant by the servo mechanism. This cycle is continued until the sample reaches shear failure. At intermediate points, the dimensions of the deforming periodic space and the average stress tensor σ_{ij} is read. The average stress tensor gives the stress state of the macroscopic element. The volumetric strain of the sample at any time step is calculated based on the dimensions of the periodic space at that time step and the dimension of the sample at the end of consolidation.

Results of the triaxial test are presented by means of two graphs: variation of deviatoric stress; $\sigma_{zz} - (\sigma_{xx} + \sigma_{yy})/2$ in this case, with the shear strain ϵ_q $(= 2/3(\epsilon_1 - \epsilon_3))$ and variation of volumetric strain ϵ_v with shear strain ϵ_q. The program verifies the results of this numerical simulation by checking on the variation of mean effective stress with deviatoric stress. For a drained triaxial stress, a plot of mean effective stress against deviatoric stress would give a straight line originating from the effective consolidation stress, and running at a slope of

1:3 until failure. A typical input data file used for a drained triaxial test simulation is given in Appendix C.6.

5.3 Simulations Using a Granular Assembly

Although the sample used for simulations was selected based on the particle size distribution of the silty sand used in the physical tests, it was not an exact one on one geometrical representation. There is no record of past research work where exact geometric representations have been used to achieve successful simulations of physically observed behavior. Results of the 2-D triaxial test simulations carried out by Ting et al. (1989) were not successful in predicting physically observed behavior even though particle size distribution was exactly modeled and centrifugal scaling laws were used to scale down the physical tests to its microscopic counterparts.

In this study the numerical model TRUBAL was modified to include the lubricating effects of pore fluid and this modified program was used to support and consolidate the results of the physical experiments.

As an initial verification of the modified program, simulation of granular soils, ignoring 'viscous effects' were carried out for drained and undrained triaxial tests. Descriptions of the test samples used in the simulations are given in Table D.1. The undrained triaxial test simulation was carried out conforming to the method described by Ratnaweera and Meegoda (1991b).

Initially a loose-sand was modeled, using a sample type S1 (Table D.1) for drained and undrained triaxial test conditions. The results of these two simulations as shown in Figures D.1 and D.2 follow typical triaxial test results for loose sands. Adopting a new sample type S2 (Table D.1) with an increased number of particles a medium-dense sand was modeled for drained triaxial test conditions subjected to three effective consolidation pressures of 75000, 100000, and 125000 stress units. The results of these simulations are given in Figures D.3 through D.5, showing the variation of deviatoric stress with shear strain, the variation of volumetric strain with shear strain and variation of deviatoric stress with mean effective stress. Variation of deviatoric stress, q with mean effective stress p′ also show that at low effective consolidation pressures, normalizing q with respect to p′ is not possible as discussed in Article 1.2.

For the simplicity it offers in computations, only two particle sizes were used in the simulations. The particle size distribution curve of the silty sand was used to select particle sizes of the representative sample and their distribution.

Two particle sizes were selected to represent the finer two thirds of the total particle size distribution and the coarser one third remaining. The average particle sizes of these two segments were found to be in 2:3 proportion. Since the particle sizes that can be used in TRUBAL lie between 5-25 TRUBAL units in radius, particle sizes of 10 and 15 TRUBAL units in radii were selected to be in proportion of 2:1, in numbers.

To select a sample that would give a better representation of a medium-dense sand, simulations were performed using three different samples. The first comprised of 100 spheres of radius 10 units and 50 spheres of radius 15 units while the second sample comprised of 200 spheres of radius 10 units and 100 spheres of radius 15 units, respectively. The third sample had 400 and 200 spheres of radii 10 and 15 respectively. The three samples were used to simulate a dry granular soil subjected to drained triaxial test conditions. These samples were consolidated at an effective consolidation stress of 100000 units and sheared at a strain rate of 5×10^{-4} units until failure. Subjected to this consolidation stress, the three samples consisting of particles 150, 300 and 600 had developed porosities of 0.358, 0.365 and 0.357 respectively.

The first sample consisting of 150 spheres failed to give the expected stress-strain behavior pattern but the responses of the latter two samples of 300 and 600 spheres were successful (Figure D.6(a)). Although the peak deviatoric stresses were slightly different, both samples achieved the same residual deviatoric stress. The variation of volumetric strain with vertical strain showed a similar trend but since the initial porosities were not the same, at higher vertical strains, volumetric strains deviated significantly (Figure D.6(b)). This simulation shows that the sample with a lower initial porosity expands more than the one with a higher initial porosity. This is similar to the observations made in the experiments and also supports the Critical Void Ratio concept explained in Article 1.3.

The co-ordination number r and the constraint ratio, R play important roles in understanding force-displacement behavior at the microscopic level. The co-ordination number, r is defined as the number of contacts per sphere while the constraint ratio, R expressed as:

$$R = \frac{r}{3}(2 - S)$$

where S is the fraction of the contacts sliding, indicates the amount of constraints on the particles. Figures D.6(c) and D.6(d) show the variation of co-ordination number with vertical strain and the variation of constraint ratio with vertical strain for all three samples.

For a deforming granular assembly the constraint ratio is identified as an important parameter governing the microscopic failure mechanism (Cundall and Strack, 1983). A constraint ratio, R greater than unity indicates an over constrained sample while a constraint ratio less than unity indicates that the sample is under constrained. When constraint ratio approaches unity, the sample is identified to be at a limiting stress. This case; R = 1 also corresponds to a particular failure mode which shows deformation at a constant stress. R is found to be closely related to the strength than to density or porosity (see Figures D.6(a) and D.6(c)) (Cundall and Strack, 1983).

Figures D.6(b) and D.6(d), closely follow the same trend indicating that the co-ordination number, r governs the volume change behavior of a granular medium.

The initial co-ordination numbers of the samples of 150 and 600 spheres are the same indicating that they have the same initial porosity. The variation of co-ordination number with vertical strain of both these samples are similar indicating similar volumetric change behavior.

Based on the constraint ratio R, the sample with 300 spheres was selected for the simulations, since at higher vertical strains, constraint ratio of this sample approaches unity indicating that it will reach a constant residual stress beyond the peak stress.

All quantities are measured in TRUBAL units. Table D.2 gives the relationship between TRUBAL units and standard physical units. Figure D.11 shows the simulated stress-strain behavior for an effective consolidation stress of 75 kPa.

5.4 Simulations Using Iterative Method

In the iterative method, the force generated due to the lubricating effect of the pore fluid is found through a long and tedious process of iteration. Although the iterative process is time consuming and demands more CPU time, this gives the exact value of the force, calculated using all the parameters involved.

Considering the iterations that would be required for each contact for each sphere for each cycle, simulations in this method requires more computer CPU time and this reason alone limits the number of particles and sizes that can be used for the simulation.

For the simulations carried out in this method the number of spheres was limited to 20 and were to be of a single size. Since a dense sand sample cannot be successfully represented by 20 spheres, a loose sand was selected for the simulations. The description of the selected sample type S3 is given in Table D.1. Simulations were carried out for three pore fluid viscosities of 0.02, 0.05 and 0.1 units and for a ''dry test'' where the viscosity was taken to be zero. Figure D.7

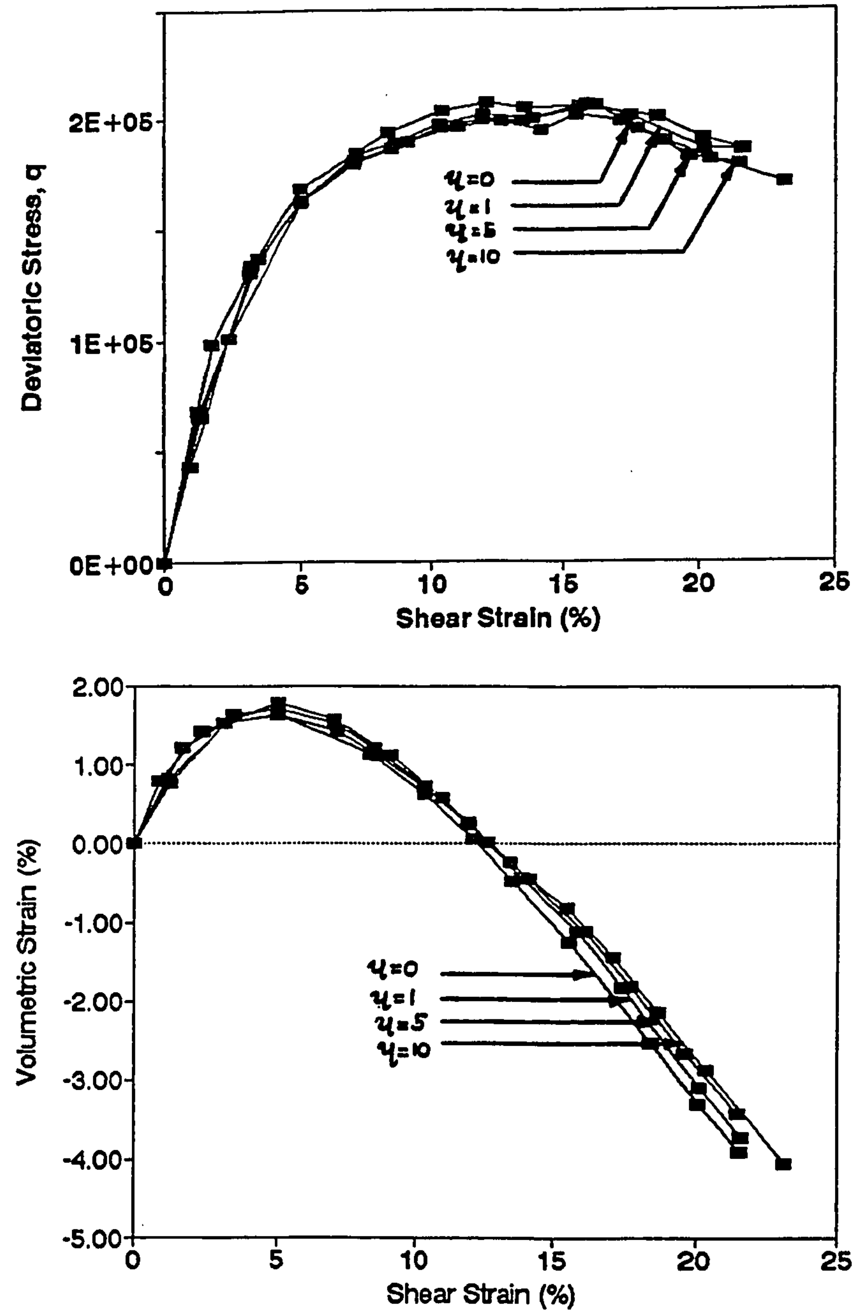

Figure 5.1 Drained Stress-Strain Behavior of a Medium-Dense Sand with Different Pore Fluid Viscosities Simulated at an Effective Consolidation Stress of 75000 Stress Units

shows the variation of the deviatoric stress with vertical stress and variation of volumetric strain with vertical strain for these simulations.

5.5 Simulations Using Database Method

In this approach, the force generated at the particle contacts due to the lubrication effect of pore fluid is made available to the computer program through a data base, avoiding the tedious computation involved in the iterations. This allows large numbers of spheres and more particle sizes to be used in the computer simulations.

In this analysis an assembly of 300 spheres of two particle sizes were used to demonstrate the effects of pore fluid viscosity on soil behavior. The description of the selected sample type S.2 is given in Table D.1. Simulations were carried out for medium-dense sand under drained triaxial test conditions, subjected to three different effective consolidation pressures of 75000, 100,000 and 125000 stress units and for samples with 4 different pore fluid viscosities of 0, 1, 5 and 10 units. Figures D.8 through D.10 give the results of these simulations. Figure 5.1 shows the variations of deviatoric stress with shear strain and volumetric strain with shear strain for granular assemblies with different pore fluid viscosities, simulated at an effective consolidation stress of 75000 units.

5.6 Results and Discussion

The results of the simulations carried out for loose and medium-dense sand, neglecting viscous effects of pore fluid, agree with typical stress-strain behavior observed in the triaxial tests. These initial simulations were carried out to verify the validity of the modified program to model granular soils and the results indicated that the model is successful although limited to qualitative studies at this stage. Figures D.3 through D.5 show the simulated stress strain behavior patterns of a medium dense sand tested under three effective consolidation pressures. It is apparent that even though it is not possible to quantify strength of a soil at this stage, the model is successful in showing the trends.

Figure D.7 shows the results of the simulations carried out in the iterative method for loose sand samples with different pore fluid viscosities. These results in general follow typical stress-strain behavior of a loose sand. The stress-strain behavior patterns show a consistent variation with the variation of pore fluid viscosity. However, the limitations of the iterative method make it impracticable in simulating an acceptably good representative sample for soil.

The database method of simulation allows larger numbers as well as different sizes of particles to be used in modeling, thus making it possible to achieve a more realistic representation of soil. Figures D.8 through D.10 show the results of the drained triaxial test simulations carried out for medium-dense sand subjected to three different effective consolidation pressures. In general the simulated stress-strain behavior seem to follow typical experimental results for medium-dense sand.

The variation of deviatoric stress with vertical strain for soil samples with different pore fluid viscosities but tested under same effective consolidation pressure takes the same trend and shows very little deviation. A slight deviation is observed at the peak stress and beyond. Simulations for samples subjected to higher effective consolidation pressures give similar results but yield higher deviatoric stresses. The rate of increase in the deviatoric stress with vertical strain increases as the effective consolidation pressure is increased and the peak stress is reached earlier.

The variations of volumetric strain with the vertical strain, also follow typical patterns of results and are consistent with each other for samples tested under different effective consolidation pressures. Initially the samples undergo compaction but with increasing vertical strain the samples show expansion. The samples with higher pore fluid viscosities fail at more compacted states.

The results in general agree with typical stress-strain behavior patterns observed in physical tests. But beyond peak stress at higher strains, the samples do not attain residual strengths nor constant volumetric strains. As a result, neither residual stresses nor critical void ratios can be obtained from these graphs, to produce a plot of residual shear strength against critical voids ratio. Such a plot if it was possible would have enabled a direct comparison with the results of the physical tests (Chapter 3.0). This is due to a shortcoming in the mathematical scheme employed in TRUBAL, independent of the modifications made to include pore fluid viscosity. At higher strains, beyond the peak stress, the outward movements of the spheres reduce particle contacts and create void spaces. The program calculates the average number of contacts per sphere at each time step and as the straining progresses, this number is seen to reduces from an average of 5.5 to 4.2. Further increase in strain continuously moves particles outwards creating more void spaces, deleting the particle contacts. As such the void ratio of the sample will not stabilize at a residual void ratio as expected. Similarly, beyond the peak strength, the deviatoric stress decreases continuously without stabilizing. Deletion of particle contacts decreases the strength of the soil sample since the strength is governed by the particle contacts. Therefore the shear strength of the soil will not reach a residual stress.

However, the results of the simulations clearly show that the pore fluid viscosity does affect the shear strength and stress-strain behavior of a soil. The graphs of deviatoric stress versus shear strain show that there is a significant change in the angle of internal friction while the graphs of volumetric strain versus vertical strain show that samples with higher pore fluid viscosities fail at higher densities. These results support the hypothesis that the pore fluid viscosity influences the shear strength and stress strain behavior of a granular soil through a locally occurring process of lubrication at particle level.

CHAPTER 6
SUMMARY AND CONCLUSIONS

6.1 Summary

In this study a two fold path of investigation was carried out to investigate the influence of pore fluid viscosity on deformation characteristics of granular soils. An attempt was made to verify the hypothesis that changes in the pore fluid viscosity of granular soils are associated with changes in the stress-strain behavior. A series of drained triaxial tests were carried out to investigate this, followed by a series of numerical simulations using a microscopic model to verify the observed behavior.

A series of drained triaxial tests were performed on a medium-dense silty sand, subjected to three different effective consolidation pressures. Using glycerol/water solutions of different proportions, sandy silt samples with four different pore fluid viscosities were prepared. The residual shear strength values of these sand samples were plotted against the corresponding critical void ratios to obtain a family of curves, identifiable by their pore fluid viscosities. For a given critical void ratio, as the pore fluid viscosity increased, the residual shear strength decreased indicating that the pore fluid viscosity does influence the stress-strain behavior of granular soils.

For a given critical void ratio, the residual shear strength of a soil with lower pore fluid viscosity was found to be higher than that of a soil with higher pore fluid viscosity. Similarly, for a given residual shear strength, granular soils with higher pore fluid viscosity showed a lower critical void ratio.

Since the strength of a saturated granular soil is governed by mineral to pore fluid contacts in presence of a pore fluid, the observed changes in the stress strain behavior could be reasoned to be associated with changes in the contact properties. Therefore the soil behavior at particle level was studied in order to understand the fundamental mechanism responsible for the observed behavior.

A microscopic numerical model TRUBAL developed based on the Distinct Element Method was used in this study. Since TRUBAL had been developed to model only dry granular material, it was modified to incorporate the effects of pore fluid on mineral to mineral contacts. The Reynolds equation for hydrodynamic lubrication was adopted to explain and quantify the forces generated due to pore fluid viscosity at mineral-mineral contacts in the presence of pore fluids. These forces were calculated by summing up the pressures over the projected area of contact using a finite difference formulation.

The modification to incorporate the effects of mineral to mineral contacts in the presence of a pore fluid was introduced in two ways; directly, including a lengthy iterative calculation, and through a data base which eliminates the need for time consuming iterations. In the data base method all the information sought from the iterative method is made available to the program through a data base. In both the methods, the granular assemblies were generated, consolidated and sheared until failure in the same manner.

After several trials, an optimum combination of 200 spheres of radius 10 units and 100 spheres of radius 15 units was selected to model a medium-dense granular assembly and this was used to simulate drained triaxial behavior of a silty sand. However the limitations imposed by the computer CPU time would not allow this sample to be used in the iterative method of simulation forcing the use of a smaller sample of 20 spheres of single size. Since 20 spheres could not be used as an acceptable representative sample to model a medium-dense sand, this assembly was used to simulate the stress-strain behavior of a loose sand, mainly to demonstrate the use of Reynolds equation in TRUBAL program.

The results of the simulations support the view of the past researchers that numerical models can only be used for qualitative simulations of soil behavior. The trends of the numerical simulations were consistent with those of the physical drained triaxial tests. The observations indicate that for the strain rates used in this study the angle of internal friction did not change with the change in pore fluid viscosity.

The numerical simulations also show a trend similar to that observed in the physical tests for the variation of the volumetric strain with the vertical strain except for the fact that the samples did not stabilize at a critical void ratio. This may be an inherent deficiency of TRUBAL since to date, all numerical simulations using TRUBAL used in comparative studies with physical tests have been performed at low shear strains. The results also demonstrated that samples with higher pore fluid viscosities failed at higher densities than those with lower pore fluid viscosities.

6.2 Conclusions

The results of both the physical tests and numerical simulations support the hypothesis that the pore fluid viscosity influences the deformation characteristics of granular soils.

The results of the drained triaxial tests (Figure 3.1) show that for a given critical void ratio, soil samples with different pore fluid viscosities develop different residual shear strengths; the samples with higher pore fluid viscosities reach lower residual strengths and samples with lower pore fluid viscosities reach higher residual strengths. Conversely for sand samples reaching any given residual shear strength, the samples with higher pore fluid viscosities show lower critical void ratios. Thus soils with higher pore fluid viscosities are shown to fail at denser states.

Although a graph showing the variation of residual shear strength with critical void ratio could not be produced as explained in Article 6.1, the results of the simulations in general agree with those of the triaxial tests.

These numerical simulations indicate that the pore fluid viscosity influences deformation characteristics of granular soils. However, it must be noted that these tests were carried out at very low strain rates which may allow dissipation of pore pressures generated during shearing.

At low strain rates, in both drained tests and the numerical simulations, the angle of internal friction remained constant with the changes in pore fluid viscosity.

6.3 Recommendations for Future Research

A microscopic model which could be used exclusively to model soil behavior is yet to be developed. Although researchers have added many improvements to their models such as different sizes, shapes etc., these models fail in modeling physically observed phenomena such as the stress-dilatancy behavior.

Once the above has been addressed, a further step could be taken towards quantitative mathematical modeling. This involves proper scaling of microscopic parameters and their corresponding physical counterparts, and accurate experimental determination of microscopic model parameters.

APPENDIX A
Figures and Tables Cited

Table A.1 Model Parameters used in TRUBAL Simulations (Ratnaweera and Meegoda, 1991a)

Microscopic Model TRUBAL	A1
Model Variables	
Particles with Radius 10 units	100
Particles with Radius 15 units	50
Soil Parameters	
Normal Stiffness k_n	$1x10^8$
Shear Stiffness k_s	$2x10^8$
Coefficient of Static Friction, μ	1.0
Stress State	
Initial Stress, p_o'	75000
Porosity	0.349

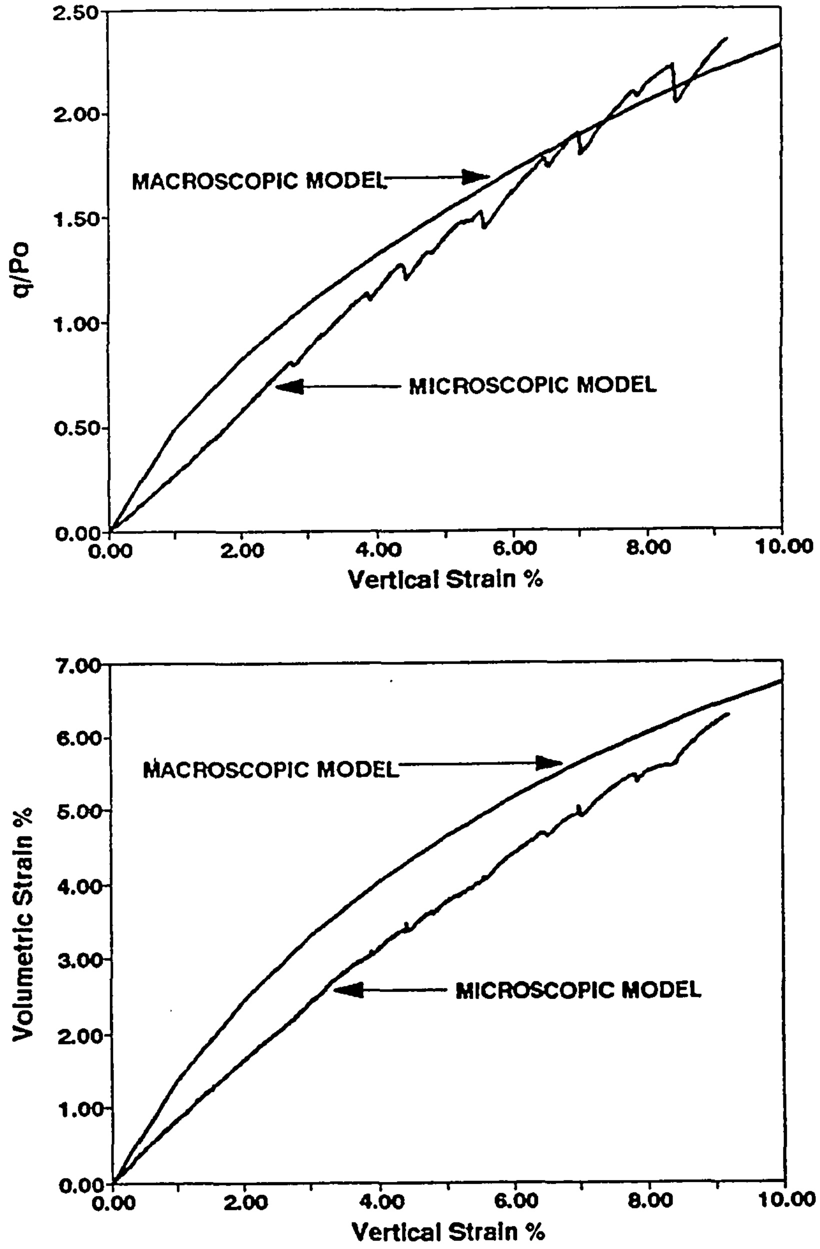

Figure A.1 Simulated Drained Stress-Strain Behavior of a Conventional Triaxial Test Using Microscopic and Macroscopic Models (Ratnaweera and Meegoda, 1991a)

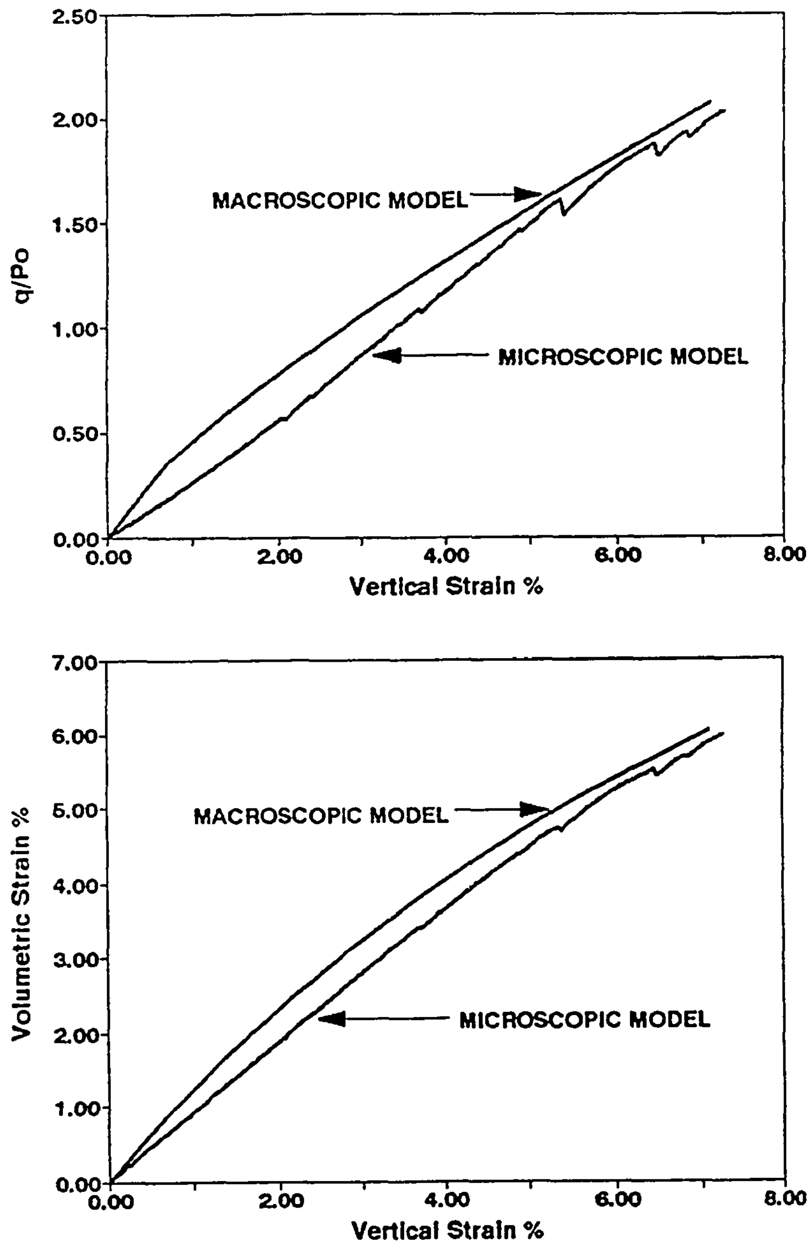

Figure A.2 Simulated Drained Stress-Strain Behavior of a Plane Strain Triaxial Test Using Microscopic and Macroscopic Models (Ratnaweera and Meegoda, 1991a)

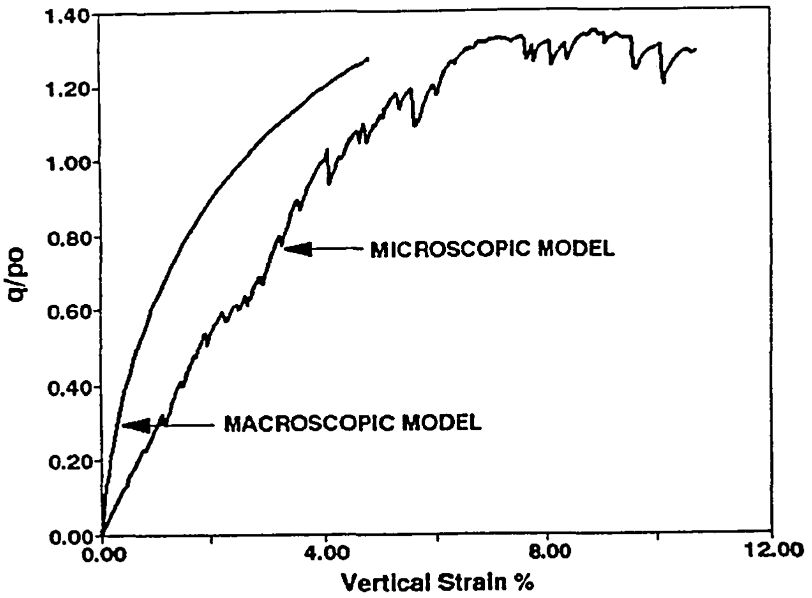

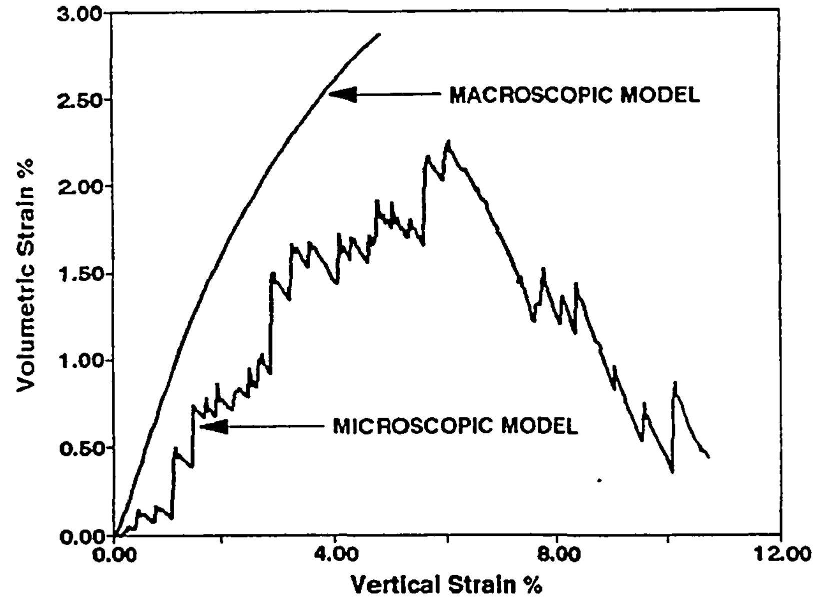

Figure A.3 Simulated Drained Stress-Strain Behavior of a Constant Pressure Triaxial Test Using Microscopic and Macroscopic Models (Ratnaweera and Meegoda, 1991a)

APPENDIX B
Experimental Program

Table B.1 Physical Properties of Pore Fluid

Fluid	Mass Density (kg/m^3)[a]	Absolute Viscosity (cps)[b]
Water	998.0	0.89
16.54% Glycerol + Water	1040.0	1.18
28.39% Glycerol + Water	1071.0	1.63
44.22% Glycerol + Water	1113.0	3.83

[a] CRC Handbook (1989)
[b] Rajapakse (1989)

Table B.2 Results of the Drained Triaxial Test

Sample ID No.	Glycerol (%)	p_o'	v_i	q_{peak} (kPa)	ϵ_1 (%)	ϵ_v (%)	e_{cv}	q_{res} (kPa)
A50	0	50	1.649	183	14.5	-2.43	0.688	167
A75	0	75	1.676	226	14.25	-0.185	0.679	214
A125	0	125	1.628	408	12.5	-1.38	0.650	371
B50	16.5	50	1.653	183	16.1	-1.58	0.678	169
B100	16.5	100	1.619	350	15.2	-1.4	0.642	335
B125	16.5	125	1.610	439	9.3	-1.22	0.630	393
C50	28.39	50	1.652	173	12.9	-1.34	0.674	160
C100	28.39	100	1.609	325	16	-2.21	0.644	290
C125	28.39	125	1.614	389	15	-0.664	0.625	365
D50	44.22	50	1.638	147	19	-1.1	0.656	141
D100	44.22	100	1.627	284	14.1	-0.1	0.629	272
D125	44.22	125	1.593	375	14.7	-1.58	0.618	351

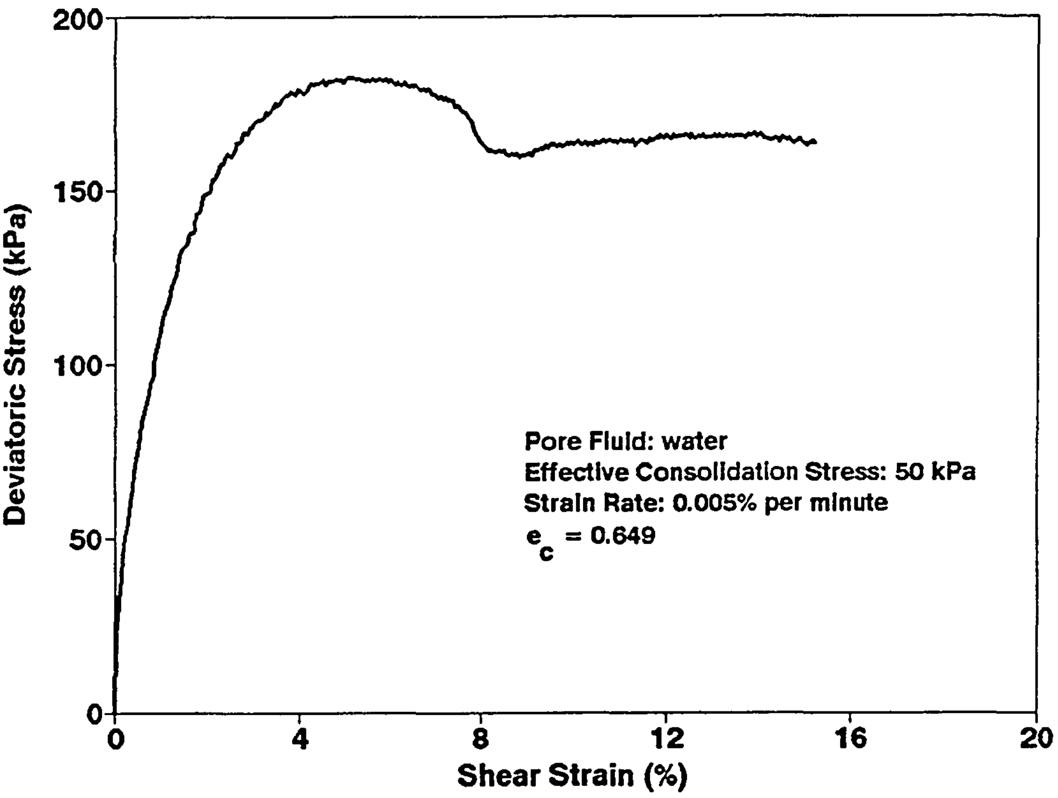

Figure B.1 Variation of Deviatoric Stress with Shear Strain for test A-50.

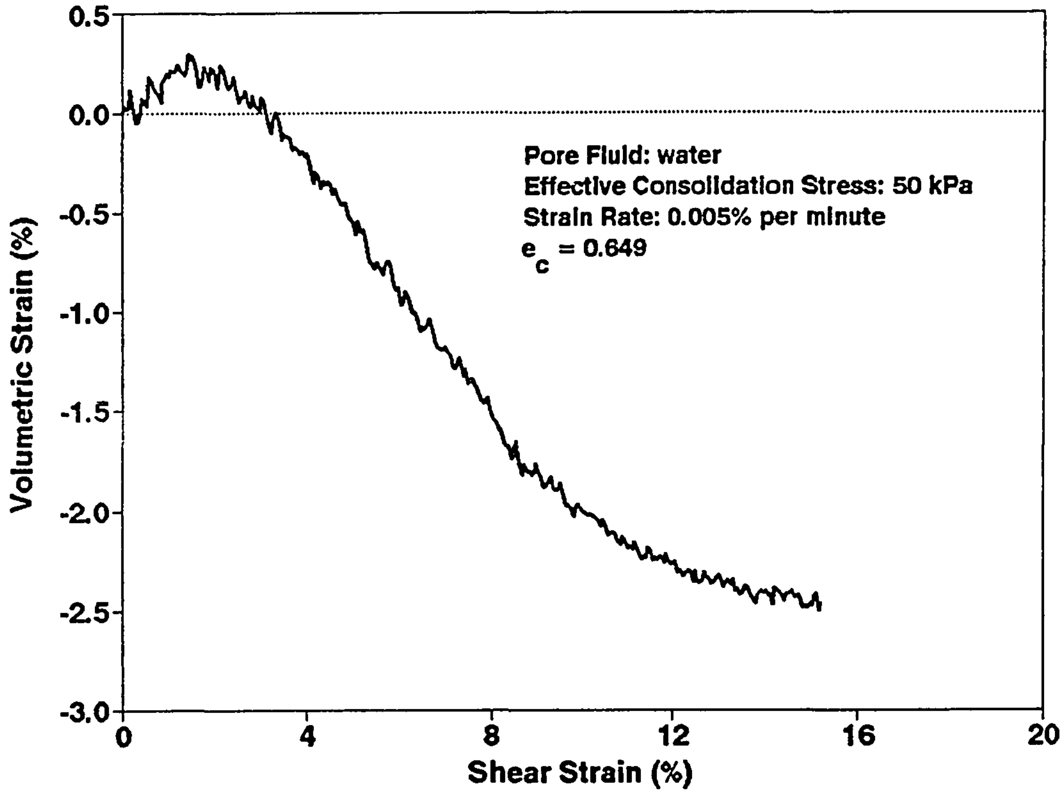

Figure B.2 Variation of Volumetric Strain with Shear Strain for test A-50.

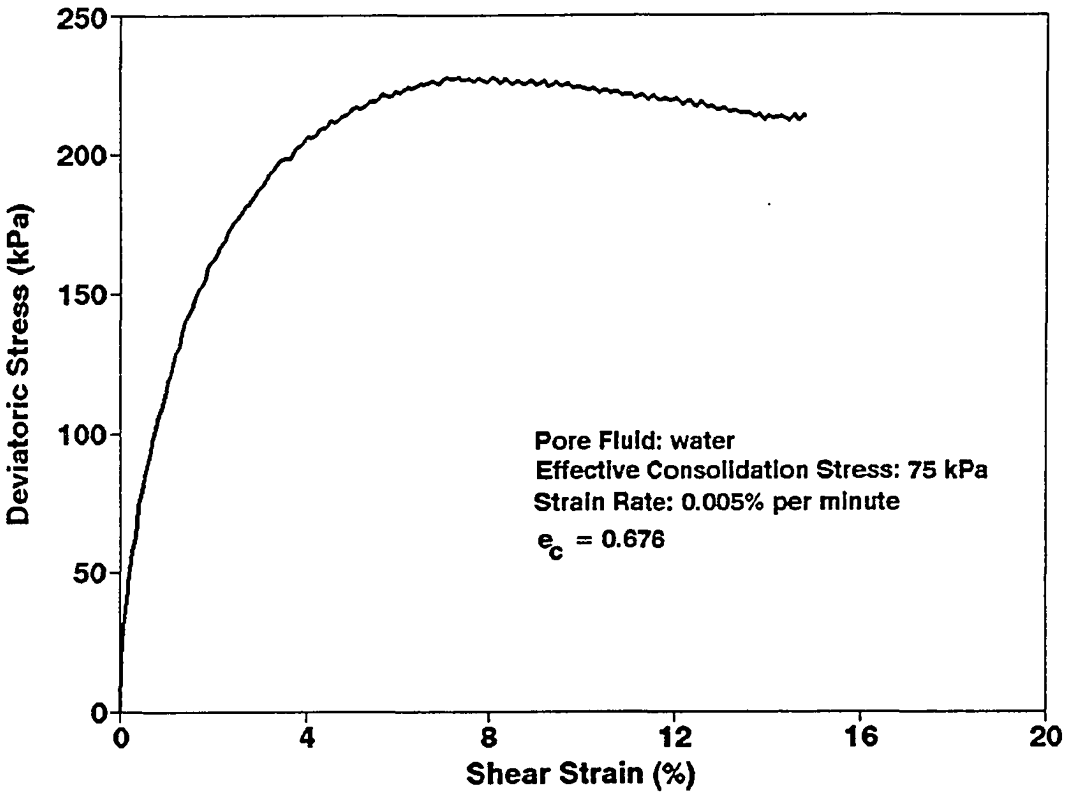

Figure B.3 Variation of Deviatoric Stress with Shear Strain for test A-75.

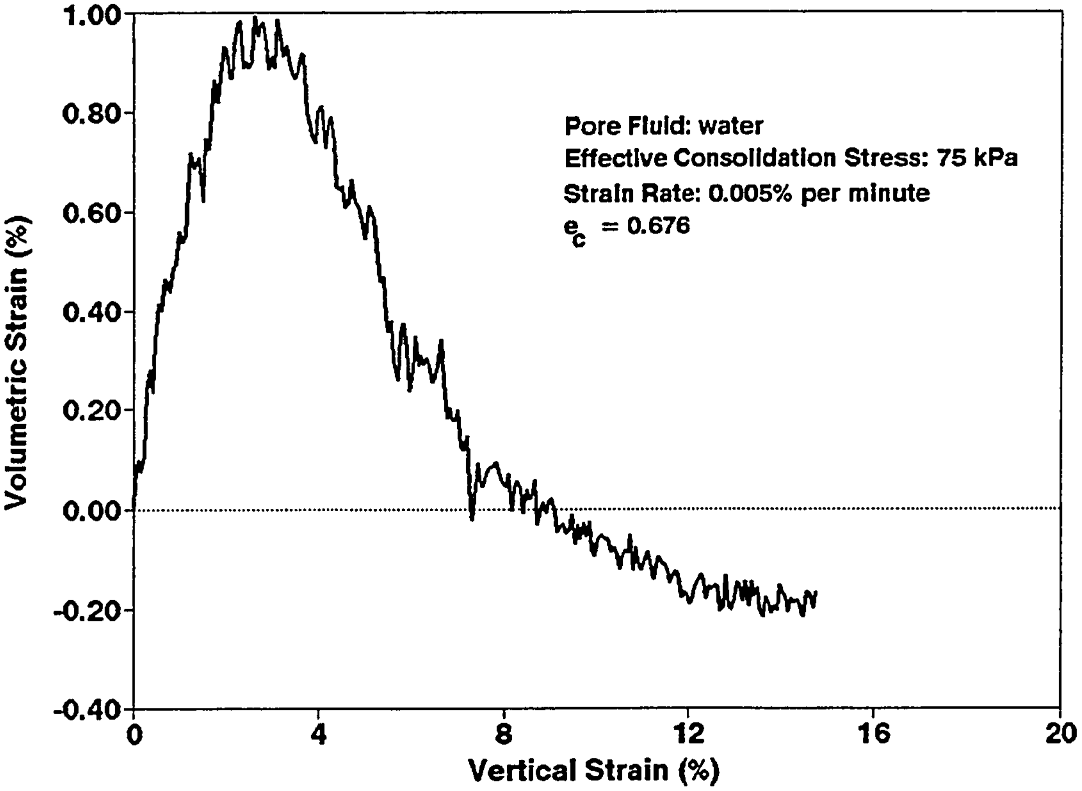

Figure B.4 Variation of Volumetric Strain with Shear Strain for test A-75.

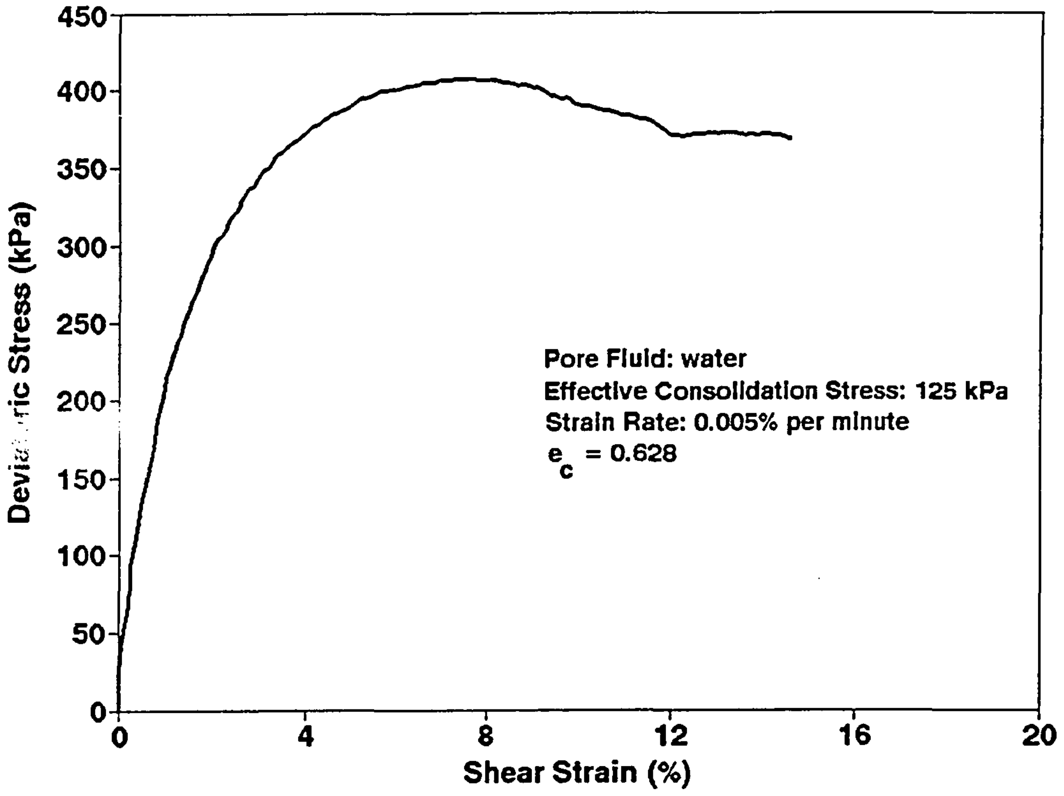

Figure B.5 Variation of Deviatoric Stress with Shear Strain for test A-125.

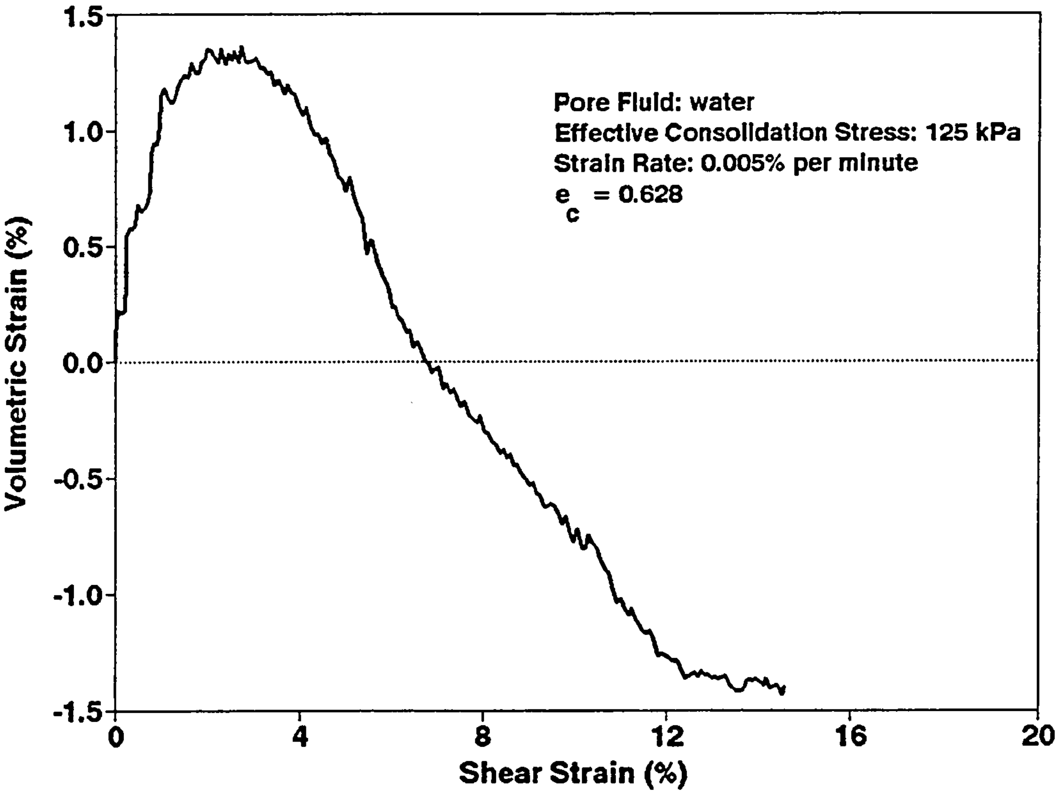

Figure B.6 Variation of Volumetric Strain with Shear Strain for test A-125.

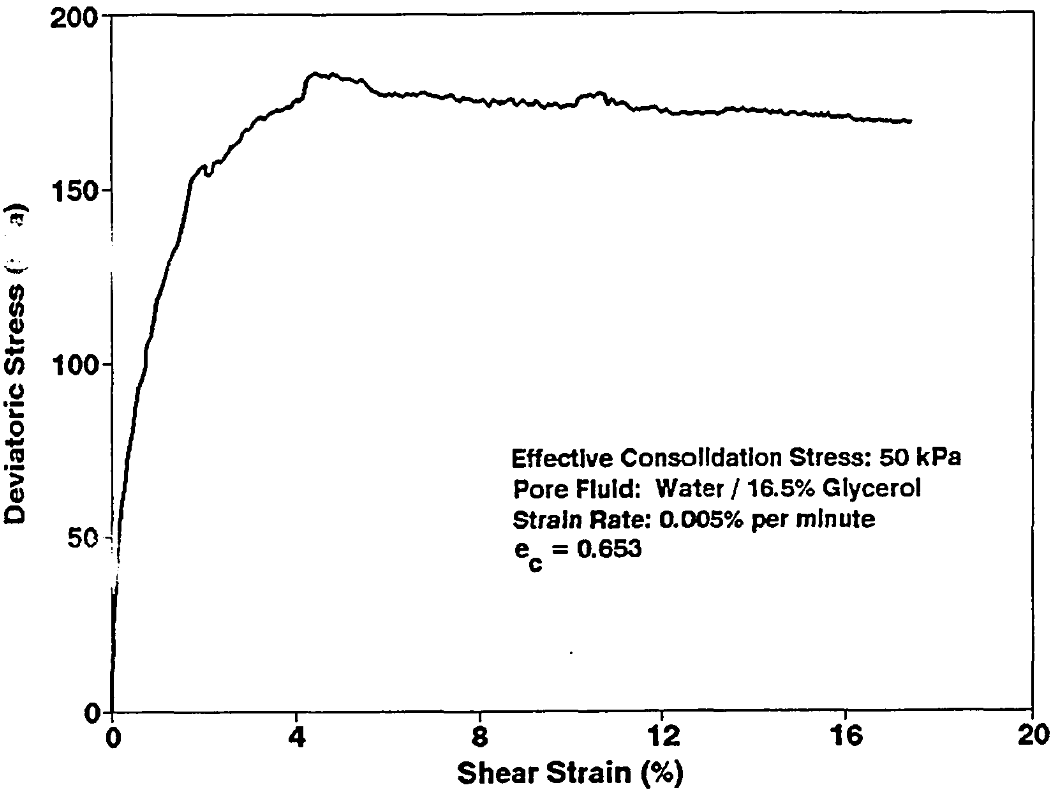

Figure B.7 Variation of Deviatoric Stress with Shear Strain for test B-50.

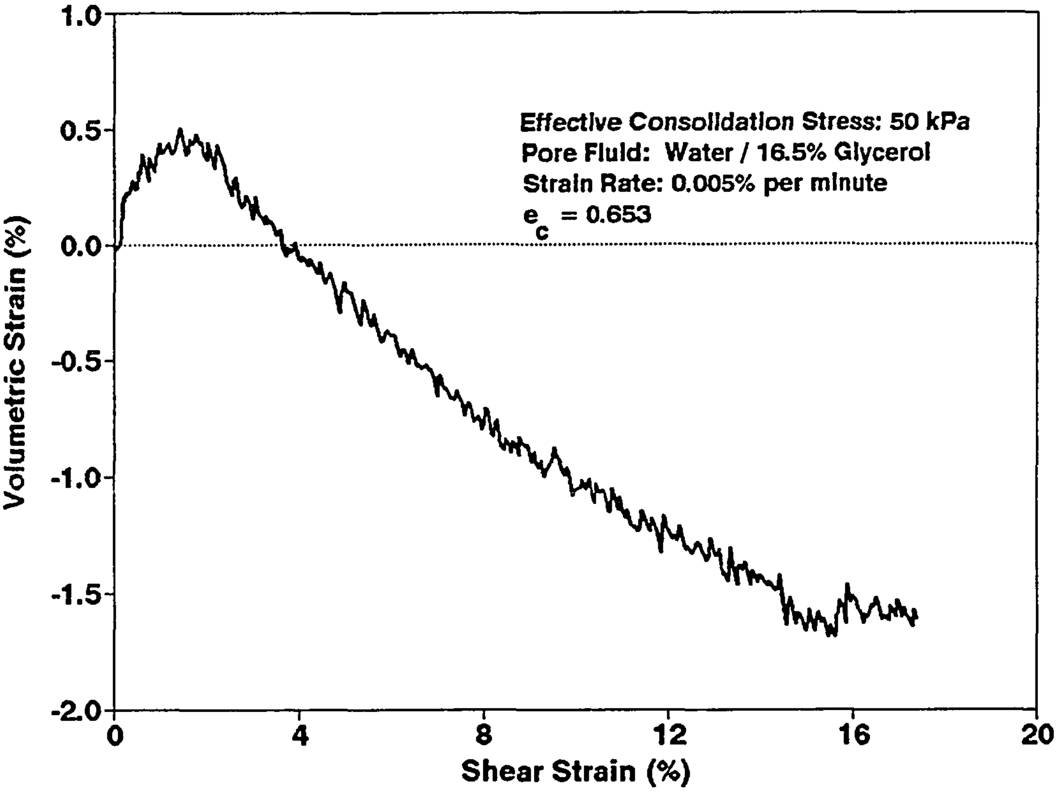

Figure B.8 Variation of Volumetric Strain with Shear Strain for test B-50.

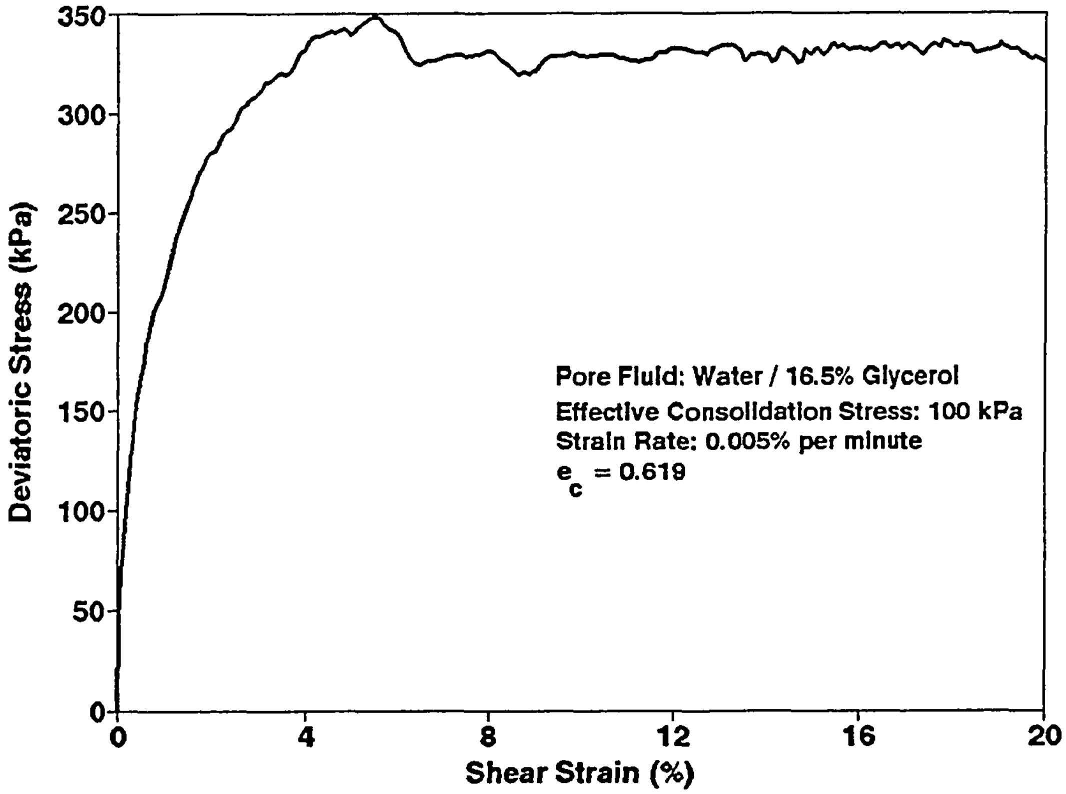

Figure B.9 Variation of Deviatoric Stress with Shear Strain for test B–100.

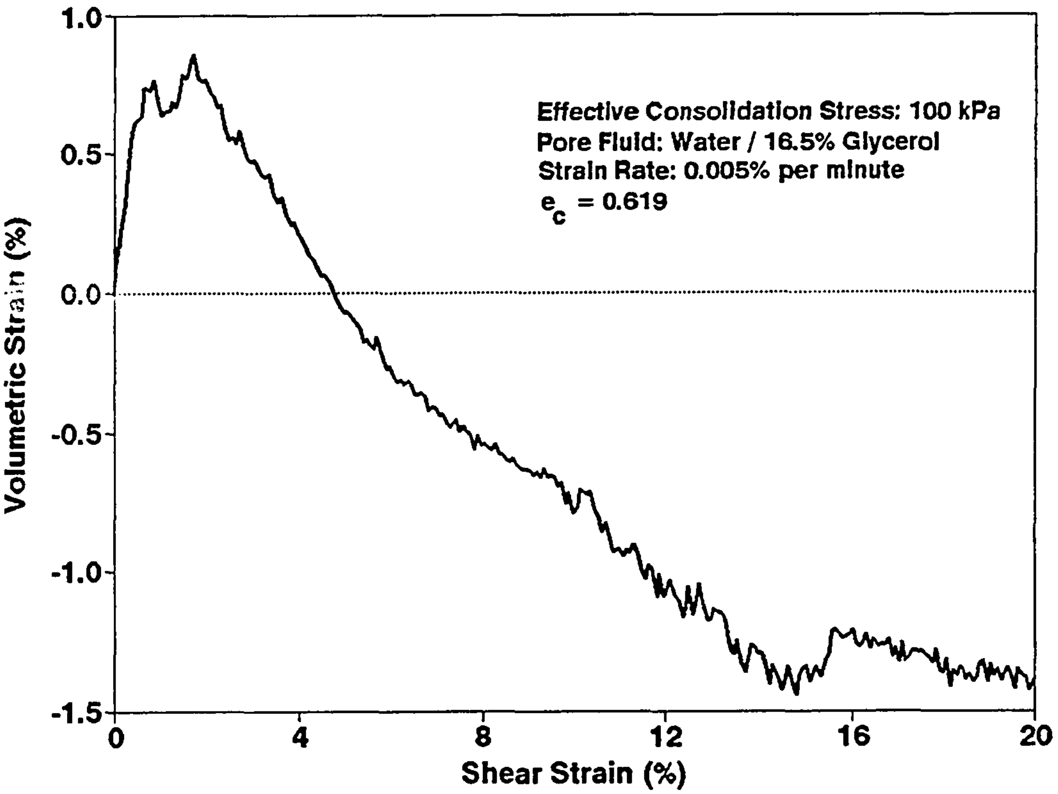

Figure B.10 Variation of Volumetric Strain with Shear Strain for test B-100.

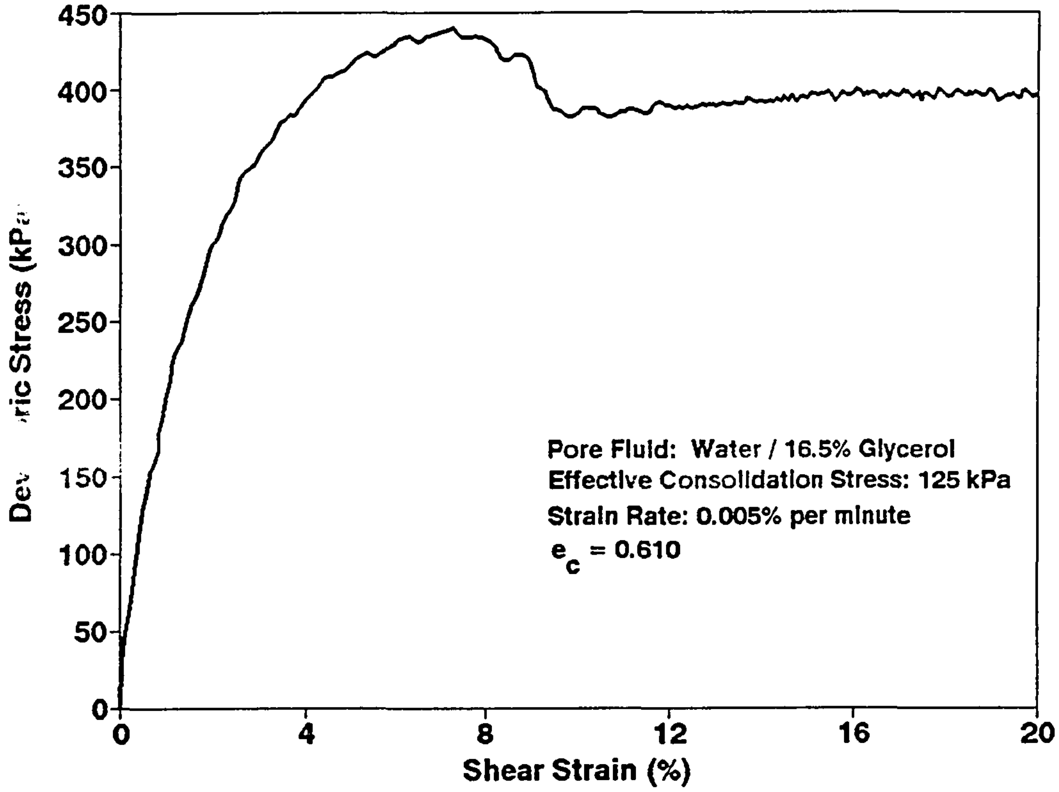

Figure B.11 Variation of Deviatoric Stress with Shear Strain for test B-125.

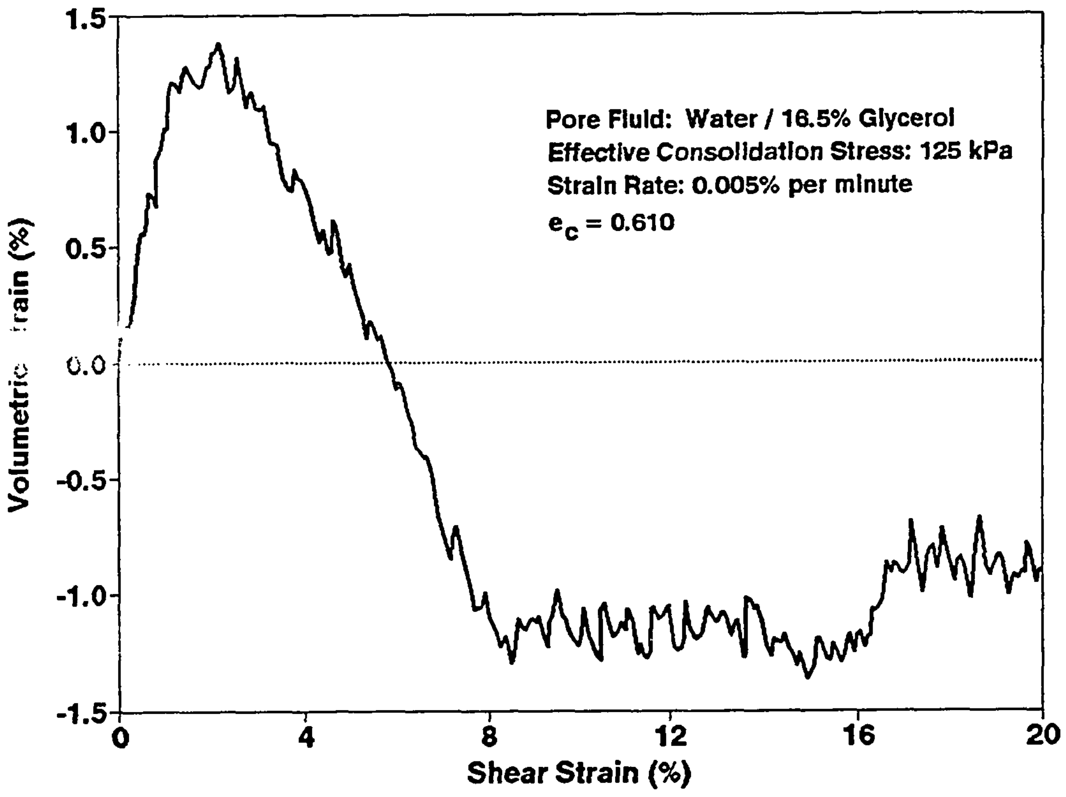

Figure B.12 Variation of Volumetric Strain with Shear Strain for test B-125.

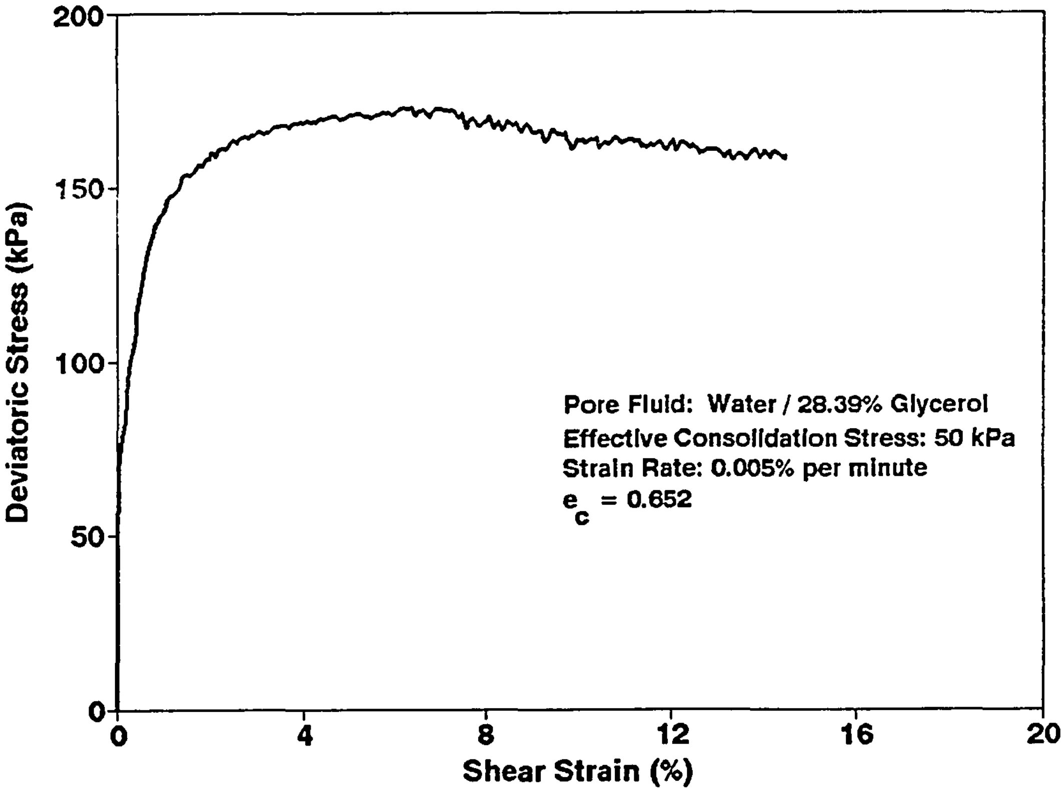

Figure B.13 Variation of Deviatoric Stress with Shear Strain for test C-50.

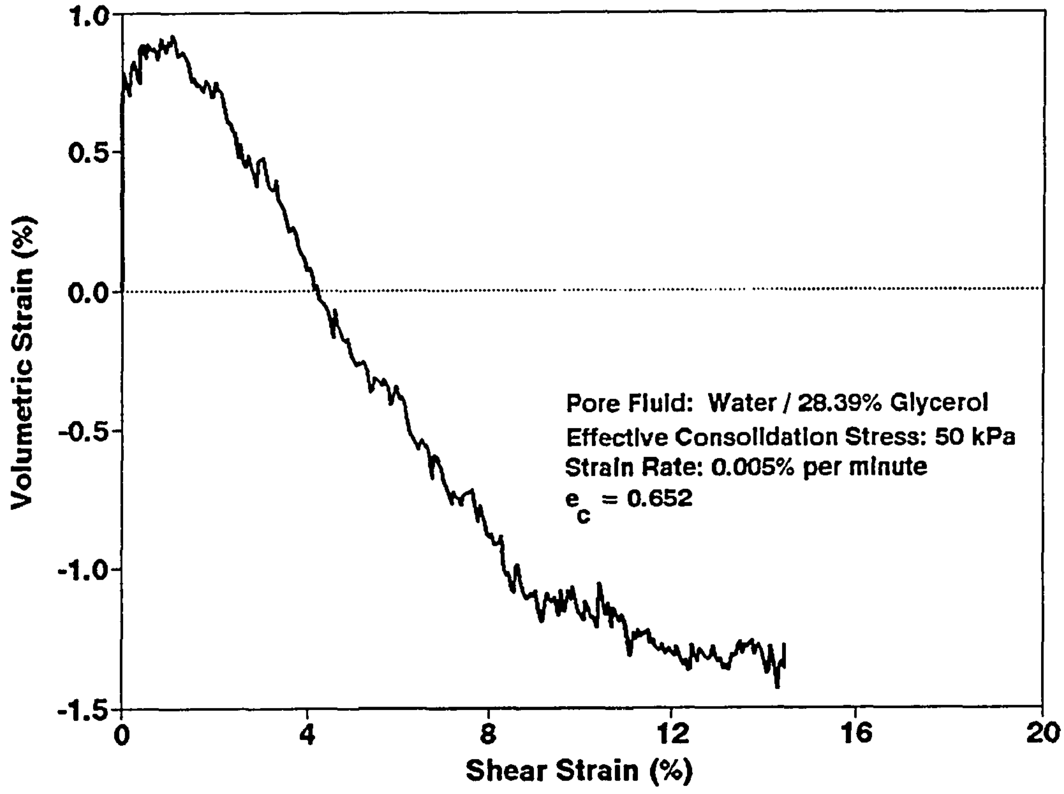

Figure B.14 Variation of Volumetric Strain with Shear Strain for test C-50.

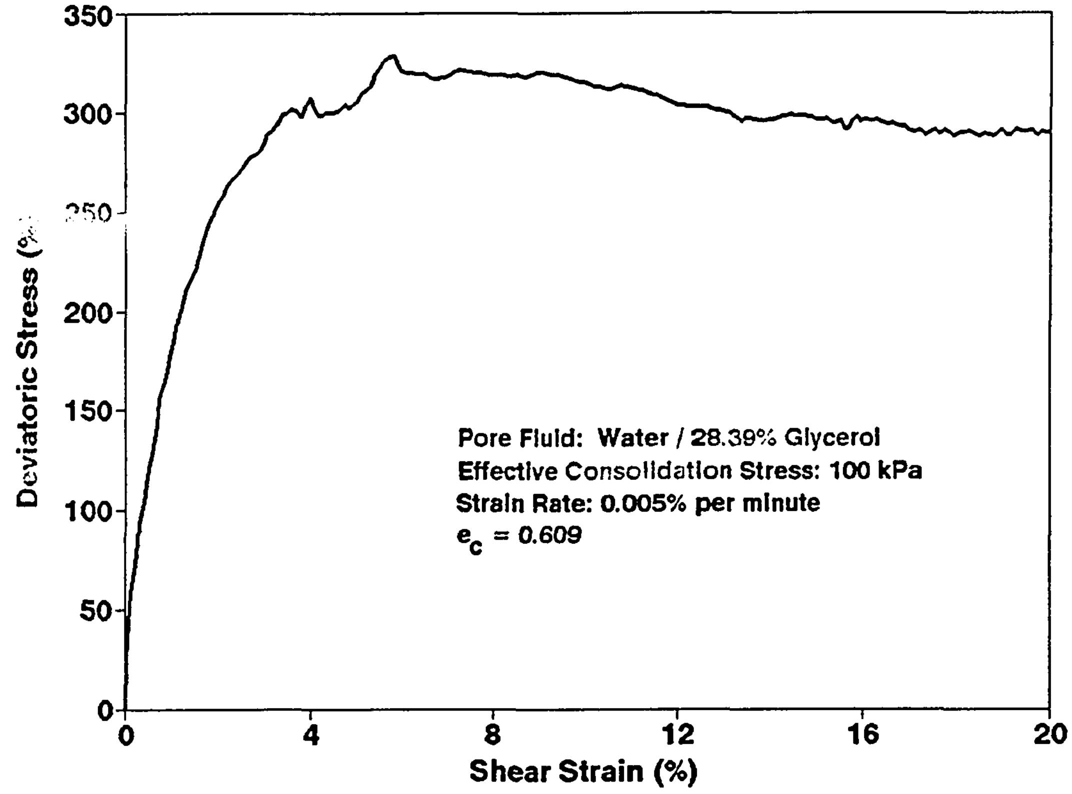

Figure B.15 Variation of Deviatoric Stress with Shear Strain for test C-100.

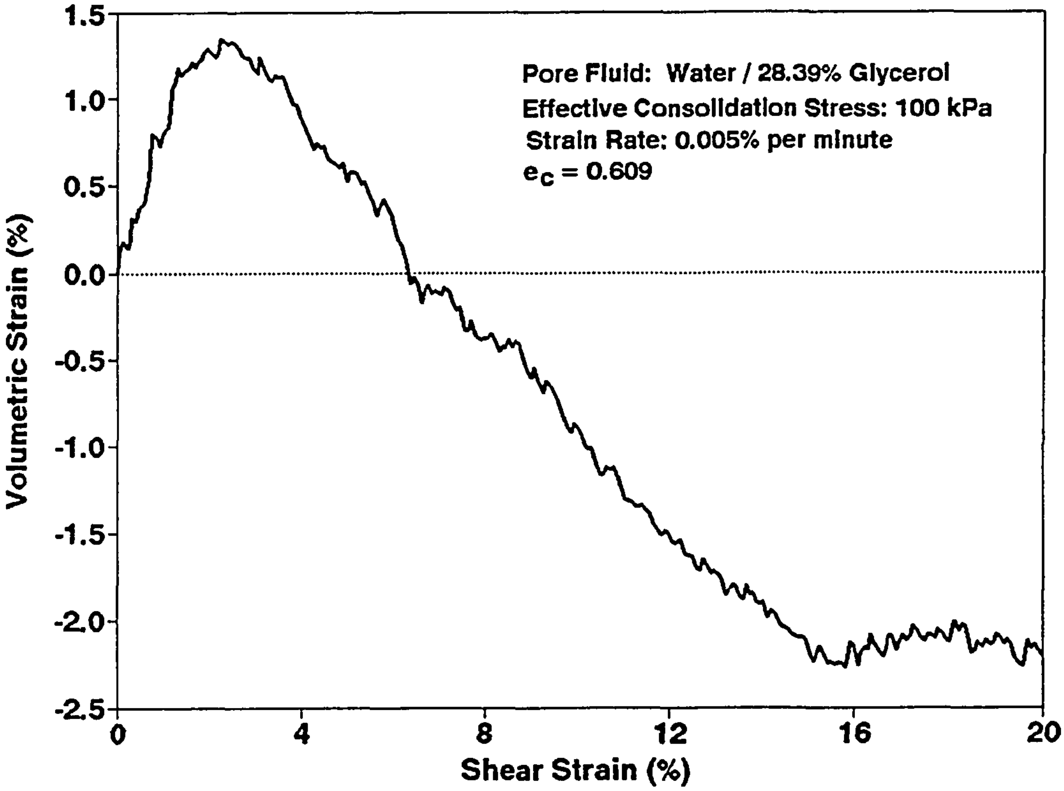

Figure B.16 Variation of Volumetric Strain with Shear Strain for test C-100.

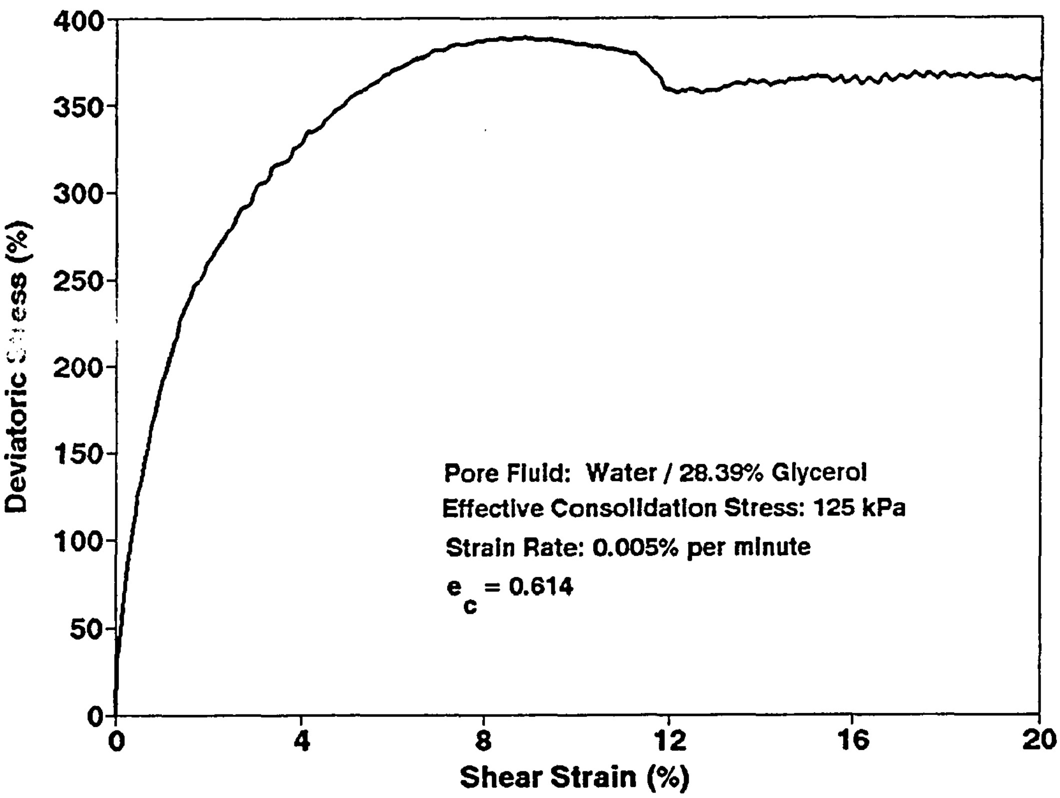

Figure B.17 Variation of Deviatoric Stress with Shear Strain for test C-125.

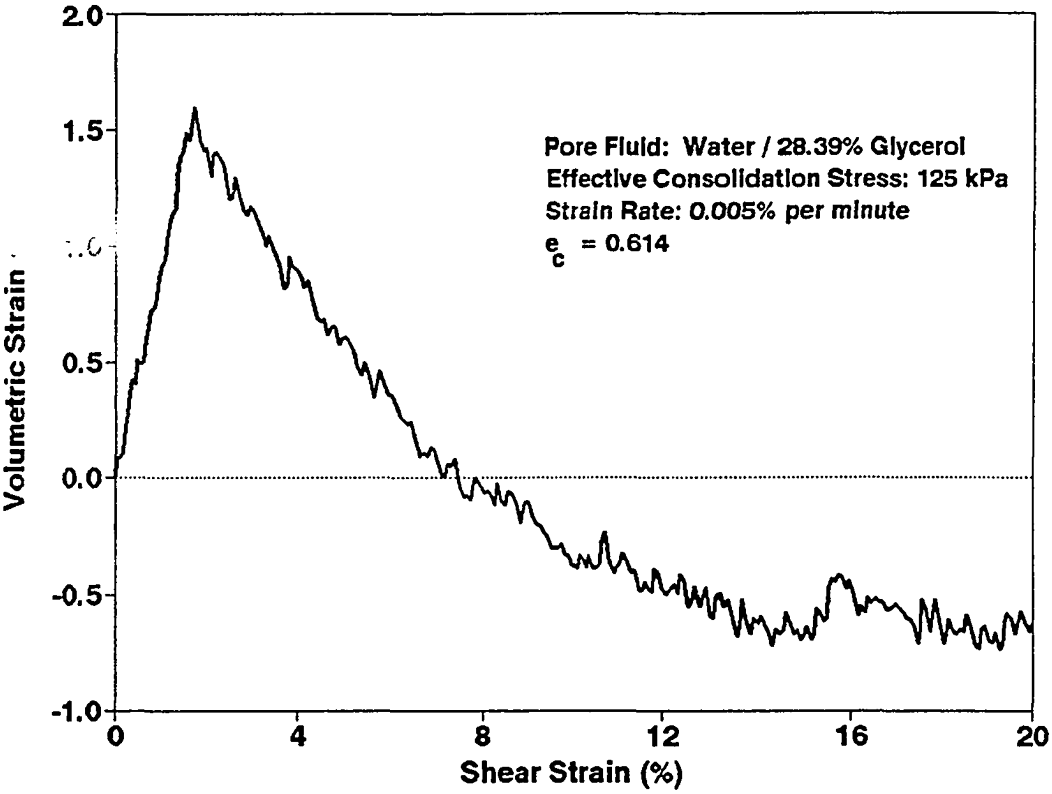

Figure B.18 Variation of Volumetric Strain with Shear Strain for test C-125.

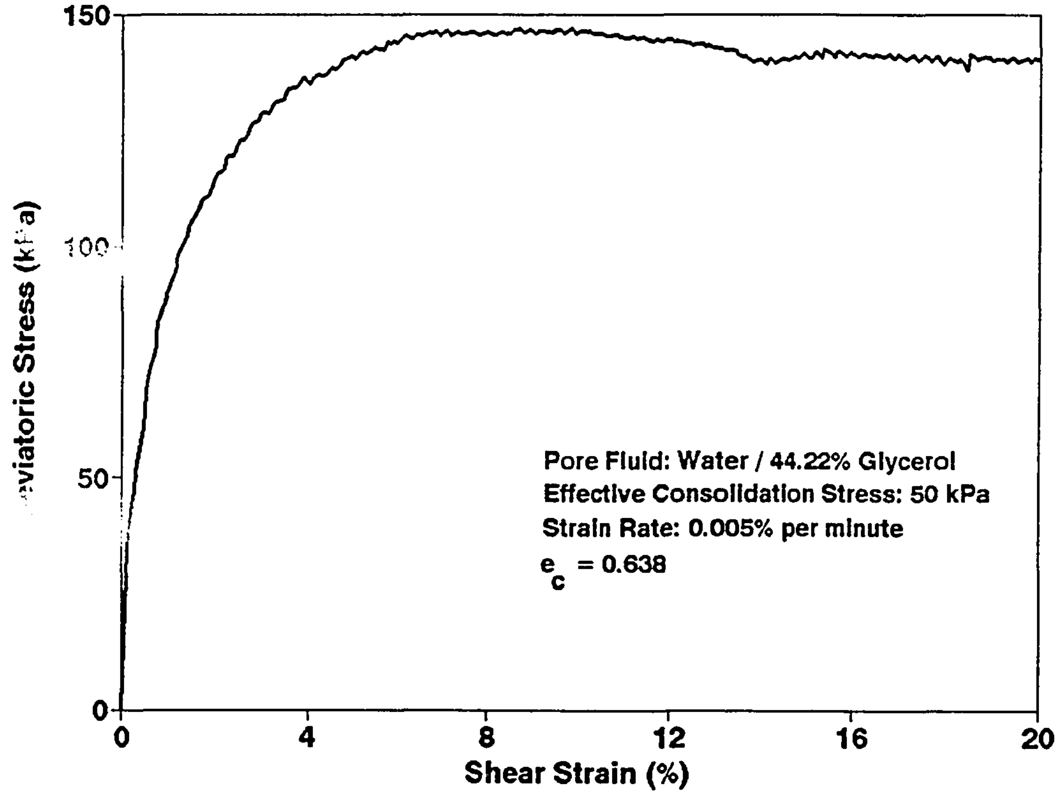

Figure B.19 Variation of Deviatoric Stress with Shear Strain for test D-50.

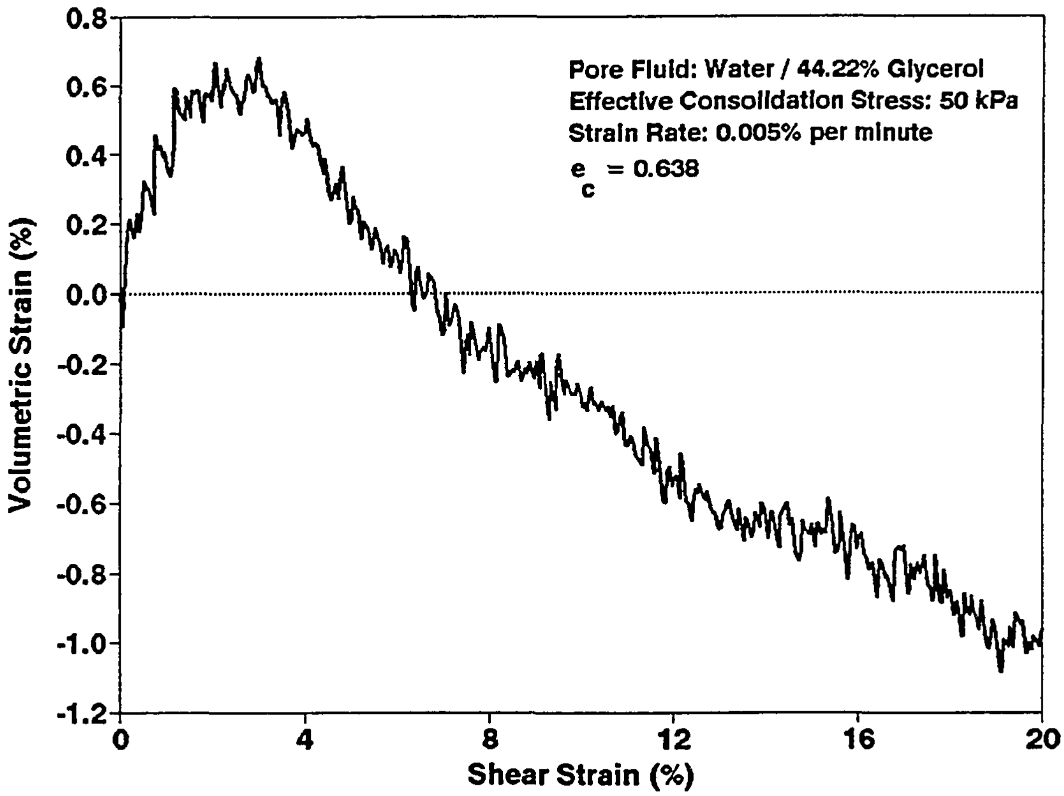

Figure B.20 Variation of Volumetric Strain with Shear Strain for test D-50.

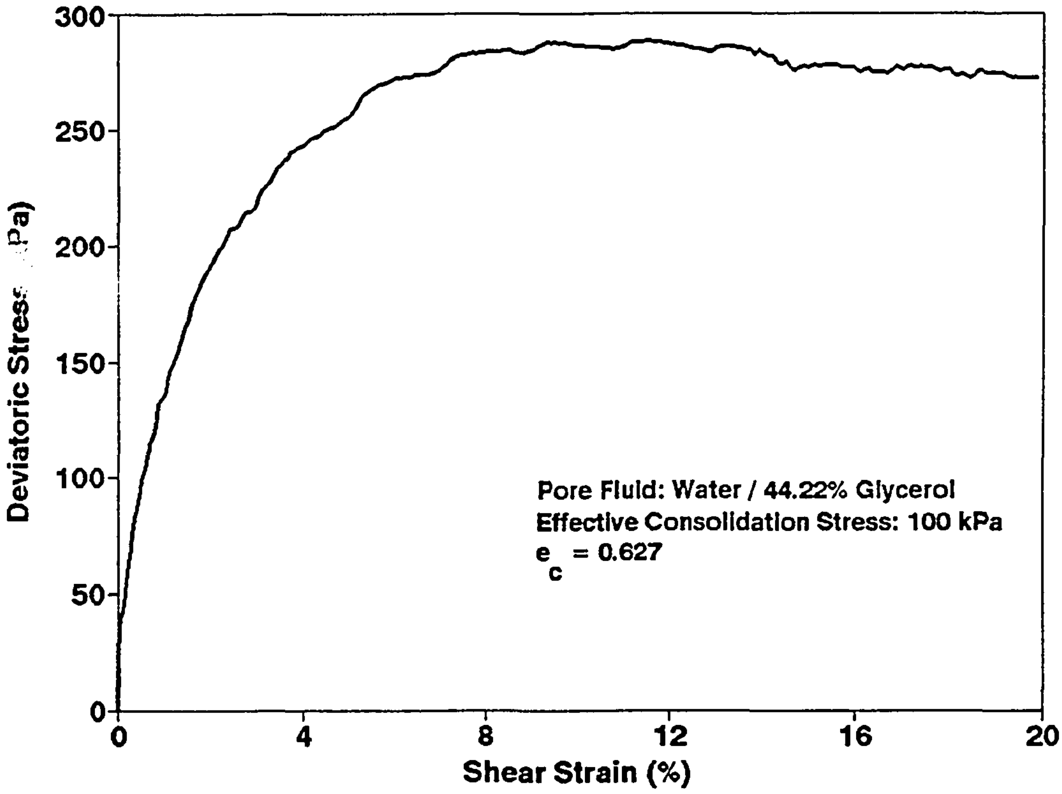

Figure B.21 Variation of Deviatoric Stress with Shear Strain for test D-100.

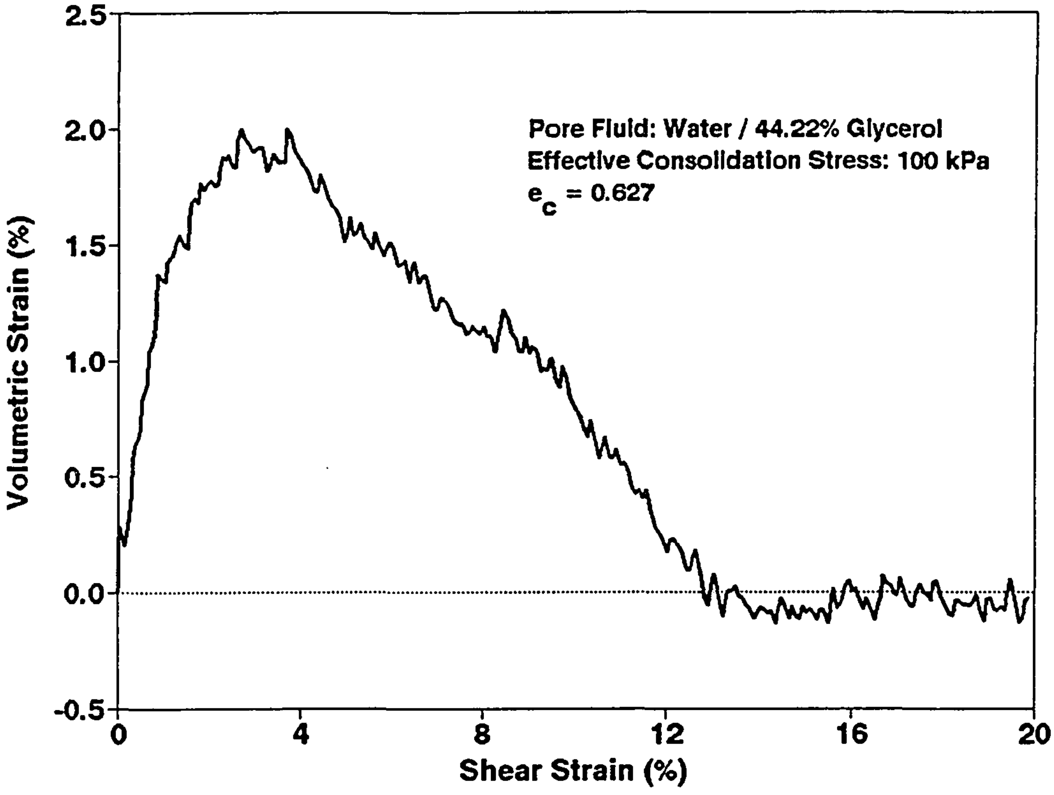

Figure B.22 Variation of Volumetric Strain with Shear Strain for test D-100.

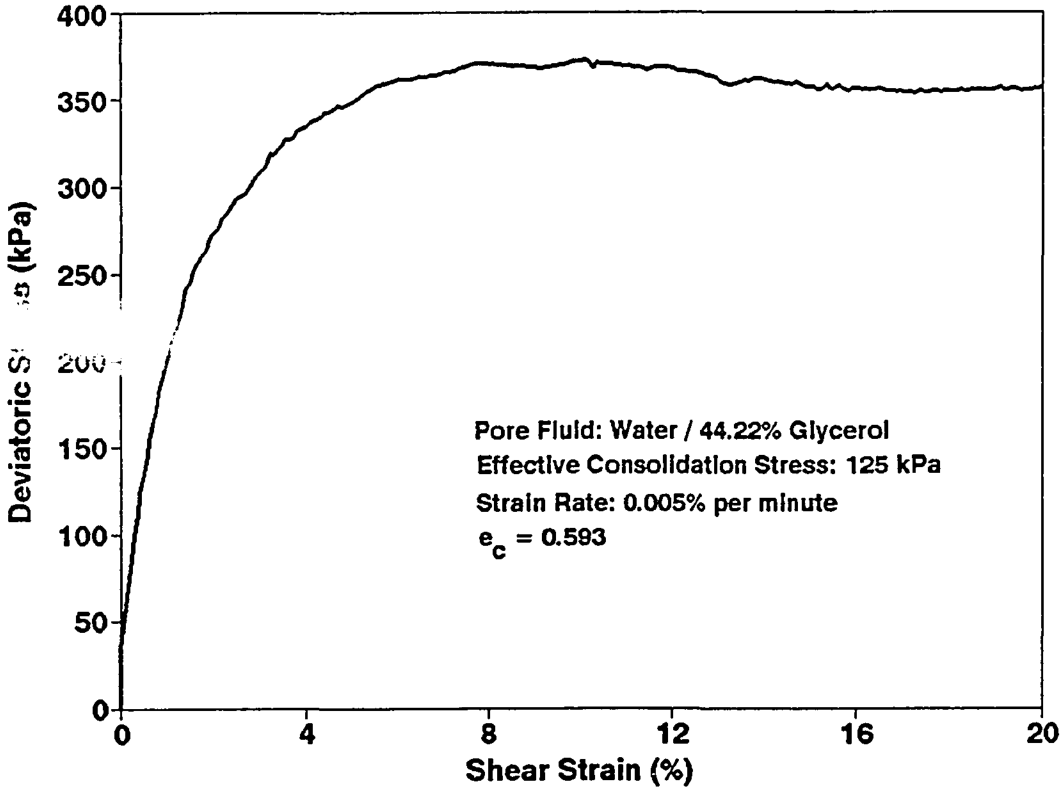

Figure B.23 Variation of Deviatoric Stress with Shear Strain for test D-125.

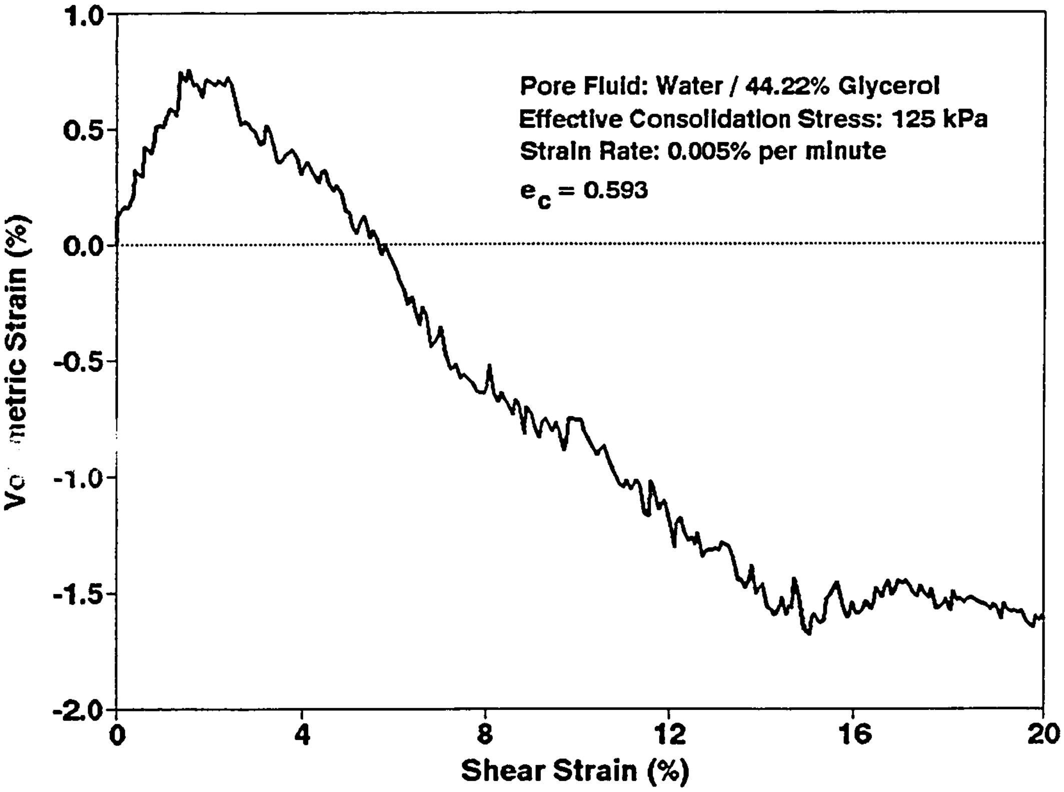

Figure B.24 Variation of Volumetric Strain with Shear Strain for test D-125.

APPENDIX C
TRUBAL and Viscous Modification

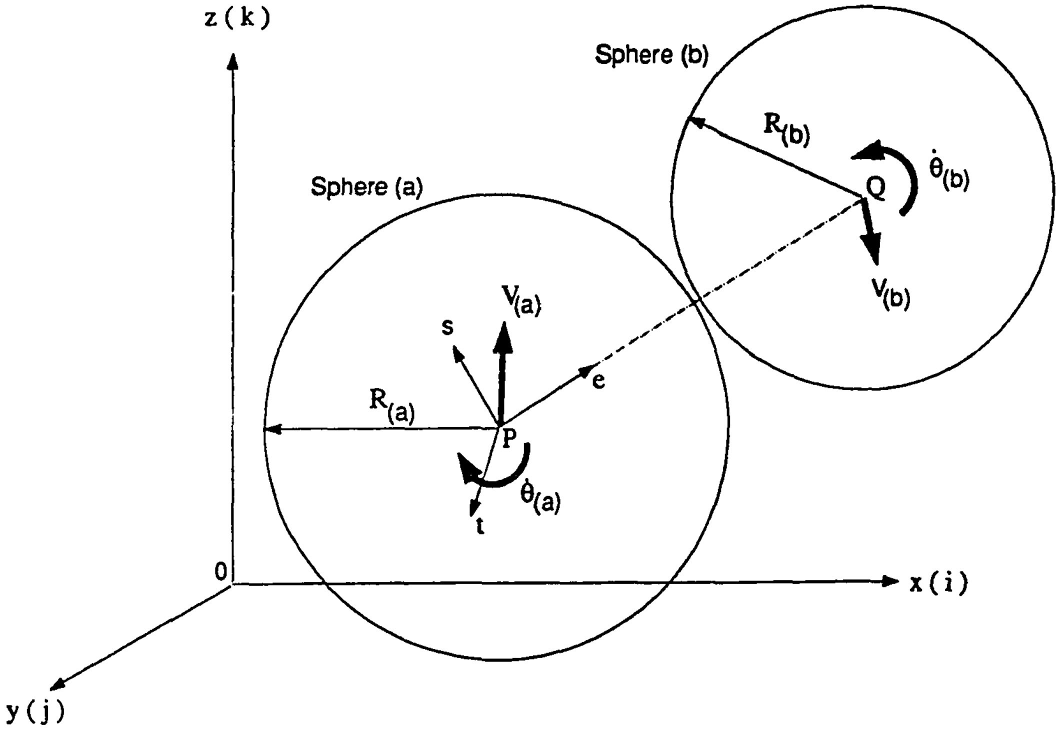

i, j, k - Unit Vectors in Global Cartesian Co-ordinate system
t,s, e - Unit Vectors in Local Cartesian Co-ordinate system

Figure C.1 Kinetics of Two Spheres as Modeled in TRUBAL

C.1 Formulation of Subroutines FORD and MOTION

In the numerical scheme employed in TRUBAL, the interactions and movements of particles are monitored, particle by particle, at each contact point, at each time step by cyclic application of Force-Displacement law and Newtons Second Law of motion. This is achieved by alternating the computation between subroutines FORD and MOTION.

C.1.1 Mathematical Formulation for Subroutine FORD

In the subroutine FORD, force displacement laws are applied at each contact for each sphere to find the forces acting at each contact, and the vectorial sum of these forces are determined to yield the resultant force acting on each sphere. The mathematical formulation behind the subroutine FORD can be described as follows:

Consider two spheres (a) and (b) (Figure C.1) which are in contact having centers $x_i = (x_1, x_2, x_3)$ and $y_i = (y_1, y_2, y_3)$. The linear velocities of each sphere at their centers are given by $\dot{x}_i$ and $\dot{y}_i$. The corresponding angular velocities are $\dot{\theta}_{(a)}$ and $\dot{\theta}_{(b)}$, positive in counter-clockwise direction. The masses and radii of the spheres are $m_{(a)}$, $m_{(b)}$ and $R_{(a)}$, $R_{(b)}$ respectively.

The unit vector along the line joining the centers of the spheres, e_i, is expressed as:

$$e_i = \frac{y_i - x_i}{D} \tag{C.1}$$

where D is the distance between the centers of the spheres. The two spheres will be in contact when D is less than or equal to the sum of their radii. The incremental forces at the points of contact are determined from the relative displacements in the normal and tangential directions, Δn and Δs, and are given by:

$$\Delta F_n = k_n \Delta n \tag{C.2}$$

$$\triangle F_s = k_s \triangle s \tag{C.3}$$

where k_n and k_s are the normal and shear stiffnesses of the two spheres. The normal and tangential displacements $\triangle$ n and $\triangle$ s are obtained by numerically integrating the relative velocities in the normal and tangential directions. The relative velocity, between the two contact points $P_{(a)}$ and $P_{(b)}$ may be expressed as:

$$\dot{X}_i = (\dot{x}_i - \dot{y}_i) - \left(\dot{\theta}_{(a)}R_{(a)} + \dot{\theta}_{(b)}R_{(b)}\right) \tag{C.4}$$

The normal and tangential components of the relative velocities are obtained from the dot product of the relative velocity vector with e_i and t_i respectively. They are expressed as:

$$|\dot{n}_i| = \dot{X}_i.e_i = (\dot{x}_i - \dot{y}_i).e_i - \left(\dot{\theta}_{(a)}R_{(a)} + \dot{\theta}_{(b)}R_{(b)}\right).e_i \tag{C.5}$$

$$s_i = \dot{X}_i - \left(\dot{X}_i.e_i\right)e_i \tag{C.6}$$

The relative displacements $\triangle n$ and $\triangle s$ are expressed as:

$$|\triangle n| = |\dot{n}|\triangle t \tag{C.7}$$

and

$$|\triangle s| = |\dot{s}|\triangle t \tag{C.8}$$

At each time step, the force increments $\triangle F_n$ and $\triangle F_s$ are added to the sum of all force increments, $(F_n)_{N-1}$ and $(F_s)_{N-1}$, determined for the previous time step and are expressed as:

$$(F_n)_N = (F_n)_{N-1} + \triangle F_n \tag{C.9}$$

$$(F_s)_N = (F_s)_{N-1} + \Delta F_s \tag{C.10}$$

where indices N and N-1 refer to forces corresponding to current time step, t_N, and to the previous time step, t_{N-1} and $\Delta t = t_N - t_{N-1}$. Relative translation between two grains is assumed to occur when the tangential force exceeds the maximum permissible resisting force calculated from the Mohr-Coulomb law for the granular material. Once the F_s is computed, it is checked against a Coulomb-type friction law expressed as:

$$|F_s|_{max} = |F_n| \tan \varphi_{mic} \tag{C.11}$$

where φ_{mic} is the inter-particle friction angle between contact surfaces of the spheres. Once the forces F_n and F_s are computed for a given time step for a given sphere, the sum of forces and the moments for the system of particles can be found. The resultant force acting on each sphere is used to compute the average stress tensor. The resultant forces and moments, according to Newton's second law are used to determine the linear and angular accelerations for the next time-step.

C.1.2 Mathematical formulation of Subroutine MOTION

The subroutine Motion uses Newton's second law of motion to find the new acceleration for each particle subjected to the forces computed by subroutine FORD. An explicit numerical scheme is employed to find the local velocities and displacements produced by these acceleration at the end of a time step. The mathematical formulation for subroutine MOTION can be given as follows.

The resultant force and moment computed in the previous cycle are considered to be constant during the time interval Δt from $t_{N-1/2}$ to $t_{N+1/2}$. For any sphere (a), according to Newton's second law of motion, the linear and angular acceleration can be obtained by calculating the resultant force and moment acting on sphere (a) (see Figure C.1) due to all the contacts and may be expressed as:

$$m_{(a)}\ddot{x}_i = \sum F_{(a)i} \tag{C.12}$$

$$I_{(a)}\ddot{\theta}_i = \sum M_{(a)} \tag{C.13}$$

where $m_{(a)}$, $I_{(a)}$ are mass and moment of inertia of sphere (a). The summation of forces (equation (C.12)) and moments (equation (C.13)) is taken over all the contact points of (a). The forces and moments acting on each disc due to contact are used to compute the new linear and angular accelerations for the next time step. These accelerations in turn determine the new linear and angular velocities and displacements as shown below.

$$(\dot{x}_i)_{N+1/2} = (\dot{x}_i)_{N-1/2} + \left[\frac{\sum F_{(a)i}}{m_{(a)}}\right]_N \Delta t \tag{C.14}$$

$$\left(\dot{\theta}_i\right)_{N+1/2} = \left(\dot{\theta}_i\right)_{N-1/2} + \left[\frac{\sum M_{(a)}}{I_{(a)}}\right]_N \Delta t \tag{C.15}$$

Therefore,

$$(x_i)_{N+1} = (x_i)_N + (\dot{x}_i)_{N+1/2}\Delta t \tag{C.16}$$

$$(\theta_i)_{N+1} = (\theta_i)_N + \left(\dot{\theta}_i\right)_{N+1/2}\Delta t \tag{C.17}$$

TRUBAL does not include damping forces associated with applied strain. The only damping mechanism provided is the damping of the motion at global level relative to the straining of space. Therefore, for higher loading rates, more damping should be provided. The global damping constants C and C* are considered to be proportional to the mass and the moment of inertia of each sphere as shown below.

$$C = \alpha m_{(a)}$$

$$C^* = \alpha I_{(a)}$$

where α is a constant determined based on the numerical stability of the program. When damping is present, the equations of motion (C.12) and (C.13) can be written as:

$$m_{(a)}\ddot{x}_i = \sum F_{(a)i} - C\dot{x}_i \tag{C.18}$$

$$I_{(a)}\ddot{\theta}_i = \sum M_{(a)} - C^*\dot{\theta}_{(a)} \tag{C.19}$$

The velocities for the next time-step can be discretized as:

$$(\dot{x}_i)_N = \frac{1}{2}\left[(\dot{x}_i)_{N-1/2} + (\dot{x}_i)_{N+1/2}\right] \tag{C.20}$$

and

$$\left(\dot{\theta}_i\right)_N = \frac{1}{2}\left[\left(\dot{\theta}_i\right)_{N-1/2} + \left(\dot{\theta}_i\right)_{N+1/2}\right] \tag{C.21}$$

which yields new linear and angular velocities:

$$(\dot{x}_i)_{N+1/2} = (\dot{x}_i)_{N-1/2}\left[1 - \alpha\frac{\Delta t}{2}\right] + \sum \left(F_{(a)i}\right)_N \frac{\Delta t}{m_{(a)}} \Big/ \left(1 + \alpha\frac{\Delta t}{2}\right) \tag{C.22}$$

$$\left(\dot{\theta}_{(a)}\right)_{N+1/2} = \left(\dot{\theta}_{(a)}\right)_{N-1/2}\left[1 - \alpha\frac{\Delta t}{2}\right] + \sum \left(M_{(a)i}\right)_N \frac{\Delta t}{I_{(a)}} \Big/ \left(1 + \alpha\frac{\Delta t}{2}\right) \tag{C.23}$$

and new linear and angular displacements:

$$(x_i)_{N+1} = (x_i)_N + (\dot{x}_i)_{N-1/2}\left[1 - \alpha\frac{\Delta t}{2}\right] + \sum \left(F_{(a)i}\right)_N \frac{\Delta t}{m_{(a)}} \Big/ \left(1 + \alpha\frac{\Delta t}{2}\right) \tag{C.24}$$

$$(\theta_{(a)})_{N+1} = (\theta_{(a)})_N + \left(\dot{\theta}_{(a)}\right)_{N-1/2}\left[1 - \alpha\frac{\Delta t}{2}\right] + \sum (M_{(a)})_N \frac{\Delta t}{I_{(a)}} \Big/ \left(1 + \alpha\frac{\Delta t}{2}\right) \tag{C.25}$$

Equations (C.24), (C.25), and (C.23) give the new position, orientation and the angular velocity respectively, of each sphere for the next time-step. The velocity due to prescribed strain rate and the velocity due to contact (Equation (C.22)) determine the resultant velocity of each sphere for the next time-step.

C.2 User Manual for TRUBAL

CReate x y z isize isurf

A sphere is created at location (x,y,z) with size type isize and surface type isurf. A radius must have been already defined for size type isize - see the Radius command. Currently TRUBAL allows 5 size-types (1 through 5) and 5 surface-types. TRUBAL does not prevent overlapping particles from being specified, but it make no sense.

Cycle n [S0] v
[S1MS2] v
[S22] v
[S33] v
[RING] v

The program executes n calculation cycles, and returns control to the user (or input file) when they are complete.

The optional keywords denote that the servo-control will attempt to hold the specified variable constant at the value of v. Keyword S0 corresponds to mean stress, σ_o, where $\sigma_o=(\sigma_{11}+\sigma_{22}+\sigma_{33})/3$. Keyword S1MS2 is similar, but corresponds to the two dimensional mean stress $(\sigma_{11}+\sigma_{22})/2$. Individual stresses, σ_{11}, σ_{22}, and σ_{33} are controlled by the keywords S11, S22 and S33, respectively. Ring controls the angle of major principal stress in a ring shear test.

Combinations of control keywords may be used when this physically reasonable. See related commands Gain and Mode.

DAamping frac freq imass istiff

Damping is specified in terms of the Rayleigh damping parameters: frac is the fractional of critical damping at the modal frequency freq. Rayleigh damping involves mass proportional damping and stiffness proportional damping: the former may be switched off by giving imass as 1, and the latter may be switched off by giving istiff as 1. Otherwise these parameters should be set to zero for full Rayleigh damping. Note that stiffness proportional damping requires a reduction in time step for numerical stability. If in doubt, give istiff as 1.

Density d isize

d is taken as the mass-density of all particles of size type isize

Fix ix iy iz irx iry irz iadd
All

The translational or angular velocity of any particle may be held constant by setting the appropriate parameter equal to 1: ix, iy and iz control the x, y and z velocities, and irx, iry and irz the angular velocities about the x, y and z axes, respectively. The constrains may be removed by setting the parameters to zero. The final parameter, iadd, is the address of the particle to be fixed. If the word All is substituted, then all particles are affected. Note that the Fix command does not set velocities to zero - see the Zero command.

FRAction f

The fraction of critical time-step is set to f. The critical time stop Δt_{crit} is calculated by TRUBAL on the basis of one sphere, acted on by one set of linear normal and shear springs (as given by the Norm and Shear commands). The smallest mass and the largest stiffness are used. In a real assembly, each particle is acted on by several springs. To allow for this increase in apparent stiffness, Δt_{crit} is reduced by factor f, which is typically taken as 0.05 for a three dimensional assembly. If numerical instability is suspected, f should be reduced even further.

FRiction amu isurf jsurf

The friction coefficient is set to amu for contact between two particles of surface types isurf and jsurf. Note that the friction is given as a coefficient, not as an angle.

GAIN g edmax

The servo gain, g, and the allowed strain-rate, edmax, are set. In mode 0 (see Mode command), the parameter g represents $\Delta\dot{\epsilon}/\sigma_{\text{error}}$, where $\Delta\dot{\epsilon}$ is the change in grid strain-rate that occurs for an error in the controlled stress of σ_{error}. The controlled stress is the one given on the Cycle command, and the "error" is the difference between the given value and the measured value for the assembly of particles. For mode 1 operation, the parameter g is $\dot{\epsilon}/\sigma_{\text{error}}$. The optimum value of g is, to some extent, a matter of trial and error. If it is too high, the servo will 'hunt' or will be unstable; if g is too low, the servo will be sluggish and the error may be too large.

GENerate n isize isurf

n particles of size isize and surface type isurf are generated randomly over the whole volume of periodic space. No effort is made to fit particles into gape between other particles: if a candidate particle overlaps an existing particle, it is rejected and another one is tried. Before giving this command, a radius must already have been defined for the size type isize. If several sizes of particles are to be combined in an assembly, the larger ones should be generated first, since it is easier to fit small particles into gaps than large particles.

In the second form of the command (Gen Seed n) no particles are generated, but the random number generator produces n numbers that are discarded. This is useful when generating different distributions of the same particles.

GRAvity gx gy gz

Gravitational accelerations are prescribed for each of the coordinate directions. Note that gravity is not meaningful when full periodic boundaries are in effect.

GRID ed11 ed22 ed33 ed12 ed23 ed31

The strain-rates, $\dot{\epsilon}_{11}$, $\dot{\epsilon}_{22}$, $\dot{\epsilon}_{33}$, $\dot{\epsilon}_{12}$, $\dot{\epsilon}_{23}$, and $\dot{\epsilon}_{31}$ of periodic space are set. Not that the strain-rates $\dot{\epsilon}_{23}$, and $\dot{\epsilon}_{31}$ are not used, although they should be entered on the Grid command as zero. The components $\dot{\epsilon}_{11}$, $\dot{\epsilon}_{22}$ and $\dot{\epsilon}_{33}$ cause the periodic volume to change shape. However, the component $\dot{\epsilon}_{12}$ does not distort the periodic volume in shear; rather, there is a step in x or z displacement between bottom y-boundary and the top y-boundary. This step is shear is printed out when the Print Grid command is given.

HERTZ gmod poiss isize

This command causes TRUBAL to use a nonlinear contact law, based on the Hertz-Mindlin theory. Parameter gmod is the shear modulus and poiss is the Poisson's ratio of the solid material of the spheres. These properties are for particles of size-type isize. In this version of TRUBAL, no attempt is made to allow for different properties of the two particles comprising a contact: the properties are simply derived from one of them. Both normal stiffness and shear stiffness depend on normal force in a nonlinear way, but partial sliding is not modelled - for more details, see reference 9.

It is important to note that the time-step calculation does not recognise the Hertz contact formulation - therefore shear and normal stiffnesses should be given that correspond to the equivalent Hertz-contact stiffnesses at the prevailing stress level. These linear stiffness (given by the shear and Normal commands are only used to compute the time-step, and are not used in the mechanical calculation when Hertz mode is in effect.

Iset k iadd

The integer k is inserted into the main memory array IA() at address iadd. Great caution is needed when using this command.

Log On
OFF

This command Log On causes all commands, comments, error messages, etc., to be reproduced on a file TRUBAL.OUT. The command Log OFF suppresses this echo function, except for output from the Print command.

Mode n

This selects the type of servo control. Mode O, which is the default, selects ''velocity increment control," in which the increment in grid velocity is proportional to the error (difference between measured value and desired value). Mode 1 selects "velocity control," whereby the grid velocity is set directly by the servo. In mode 0, the increments are added to the velocities prescribed by the user: it is used normally when doing a test in which the strain rate is expected to approach a steady state. Mode 1, however, ignores any strain-rate that may have been given: it is useful for getting to an equilibrium condition of zero velocity. In such a case the mode 0 servo would be unsatisfactory because it would continue to ''hunt," without coming to final equilibrium. In the present version of TRUBAL, mode 1 only works for control of mean stress in 3-D: σ_0.

New

This program returns to the point at which it expects a Start or Restart command. The date for the current problem is lost from memory.

NOrmal akn isurf jsurf

The normal stiffness is set to akn for contact between two particles of surface types isurf and jsurf. The contact stiffness is a linear relation between normal force and normal displacement. See also command Hertz.

Plot **BOund**
Disks
Forces
Rdisp
ROtation
Save
Velocity

Wall
Wcap

The plot command produces plots of the x-y plane from TRUBAL when it is operating in 2-D mode. The 'plots' are in the form of PostScript directives on a file called TRB.PS. This file is sent to a laser printer that has PostScript capability. Each Plot command produces one plotted page. Parameter Bound produces a plot of the boundary of periodic space. Shaded circles are plotted with the Disks. The Force parameter produces a series of lines that corresponds to contact forces, where line thickness is proportional to force magnitude. The Save parameter does not produce a plot, bit it causes the current state to be saved in a memory buffer: this saved state is necessary before using parameters Rdisp and Rotation, which produce, respectively, Plots of relative displacement and relative rotation. Typical usage is:

```
plot save
cycle 200
plot bound rdis
```

In this example, the incremental displacement vectors corresponding to a 200-cycle interval will be plotted. the keyword Vel causes velocity vectors to be plotted. The final two keywords, Wall and Wcap, are described under the command Wall.

PRint **Balls**
Chist
Contacts [All]
[Gap]
Entries
Grid
Info
Map

Partitions
Stress

Printout is made of various things. The above parameters correspond, respectively, to: balls, contact histogram, contacts, box entries, grid size, general information, memory map, stress partitions, and stress tensor. The optional keyword All (after the Contact parameter) requests that all contacts are printed, rather than just those taking load, which is the default. The optional keyword Gap causes only contact overlaps and normal forces to be printed. Several keywords may be gain on the same line. To reduce the amount of output, the Window command may be given prior to the Print command.

PRObe **E11**
E22
E33
E12
E23
E31
E1M2
E1M3
E3M1

This command causes an strain increment to be made at the current state. The resulting modulus (stress/strain) is printed out. Only one of the above keywords may be given per Probe command: they correspond, respectively, to probes of Δe_{11}, Δe_{22}, Δe_{33}, Δe_{12}, Δe_{23}, and Δe_{31}, is done, and restored afterwards. During the probe, 500 cycles are done at zero strain, to get a "baseline" state; then 250 cycles of probe are done, and finally 500 cycles of zero strain are done. So a Probe takes quite a time to execute.

RAdius r isize

r is taken as the radius of particles of size type isize.

RESet

Accumulated rotations are set to zero. This has no effect on the mechanical behavior, since only incremental rotations are used in the calculation. Note that the rotations are simply the summation, over time, of the incremental rotations. They have no physical meaning, since the three components of rotation do not constitute a vector.

Restart [filename]

A previously-saved problem is restored from the file filename. If a file name is not given, a default file name of SAVE.SAV is assumed. The command Restart may only be given as the first command of a run or as the first command after a New command.

Rset r iadd

The real number r is inserted into the main memory array IA() at address iadd. Great caution is needed when using this comend.

SAve [filename]

The current problem state is saved on the file filename. If a file name is not given, a default file name of SAVE.SAV is assumed. If a file name is specified that already exists, the existing data is over-written. The saved state records all positions, velocities, forces, options and so on, at a given stage in a run; it corresponds to a 'snapshot' at a single point in time. The Save command does not record a sequence of commands.

SHear aks isurf jsurf

The shear stiffness is set to aks for contact between two particles of surface types isurf and jsurf. The contact stiffness is a linear relation between shear force and shear displacement. See also command Hertz.

Start xmax ymax zmax nbox nball nwall [Log]

This command (or the Restart command) must be the first one given to TRUBAL. The parameters xmax, ymax and zmax are the total widths of the box volume (also the periodic volume) in the x,y and z directions, respectively. nbox is the number of boxes requested, and nball is the maximum number of spheres that may be needed - there is no problem if fewer spheres are subsequently generated: the purpose of the Start command is to allocate enough memory to hold all the required boxes and particles. The parameter nwall is not used at present, and should be set to zero. The optional keyword Log turns the 'log' facility on immediately: i.e. output is echoed to the output file TRUBAL.OUT.

Stop

TRUBAL stops. The current state of the problem is not saved automatically - see command Save.

WALL	**Gain**	g	
	Nstress		sig
	Pos	ybot	ytop
	Vel	vmax	
	Xvel	xvbot	xvtop

This command sets up two sheets of particles that are controlled in velocity: they resemble rough walls. The 'walls' are perpendicular to the y axis, and can be given x velocities in order to do a shear test. The y velocities are controlled by a servo-mechanism so as to keep the average normal stress on the walls constant. Before the first WAll command is given, a stable, compacted sample must exist. The lower (low-y) and upper (high-y) wall positions are specified, respectively, by ybot and ytop, following the keyword Pos. All particles that are intersected by the two planes (at y=ybot and x=ytop) are 'captured' by the walls, and are controlled in any subsequent tests. Particles above the top wall and below the bottom wall are marked as inactive during the calculation cycle. The positions of the two planes may be plotted by the Plot Wall command, and in 2-D mode, the controlled particles may be plotted by the Plot Wcap command, which plots white circles rather than shaded circles. Keyword Xvel is used to specify the x velocities of the lower and upper walls: xvbot and xvtop, respectively. The servo control resembles that described under commands Cycle and Gain; for the wall servo, gain is specified as g, following the Gain keyword, and the limit to velocity is vmax, following the Vel keyword. The wall servo operates in velocity-increment mode - see the Mode command. Reference 10 provides an example of wall use. WARNING! The Wall logic has never been tested in 3-D mode, and probably do not work in 3-D.

Window x1 x2 y1 y2 z1 z2

This command limits the volume of space that is addressed by the Print command, when it is printing out information on spheres, contacts, etc. The volume is:

$x1 < x < x2$

$y1 < y < y2$

$z1 < z < z2$

Zero

Translational velocities of all particles are set to zero.

2-D

This command causes TRUBAL to operate in two-dimensional mode. The particles are still regarded as spheres, but they are constrained to move in the x-y plane only. Although the equations of motion are truncated to two dimensions, the force-displacement calculation (subroutine FORD) still operates in three dimensions. This could be modified, to improve running speed. In 2-d mode, the generation routine sets the z coordinate of all particles to the same value- corresponding to the center of the box volume in the z direction. Only one box should be specified in the z direction, although TRUBAL will not complain if more are requested.

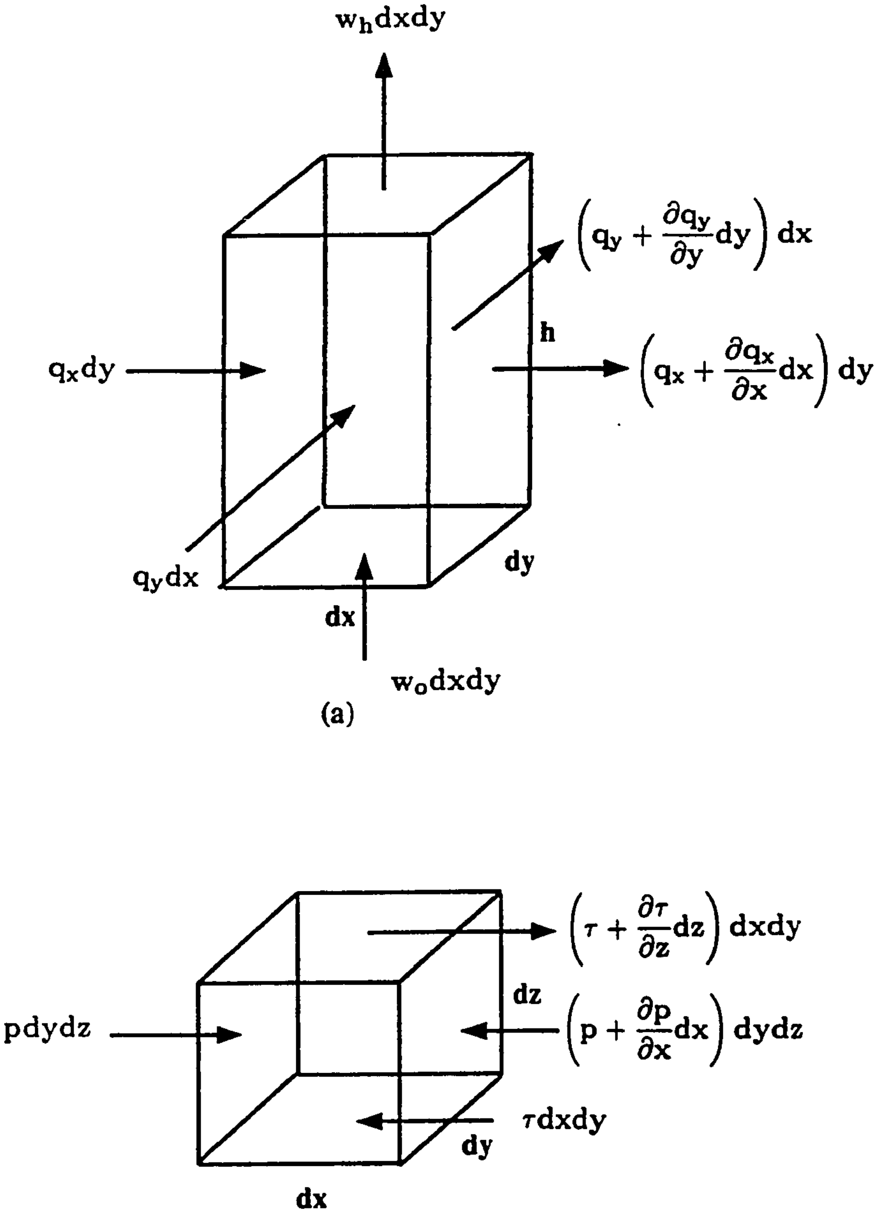

Figure C.2 (a) Continuity of Flow in a Fluid Column, (b) Equilibrium of a Fluid Element.

C.3 Derivation of Reynolds Equation

The Reynolds equation is derived based on the continuity of a fluid column and the force equilibrium of an element of fluid. In the derivation of Reynolds equation the following assumptions are made.

1. All body forces acting on the fluid are neglected.
2. The pressure is constant through the thickness of the film, since the film thickness is very small compared to the dimensions of the lubricated spheres.
3. There is no slip at the boundaries. The velocity of the fluid layer adjacent to the boundary is the same as that of the boundary.
4. The lubricant is Newtonian, *i.e.* the shear stress is proportional to rate of shear.
5. Flow is assumed to be laminar since only small strain-rate deformations are considered.
6. Fluid Inertia is neglected. Several studies have shown that even if Reynolds number is 1000, the pressures are modified only by about 5 per cent.
7. The viscosity is constant through the film thickness; a simplifying assumption, to avoid great complexities that would otherwise result.

Consider a column of fluid of height h and base dx, dy (Figure C.2(a)). Fluid flows into the column from the left at a rate q_x per unit width. The volume flow rate is ($q_x$dy), since the column is dy wide. The rate of flow out per unit width is

$$\left(q_x + \frac{\partial q_x}{\partial x} dx\right)$$

where $\partial q_x/\partial x$ is the rate of change of flow in the x direction, and dx is small enough to treat $\partial q_x/\partial x$ as linear. The actual flow out of the column in x direction is:

$$\left(q_x + \frac{\partial q_x}{\partial x} dx\right) dy$$

Similarly, the inflow in the y direction is $q_y dx$ and the outflow is:

$$\left(q_y + \frac{\partial q_y}{\partial y} dy\right) dx$$

As for the flow in the z direction, since the top surface moves at a relative velocity of w_2—w_1 in the positive z-direction, the change in the confined volume is $(w_2$—$w_1)dxdy$. For continuity of flow, the fluid being of constant density, the difference between the inflow and outflow in the x and y directions which is the flow accumulated within the column should be the same as the change in confined volume.

$$\left[q_x - \left(q_x + \frac{\partial q_x}{\partial x} dx\right)\right] dy + \left[q_y - \left(q_y + \frac{\partial q_y}{\partial y} dy\right)\right] dx = (w_2 - w_1) dxdy \qquad \text{(C.26)}$$

Hence

$$\frac{\partial q_x}{\partial x} + \frac{\partial q_y}{\partial y} + (w_2 - w_1) = 0$$

Consider the forces acting on a small element of fluid, of sides dx, dy and dz (Figure C.2(b)). The pressure p acting on the left of the element gives rise to a force pdydz in x direction. On the opposite face, the pressure being $(p + \partial p / \partial x dx)$ the corresponding forces is:

$$\left(p + \frac{\partial p}{\partial x} dx\right) dydz$$

There are shear stresses acting on the top and bottom faces, producing forces. On the bottom face the shear stress τ gives a force ($\tau dxdy$) acting to the left. On the top, the shear stress being $\tau + (\partial \tau / \partial z) dz$, acting to the right is a force

$$\left(\tau + \frac{\partial \tau}{\partial z} dz\right) dxdy$$

The forces acting to the left and right balancing each other, the equilibrium of all these forces in x direction can finally be reduced to the following relation.

$$\frac{\partial \tau}{\partial z} = \frac{\partial p}{\partial x}$$

Combining the above equation with the Newton's viscosity relation $\tau = \eta(\partial u/\partial z)$ will give

$$\frac{\partial p}{\partial x} = \frac{\partial}{\partial z}\left(\eta \frac{\partial u}{\partial z}\right) \tag{C.27}$$

Similarly, the force equilibrium in the y direction yields

$$\frac{\partial p}{\partial y} = \frac{\partial}{\partial z}\left(\eta \frac{\partial v}{\partial z}\right)$$

Consider equation (C.27) further. This equation can be integrated with respect to z, since p is not a function of z, thus

$$\eta u = \frac{\partial p}{\partial x}\frac{z^2}{2} + C_1 z + C_2 \tag{C.28}$$

Considering the limiting velocities u_1, u_2 at z=0, z=h, the velocity u in the x direction at any point z in the film is given by:

$$u = \frac{1}{2\eta}\frac{\partial p}{\partial x}(z^2 - zh) + (u_1 - u_2)\frac{z}{h} + u_2$$

The flow rate in the x direction per unit width of y, using the relation

$$q_x = \int_0^h u\,dz$$

yield

$$q_x = \frac{-h^3}{12\eta}\frac{\partial p}{\partial x} + (u_1 + u_2)\frac{h}{2} \tag{C.29}$$

Similarly, the flow rate in the y direction, q_y is

$$q_y = \frac{-h^3}{12\eta}\frac{\partial p}{\partial y} + (v_1 + v_2)\frac{h}{2} \tag{C.30}$$

where v_1, v_2 correspond to velocities in the y direction.

Combining equations (C.26) through (C.30) the mass transfer equation expressed in rectangular coordinates can be given as:

$$\frac{\partial}{\partial x}\left(\frac{h^3}{\eta}\frac{\partial p}{\partial x}\right) + \frac{\partial}{\partial y}\left(\frac{h^3}{\eta}\frac{\partial p}{\partial y}\right) = 6\left\{\frac{\partial}{\partial x}(u_1 + u_2)h + \frac{\partial}{\partial y}(v_1 + v_2)h + 2(w_2 - w_1)\right\} \tag{C.31}$$

This is the Reynolds equation in three dimension.

C.4 LUB Fortran Source Code

```
c   PROGRAM LUB
c
c   Computes the pressure distribution due to lubrication of two
c   sphere
c   Involves Gauss-Seidel type solution of Reynold's equation
c   on a circular projected area. There are M and N grid spacings
c   in the x and y directions respectively
c   dx is the spacing between two nodes in both x and y directions
c   The pressure p(i,j) is zero along the curved portion of the
c   boundary
c   Interpolation of degree two is employed at the boundary points.
c
c
c   Prasanna Ratnaweera
c   May 1992
c
c   with modified boundary conditions: relative velocity &
c   absolute rotation
c
      implicit real*8(a-h,o-z)
      parameter(ng=21)
      common/blku/u,udot,thu,thdotu,rad1,v,vdot,thv,thdotv,rad2
     *,h0,iab1,iab2,dminim,dmaxim
      common/blkr/rprime
      common/blkm/h01
      common/blkgrid/dx,x0,y0,r0,m,n,xx,yy,psi,itype,jlow,jhigh
      common/blk1/e,t,s
      common/blkvel/u1,v1,w1,u2,v2,w2,eta
      common/blkcon/a1,a2,a3,a4,nnumber
      common/blkpres/ iter,eps,sumfx,sumfy,sumfz
      dimension u(3),udot(3),thu(3),thdotu(3)
      dimension v(3),vdot(3),thv(3),thdotv(3)
      dimension undot(3),vndot(3),thndotu(3),thndotv(3)
      dimension e(3),urel(3),t(3),s(3)
      dimension xx(ng,ng),yy(ng,ng)
      dimension u1(ng,ng),v1(ng,ng),w1(ng,ng)
      dimension u2(ng,ng),v2(ng,ng),w2(ng,ng)
      dimension a1(ng,ng),a2(ng,ng),a3(ng,ng),a4(ng,ng)
      dimension itype(ng,ng),psi(ng,ng),jlow(ng),jhigh(ng)
      nnumber=1
```

```
c .
c   reading data from lub.dat file
c   reads global data for two spheres
c
c
      open(3,name='value.dat',status='old')
      read(3,*) iib,jjb,kkb,llb
      read(3,*) iif,jjf,kkf,llf
      open(4,name='h.dat',status='new')
      m=20
      n=20
      rad1=10.
      rad2=10.
      dminim=.1
      dmaxim=1.
      ncounter=0
      nstart=0
      do 120 i=iib,iib
      do 105 j=1,jjf
      do 110 k=1,kkf
      do 115 l=1,llf
      ncounter=ncounter+1
      if((i.eq.iib).and.(j.eq.jjb).and.(k.eq.kkb).and.(l.eq.llb))
     *nstart=1
      if(nstart.eq.1)goto 119
      goto 115
119       h=(i-1)*.125-3.0
      ww1=(j-21)
      tx=(k-1)*0.002
      ty=(l-1)*0.002
      ww1=ww1/200.0
      if (k.gt.l)goto 115
      udot(1)=0.0
      udot(2)=0.0
      udot(3)=0.0
      vdot(1)=0.0
      vdot(2)=0.0
      vdot(3)=ww1
      thdotu(1)=0.0
      thdotu(2)=0.0
      thdotu(3)=0.0
      thdotv(1)=tx
      thdotv(2)=ty
      thdotv(3)=0.0
```

```
 .  h0=h
    h01=h0
    r0=(rad1+rad2)/2.0/2.0
    if(h0.ge.dminim)then
    r0=(rad1+rad2)/2.0/2.0
c  ***********************************************
c  expanding the area of the surface
c
    else if (h0.lt.dminim)then
    space=(-h0+dminim)/2.0
    r00=(rad1+rad2+dminim)/2.0
    rprime=2.0*space*r00
    rprime=sqrt(rprime)
    if (rprime.gt.r0)then
    r0=rprime
c
c
    else if(rprime.le.r0)then
    r0=(rad1+rad2)/2.0/2.0
c
    end if
    end if
    x0=r0
    y0=r0
    dx=r0*2.0/m
c
c  computing the x,y coordinates of the square grid
c  and generate the node numbering system
    call grid
c
c  computing the unit vectors in the local directions
c
    call unit
c
c  computes velocities at each grid point on the two
c  surfaces projected from the square grid
c
    call velocity
c
c  generates the grid numbers
c
c  call gen
c
    call pres(dminim)
```

```
      write(4,15) i,j,k,l,iter,eps,sumfx,sumfy,sumfz
15       format(4(1x,i2),1x,i4,4(1x,e10.4))
      nnumber=nnumber+1
115       continue
110       continue
105       continue
120       continue
      close(3)
77       format(2x,i5,4(2x,e11.3))
      end
c     ********************************
      subroutine pres(dminim)
c
c     this subroutine determines the pressure at each node point (i,j)
c     using the Gauss-Siedel iterative scheme
c
      implicit real*8(a-h,o-z)
      parameter(ng=21)
      common/blkm/h01
      common/blkr/rprime
      common/blkgrid/dx,x0,y0,r0,m,n,xx,yy,psi,itype,jlow,jhigh
      common/blkcon/a1,a2,a3,a4,nnumber
      common/blkpres/ iter,eps,sumfx,sumfy,sumfz
      dimension a1(ng,ng),a2(ng,ng),a3(ng,ng),a4(ng,ng)
      dimension itype(ng,ng),psi(ng,ng),jlow(ng),jhigh(ng)
      dimension xx(ng,ng),yy(ng,ng)
c
c     maximum error epsmax
c     maximum number of iterations itmax
c
      epsmax=1.0e-1
      itmax=1000
      rovrdx=r0/dx
      eps=1.0e-6
      fm=m
      fn=n
c     initializes the pressures to zero
      do 10 i=1,m+1
      do 5 j=1,n+1
      psi(i,j)=0.0
5       continue
10       continue
20       format(11(2x,i2))
      mp1=m+1
```

```
c  . ....compute successively better approximations for
c   psi(i,j) at all grid points, iterating by gauss-
c   seidel method until convergence criterion is
c   satisfied.....
    iter=0
3     iter=iter+1
    eps=0.0
c
c   ............. for interior points .........
    do 25 i=1,m+1
    jl=jlow(i)
    jh=jhigh(i)
    if(jl.eq.jh)goto 25
    do 30 j=jl,jh
    savpsi=psi(i,j)
    alp1=(a1(i,j)/dx/dx+a2(i,j)/2.0/dx)*psi(i,j+1)
    alp2=(a1(i,j)/dx/dx-a2(i,j)/2.0/dx)*psi(i,j-1)
    alp3=4.0*a1(i,j)/dx/dx
    alp4=(a1(i,j)/dx/dx+a3(i,j)/2.0/dx)*psi(i+1,j)
    alp5=(a1(i,j)/dx/dx-a3(i,j)/2.0/dx)*psi(i-1,j)
    psi(i,j)=(alp1+alp2+alp4+alp5+a4(i,j))/alp3
    eps=eps+abs(psi(i,j)-savpsi)
30      continue
25      continue
c
c   ............ for boundary points
    do 7 i=1,mp1
    do 8 j=1,n+1
    savpsi=psi(i,j)
    if (itype(i,j).eq.0)then
    psi(i,j)=0.
    goto 8
    else if (itype(i,j).eq.1)then
    goto 8
    else if (itype(i,j).eq.4)then
    psi(i,j)=0.0
    goto 8
    end if
    fim1=i-1
    fjm1=j-1
    sq=(fm*fm/4.0-(fim1-fm/2.0)**2.0)
    xodxm1=fm/2.0-sqrt(sq)-fjm1
    xodxp1=fm/2.0+sqrt(sq)-fjm1
    sq=(fm*fm/4.0-(fjm1-fm/2.0)**2.0)
```

```
      yodxm1=fm/2.0-sqrt(sq)-fim1
      yodxp1=fm/2.0+sqrt(sq)-fim1
      bjm1=-1.0
      if (abs(xodxm1).le.1.0)psi(i,j-1)=0.0
      if (abs(xodxm1).le.1.0)bjm1=xodxm1
      bjp1=1.0
      if (abs(xodxp1).le.1.0)psi(i,j+1)=0.0
      if (abs(xodxp1).le.1.0)bjp1=xodxp1
      aim1=-1.0
      if (abs(yodxm1).le.1.0)psi(i-1,j)=0.0
      if (abs(yodxm1).le.1.0)aim1=yodxm1
      aip1=1.0
      if (abs(yodxp1).le.1.0)psi(i+1,j)=0.0
      if (abs(yodxp1).le.1.0)aip1=yodxp1
      bjm1=abs(bjm1)
      bjp1=abs(bjp1)
      aim1=abs(aim1)
      aip1=abs(aip1)
c
      baddj=bjm1+bjp1
      baddi=aim1+aip1
      bmulj=bjm1*bjp1
      bmuli=aim1*aip1
      bet1=(2.0*a1(i,j)/dx/dx/bjp1+a2(i,j)/dx)*psi(i,j+1)/baddj
      bet2=(2.0*a1(i,j)/dx/dx/bjm1-a2(i,j)/dx)*psi(i,j-1)/baddj
      bet3=2.0*a1(i,j)/dx/dx*(1.0/bmulj+1.0/bmuli)
      bet4=(2.0*a1(i,j)/dx/dx/aip1+a3(i,j)/dx)*psi(i+1,j)/baddi
      bet5=(2.0*a1(i,j)/dx/dx/aim1-a3(i,j)/dx)*psi(i-1,j)/baddi
      psi(i,j)=(bet1+bet2+bet4+bet5+a4(i,j))/bet3
      eps=eps+abs(psi(i,j)-savpsi)
8       continue
7       continue
      if (iter.ge.itmax)goto 14
      if (eps-epsmax)14,3,3
14        do 55 j=1,n+1
      do 60 i=1,m+1
c     write(3,70) xx(i,j),yy(i,j),psi(i,j),' '
c     write(3,*) xx(i,j),yy(i,j),psi(i,j)
60        continue
55        continue
70        format(1x,f8.3,1x,f8.3,2x,f9.1,a)
      sumfx=0.0
      sumfy=0.0
      sumfz=0.0
```

```
 . do 510 i=1,m+1
   do 520 j=1,n+1
   x1=xx(i,j)
   y1=yy(i,j)
   para1=x1*x1+y1*y1
   para1=sqrt(para1)
   forc=psi(i,j)*dx*dx
c  ********************************
c  half sommerfield condition
c
   if (forc.lt.0.0)forc=0.0
c  ********************************
   if (para1.gt.r0)goto 520
   if (h01.ge.dminim)then
   phi=asin(para1/r0)
   sumfz=sumfz+forc*cos(phi)
   if ((x1.eq.0.0).and.(y1.eq.0.0))goto 520
   radial=forc*sin(phi)
c  computing horizontal force vector
   xcoef=radial*-x1/para1
   ycoef=radial*-y1/para1
   else if (h01.lt.dminim)then
   if(rprime.eq.r0)then
   sumfz=sumfz+forc
   xcoef=0.0
   ycoef=0.0
   else if(rprime.lt.r0)then
   if(para1.le.rprime)then
   sumfz=sumfz+forc
   xcoef=0.0
   ycoef=0.0
   else if (para1.gt.rprime) then
   phi=asin(para1/r0)
   sumfz=sumfz+forc*cos(phi)
   radial=forc*sin(phi)
c  computing horizontal force vector
   xcoef=radial*-x1/para1
   ycoef=radial*-y1/para1
   end if
   end if
   end if
   sumfx=sumfx+xcoef
   sumfy=sumfy+ycoef
520     continue
```

```
510       continue
15       format(3x,i3,1x,f6.3,1x,i4,4(2x,e11.3))
      return
      end
c    *******************************
c
c    Reads data from lub.dat
c
c    reads radius of sphere1, sphere2
c    reads the position, linear velocity, angular position, angular velo
c    with respect to global X, Y, Z directions for sphere1
c    reads the same parameters for sphere2
c
c    ***********************************************
      subroutine magni(aa1,amag)
      implicit real*8(a-h,o-z)
      dimension aa1(3)
      amag=0.
      do 10 i=1,3
      amag=amag+aa1(i)*aa1(i)
10       continue
      amag=sqrt(amag)
      return
      end
c    *******************************
      subroutine cross(aa,bb,cc)
      implicit real*8(a-h,o-z)
      dimension aa(3),bb(3),cc(3)
      cc(1)=aa(2)*bb(3)-aa(3)*bb(2)
      cc(2)=aa(3)*bb(1)-aa(1)*bb(3)
      cc(3)=aa(1)*bb(2)-aa(2)*bb(1)
      return
      end
c    ********************************
      subroutine dot(e,f,dsum)
      implicit real*8(a-h,o-z)
      dimension e(3),f(3)
      dsum=e(1)*f(1)+e(2)*f(2)+e(3)*f(3)
      return
      end
c    ************************
      subroutine grid
c
c    computing the x,y coordinates of the square grid
```

```
c  . and generate the node numbering system
c
c   this subroutine identifies interior, exterior and boundary node
c   points. It also computes the length of each leg extending from
c   that particular node point
c
      implicit real*8(a-h,o-z)
      common/blkgrid/dx,x0,y0,r0,m,n,xx,yy,psi,itype,jlow,jhigh
      parameter(ng=21)
      dimension xx(ng,ng),yy(ng,ng)
      dimension psi(ng,ng),itype(ng,ng),jlow(ng),jhigh(ng)
      xratio=x0/dx
      rratio=r0/dx
      yratio=y0/dx
      do 10 i=1,m+1
      fim1=i-1.0
      a1=fim1-yratio
      sqr=sqrt(rratio*rratio-a1*a1)
      xratmin=xratio-sqr
      xratmax=xratio+sqr
      do 20 j=1,n+1
      itype(i,j)=0
      fj=j-1.0
      if (fj.eq.xratmin)itype(i,j)=4
      if ((fj.gt.xratmin).and.(fj.lt.xratmax))itype(i,j)=2
      if (fj.eq.xratmax)itype(i,j)=4
      a1=fj-yratio
      sqr=sqrt(rratio*rratio-a1*a1)
      yratmin=yratio-sqr
      yratmax=yratio+sqr
      xx2r=fj+1.0
      xx1r=fj-1.0
      yy2r=fim1+1.0
      yy1r=fim1-1.0
      if((xx2r.le.xratmax).and.(xx1r.ge.xratmin).and.(yy1r.ge.
     *yratmin).and.(yy2r.le.yratmax))itype(i,j)=1
20       continue
10       continue
30       format(21(1x,i1))
      do 40 i=1,m+1
      do 50 j=1,n+1
      xx(i,j)=dx*(j*1.0-1.0-n/2.0)
      yy(i,j)=dx*(i*1.0-1.0-m/2.0)
      if(itype(i,j).ne.1)goto 50
```

```
      if(itype(i,j-1).ne.1)jlow(i)=j
      if(itype(i,j+1).ne.1)jhigh(i)=j
50       continue
40       continue
      return
      end
c    *******************************************
      subroutine velocity
      implicit real*8(a-h,o-z)
      parameter(ng=21)
      common/blkgrid/dx,x0,y0,r0,m,n,xx,yy,psi,itype,jlow,jhigh
      common/blku/u,udot,thu,thdotu,rad1,v,vdot,thv,thdotv,rad2
     *,h0,iab1,iab2,dminim,dmaxim
      common/blkr/rprime
      common/blk1/e,t,s
      common/blkvel/u1,v1,w1,u2,v2,w2,eta
      common/blkcon/a1,a2,a3,a4,nnumber
      dimension u(3),udot(3),thu(3),thdotu(3)
      dimension v(3),vdot(3),thv(3),thdotv(3)
      dimension undot(3),vndot(3),thndotu(3),thndotv(3)
      dimension e(3),urel(3),t(3),s(3)
      dimension xx(ng,ng),yy(ng,ng)
      dimension u1(ng,ng),v1(ng,ng),w1(ng,ng)
      dimension u2(ng,ng),v2(ng,ng),w2(ng,ng)
      dimension a1(ng,ng),a2(ng,ng),a3(ng,ng),a4(ng,ng)
c    transferring global velocities to local values
c
c    resolves the global linear velocity of sphere(1) udot(i) to local
c    velocities in t, s, e directions
c
      call dot(udot,t,umag1)
      call dot(udot,s,umag2)
      call dot(udot,e,umag3)
      undot(1)=umag1
      undot(2)=umag2
      undot(3)=umag3
c
c    resolves the global angular velocity of sphere(1) thdotu(i) to local
c    velocities in t, s, e directions
c
      call dot(thdotu,t,umag1)
      call dot(thdotu,s,umag2)
      call dot(thdotu,e,umag3)
      thndotu(1)=umag1
```

```
      thndotu(2)=umag2
      thndotu(3)=umag3
c
c   resolves the global linear velocity of sphere(2) thdotu(i) to local
c   velocities in t, s, e directions
c
      call dot(vdot,t,vmag1)
      call dot(vdot,s,vmag2)
      call dot(vdot,e,vmag3)
      vndot(1)=vmag1
      vndot(2)=vmag2
      vndot(3)=vmag3
c
c   resolves the global angular velocity of sphere(2) thdotu(i) to local
c   velocities in t, s, e directions
c
      call dot(thdotv,t,vmag1)
      call dot(thdotv,s,vmag2)
      call dot(thdotv,e,vmag3)
      thndotv(1)=vmag1
      thndotv(2)=vmag2
      thndotv(3)=vmag3
      eta=1.0
      rinv=1.0/rad1+1.0/rad2
c
c   computing linear velocites on the surface of each sphere
c   corresponding to nodal points (i,j)
c
      do 251 i=1,m+1
      do 252 j=1,n+1
      x=xx(i,j)
      y=yy(i,j)
      xyrat=(x*x+y*y)/2.
      const=sqrt(xyrat*2.0)
c
c   corresponding velocities for sphere (1)
c   computing velocities U1(i,j),V1(i,j),W1(i,j)
c
      xyu=rad1-xyrat/rad1
      u1(i,j)=undot(1)+thndotu(2)*xyu-thndotu(3)*y
      v1(i,j)=undot(2)-thndotu(1)*xyu+thndotu(3)*x
      w1(i,j)=undot(3)+y*thndotu(1)-thndotu(2)*x
c
c   corresponding velocities for sphere (1)
```

```
c  . computing velocities U1(i,j),V1(i,j),W1(i,j)
c
      xyv=-rad2+xyrat/rad2
      u2(i,j)=vndot(1)+thndotv(2)*xyv-thndotv(3)*y
      v2(i,j)=vndot(2)-thndotv(1)*xyv+thndotv(3)*x
      w2(i,j)=vndot(3)+y*thndotv(1)-thndotv(2)*x
c
c    the height, h between the two points considered
c
      if (h0.ge.dminim)then
      h=h0+xyrat*rinv
      a1(i,j)=h*h*h/eta
      a2(i,j)=3.0*h*h*x/eta*rinv
      a3(i,j)=3.0*h*h*y/eta*rinv
      const1=-x/rad1*thndotu(2)+x/rad2*thndotv(2)+y/rad1
     **thndotu(1)-y/rad2*thndotv(1)
      const2=(u1(i,j)+u2(i,j))*x*rinv+(v1(i,j)+v2(i,j))*y*rinv
      a4(i,j)=-6.0*(const1*h+const2+2.0*(w2(i,j)-w1(i,j)))
c
      else if (h0.lt.dminim)then
      if (rprime.eq.r0)then
      h=dminim
      a1(i,j)=h*h*h/eta
      a2(i,j)=0.0
      a3(i,j)=0.0
      const1=-x/rad1*thndotu(2)+x/rad2*thndotv(2)+y/rad1*
     *thndotu(1)-y/rad2*thndotv(1)
      const2=0.0
      a4(i,j)=-6.0*(const1*h+const2+2.0*(w2(i,j)-w1(i,j)))
      else if (rprime.lt.r0)then
      if (const.le.rprime)then
      h=dminim
      a1(i,j)=h*h*h/eta
      a2(i,j)=0.0
      a3(i,j)=0.0
      const1=-x/rad1*thndotu(2)+x/rad2*thndotv(2)+y/rad1*
     *thndotu(1)-y/rad2*thndotv(1)
      const2=0.0
      a4(i,j)=-6.0*(const1*h+const2+2.0*(w2(i,j)-w1(i,j)))
      else if (const.gt.rprime)then
      h=h0+xyrat*rinv
      a1(i,j)=h*h*h/eta
      a2(i,j)=3.0*h*h*x/eta*rinv
      a3(i,j)=3.0*h*h*y/eta*rinv
```

```
      const1=-x/rad1*thndotu(2)+x/rad2*thndotv(2)+y/rad1*
     *thndotu(1)-y/rad2*thndotv(1)
      const2=(u1(i,j)+u2(i,j))*x*rinv+(v1(i,j)+v2(i,j))*y*rinv
      a4(i,j)=-6.0*(const1*h+const2+2.0*(w2(i,j)-w1(i,j)))
      end if
      end if
      endif
c
c    the constants for the partial differential equation
c    a1(i,j), a2(i,j), a3(i,j), a4(i,j)
c
252         continue
251         continue
71        format(1x,f5.1,1x,f5.1,2x,f9.3,a)
      return
      end
      subroutine unit
      implicit real*8(a-h,o-z)
      common/blku/u,udot,thu,thdotu,rad1,v,vdot,thv,thdotv,rad2
     *,h0,iab1,iab2,dminim,dmaxim
      common/blkr/rprime
      common/blk1/e,t,s
      dimension u(3),udot(3),thu(3),thdotu(3)
      dimension v(3),vdot(3),thv(3),thdotv(3)
      dimension undot(3),vndot(3),thndotu(3),thndotv(3)
      dimension e(3),urel(3),t(3),s(3)
c    computing unit vector e
      e(1)=0.0
      e(2)=0.0
      e(3)=1.0
c    computing unit vectro t
      t(1)=1.0
      t(2)=0.0
      t(3)=0.0
c    computing unit vector s
      s(1)=0.0
      s(2)=1.0
      s(3)=0.0
      return
      end
```

C.5 Input File for a Sample Compaction Simulation

```
start 240 240 240 27 305 0 log
run 8 on p.c.
rad 10 1
rad 15 2
gen 100 2 1
gen 200 1 1
sh 2e8 1 1
no 2e8 1 1
fric 0.03 1 1
damp .5 .25 0 0
dens 1000 1
dens 1000 2
pr g i s
frac 0.05
grid -1e-2 -1e-2 -1e-2 0 0 0
pr g i s
c 200
pr g i s
c 200
pr g i s
c 200
pr g i s
c 200
pr g i s
c 200
pr g i s
c 200
pr g i s
c 200
pr g i s
c 200
pr g i s
c 200
pr g i s
c 200
pr g i s
```

```
c 200
pr g i s
c 200
pr g i s
c 200
pr g i s
c 200
pr g i s
c 200
pr g i s
c 200
pr g i s
c 200
pr g i s
c 200
pr g i s
c 200
pr g i s
c 200
pr g i s
grid 0 0 0 0 0 0
fric .05 1 1
gain 5e-8 3e-3
c 200 s0=-1.0e5
pr g i s
c 200 s0=-1.0e5
pr g i s
c 200 s0=-1.0e5
pr g i s
fric 0.3 1 1
c 200 s0=-1.0e5
pr g i s
c 200 s0=-1.0e5
pr g i s
c 200 s0=-1.0e5
pr g i s
c 200 s0=-1.0e5
pr g i s
```

```
c 200 s0=-1.0e5
pr g i s
c 200 s0=-1.0e5
pr g i s
c 200 s0=-1.0e5
pr g i s
c 200 s0=-1.0e5
pr g i s
c 200 s0=-1.0e5
pr g i s
c 200 s0=-1.0e5
pr g i s
c 200 s0=-1.0e5
pr g i s
c 200 s0=-1.0e5
pr g i s
c 200 s0=-1.0e5
pr g i s
c 200 s0=-1.0e5
pr g i s
c 200 s0=-1.0e5
pr g i s
c 200 s0=-1.0e5
pr g i s
c 200 s0=-1.0e5
pr g i s
c 200 s0=-1.0e5
pr g i s
c 200 s0=-1.0e5
pr g i s
c 200 s0=-1.0e5
pr g i s
c 200 s0=-1.0e5
pr g i s
c 200 s0=-1.0e5
pr g i s
c 200 s0=-1.0e5
pr g i s
```

```
c 200 s0=-1.0e5
pr g i s
c 200 s0=-1.0e5
pr g i s
c 200 s0=-1.0e5
pr g i s
save gencom22m.sav
stop
```

C.6 Input File for a Drained Triaxial Test Simulation

```
restart gencom22m.sav
gain 1.0e-8 1e-3
frac 0.05
pr g i s
grid 0 0 —5e-4 0 0 0
c 250 S1MS2=-1.0e5
pr g i s
c 250 S1MS2=-1.0e5
pr g i s
c 250 S1MS2=-1.0e5
pr g i s
c 250 S1MS2=-1.0e5
pr g i s
c 250 S1MS2=-1.0e5
pr g i s
c 250 S1MS2=-1.0e5
pr g i s
c 250 S1MS2=-1.0e5
pr g i s
c 250 S1MS2=-1.0e5
pr g i s
c 250 S1MS2=-1.0e5
pr g i s
c 250 S1MS2=-1.0e5
pr g i s
c 250 S1MS2=-1.0e5
pr g i s
c 250 S1MS2=-1.0e5
pr g i s
c 250 S1MS2=-1.0e5
pr g i s
c 250 S1MS2=-1.0e5
pr g i s
c 250 S1MS2=-1.0e5
pr g i s
c 250 S1MS2=-1.0e5
```

```
pr g i s
c 250 S1MS2=-1.0e5
pr g i s
c 250 S1MS2=-1.0e5
pr g i s
c 250 S1MS2=-1.0e5
pr g i s
c 250 S1MS2=-1.0e5
pr g i s
c 250 S1MS2=-1.0e5
pr g i s
c 250 S1MS2=-1.0e5
pr g i s
c 250 S1MS2=-1.0e5
pr g i s
c 250 S1MS2=-1.0e5
pr g i s
c 250 S1MS2=-1.0e5
pr g i s
stop
```

APPENDIX D
TRUBAL Simulations

Table D.1 Model Parameters Used in TRUBAL Simulations

Microscopic Model TRUBAL	S1	S2			S3
Model Variables					
Particles with Radius 10 units	100	200			20
Particles with Radius 15 units	50	100			
Soil Parameters					
Normal Stiffness k_n	$2x10^7$	$2x10^8$			$1x10^7$
Shear Stiffness k_s	$1x10^7$	$2x10^8$			$2x10^7$
Coefficient of Static Friction, μ	1.0	0.3			1.0
Bulk Mudulus (Undrained Test)	$1x10^7$				
Stress State					
Initial Stress, p'_0	75000	75000	100000	125000	50000
Porosity	0.349	0.371	0.365	0.359	0.273

Table D.2 Relation Between Trubal Units and Standard Physical Units

Microscopic Model Variables	Trubal Units	Physical Units
Model Variables		
Particle Radius	15	0.128mm
Size Distribution (% fraction)	33.33%	33.33%
Particle Radius	10	0.08mm
Size Distribution (% fraction)	66.67%	66.67%
Soil Parameters		
Normal Stiffness k_n	$2x10^8$	1600 N/m
Shear Stiffness k_s	$2x10^8$	1600 N/m
Coefficient of Static Friction, μ	0.3	0.3
Pore Fluid Viscosity	10	3.83cp
Stress State		
Initial Stress, p_o'	75000	75 kPa
Porosity	0.371	0.371

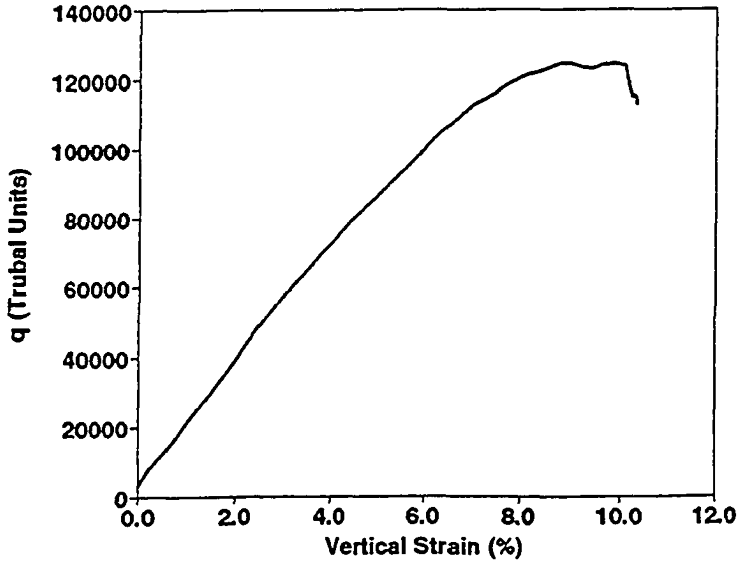

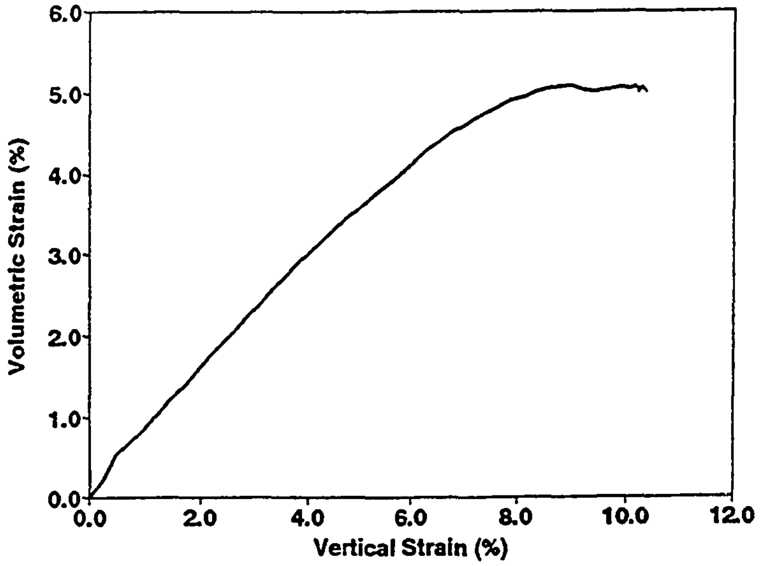

Figure D.1 Simulated Drained Triaxial Stress-Strain Behavior of a Loose Sand.

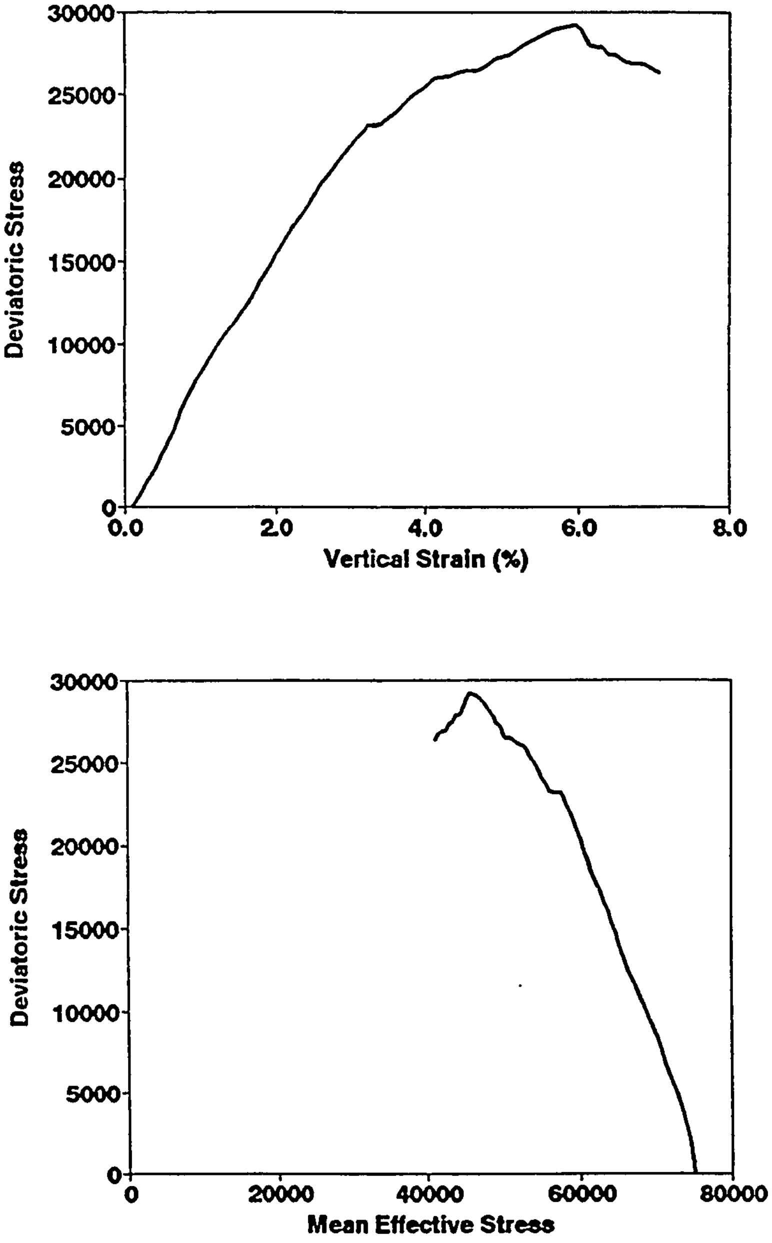

Figure D.2 Simulated Undrained Triaxial Stress-Strain Behavior of a Loose Sand.

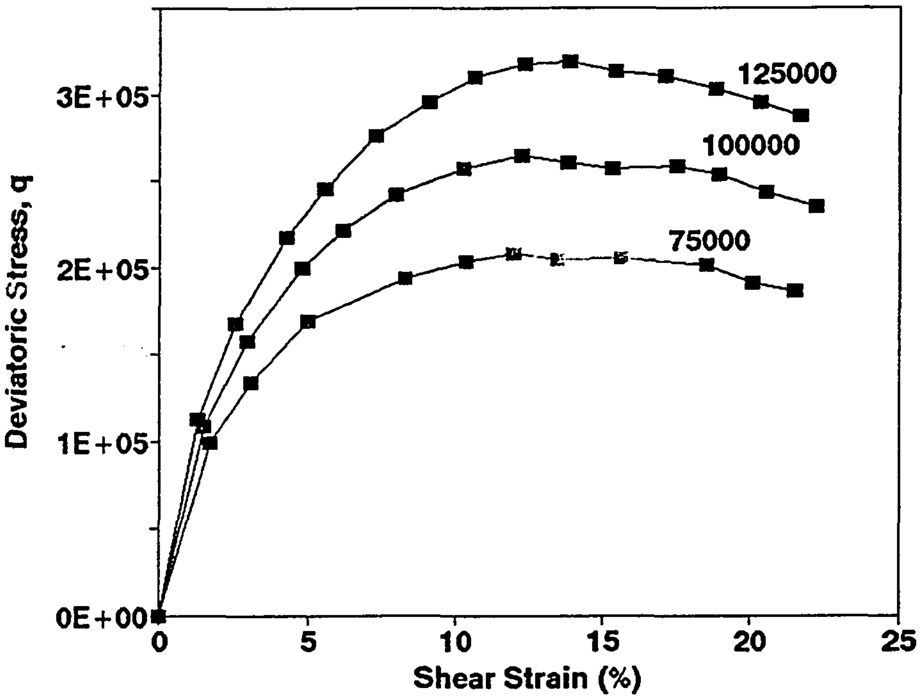

Figure D.3 Simulated Variation of Deviatoric Stress with Shear Strain of a Dry Granular Assembly at Different Consolidation Pressures.

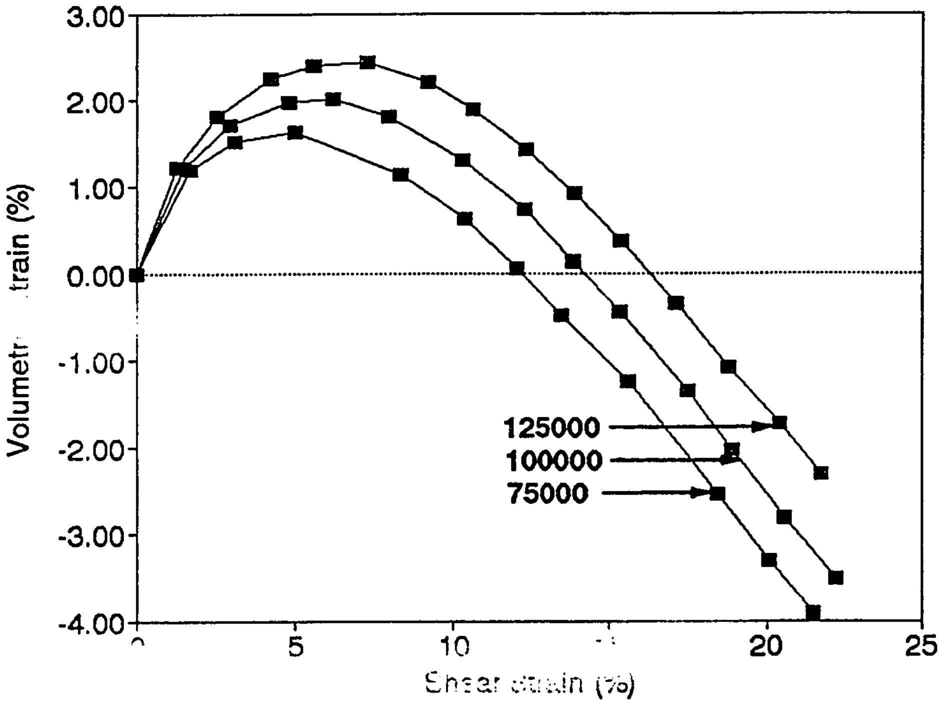

Figure D.4 Simulated Variation of Volumetric Strain with Shear Strain of a Dry Granular Assembly at Different Consolidation Pressures.

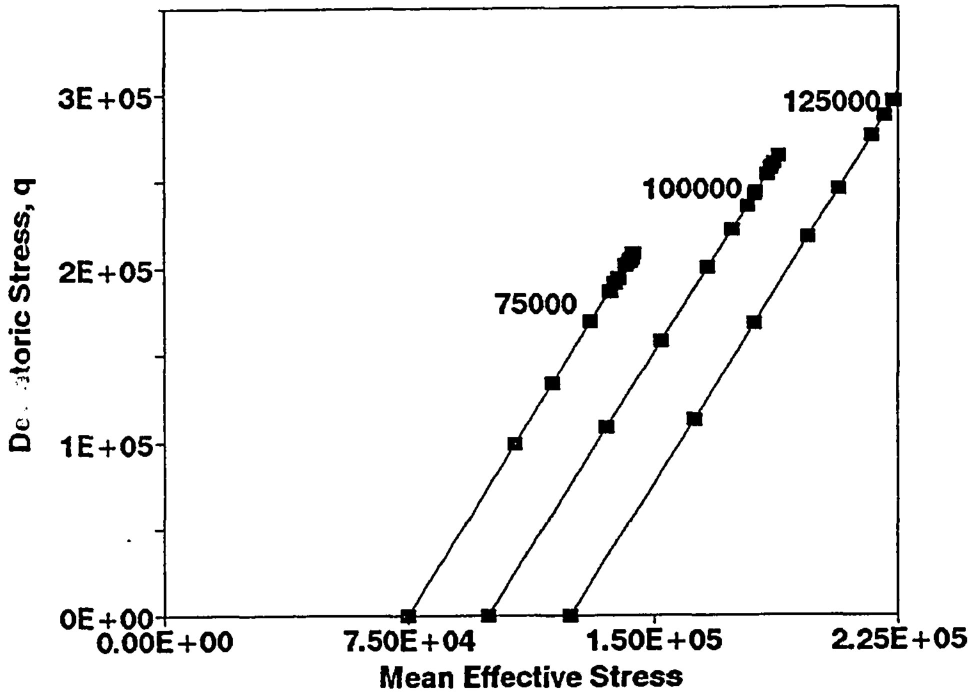

Figure D.5 Simulated Variation of Mean Effective Stress with Shear Strain of a Dry Granular Assembly at Different Consolidation Pressures.

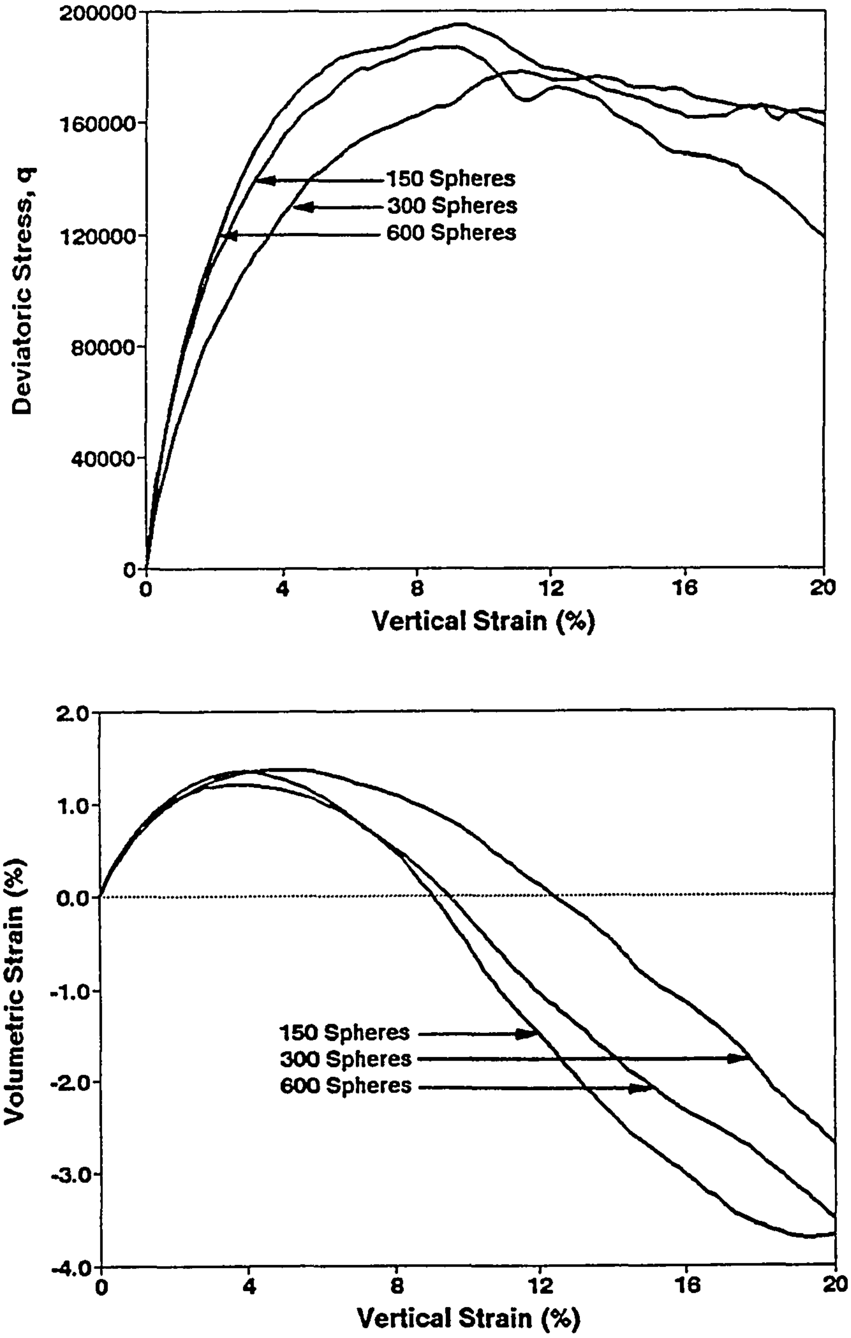

Figure D.6 Simulated Drained Triaxial Stress-Strain Behavior with Varying Sample Size (a) Deviatoric Stress vs. Shear Strain (b) Volumetric Strain vs. Shear Strain.

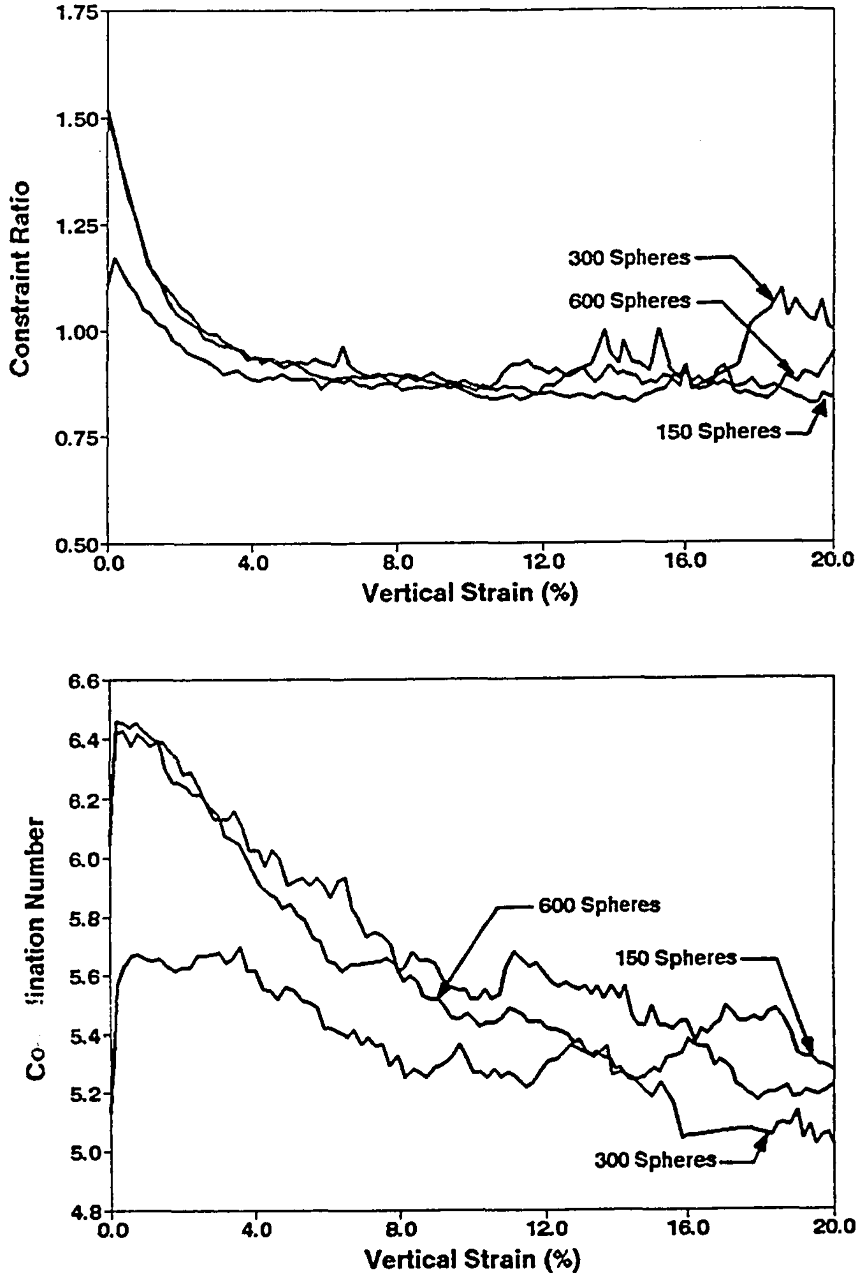

Figure D.6 Simulated Drained Triaxial Stress-Strain Behavior with Varying Sample Size (c) Constraint Ratio vs. Shear Strain (d) Co-ordination Number vs. Shear Strain.

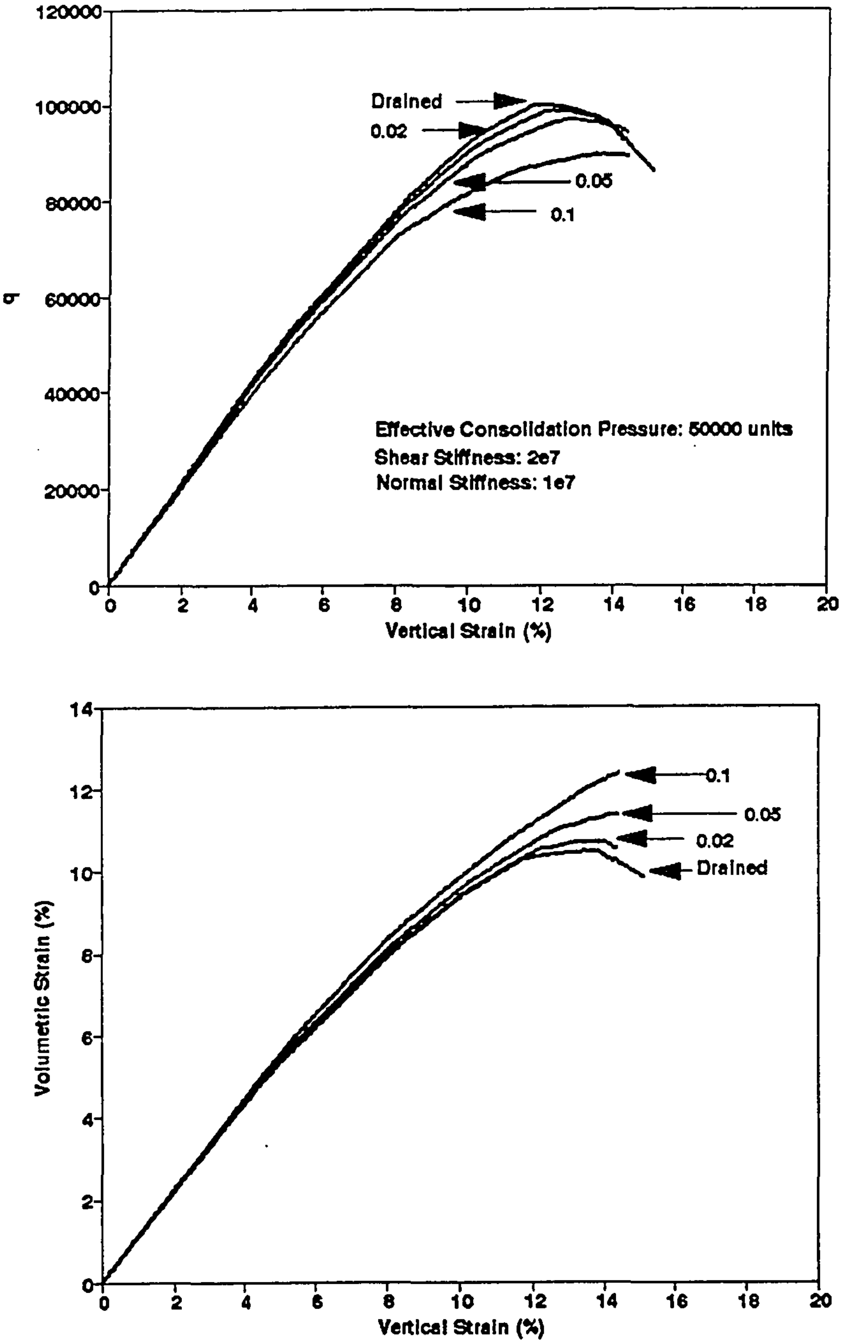

Figure D.7 Simulated Drained Stress-Strain Behavior of a Loose Sand with Different Pore Fluid Viscosities.

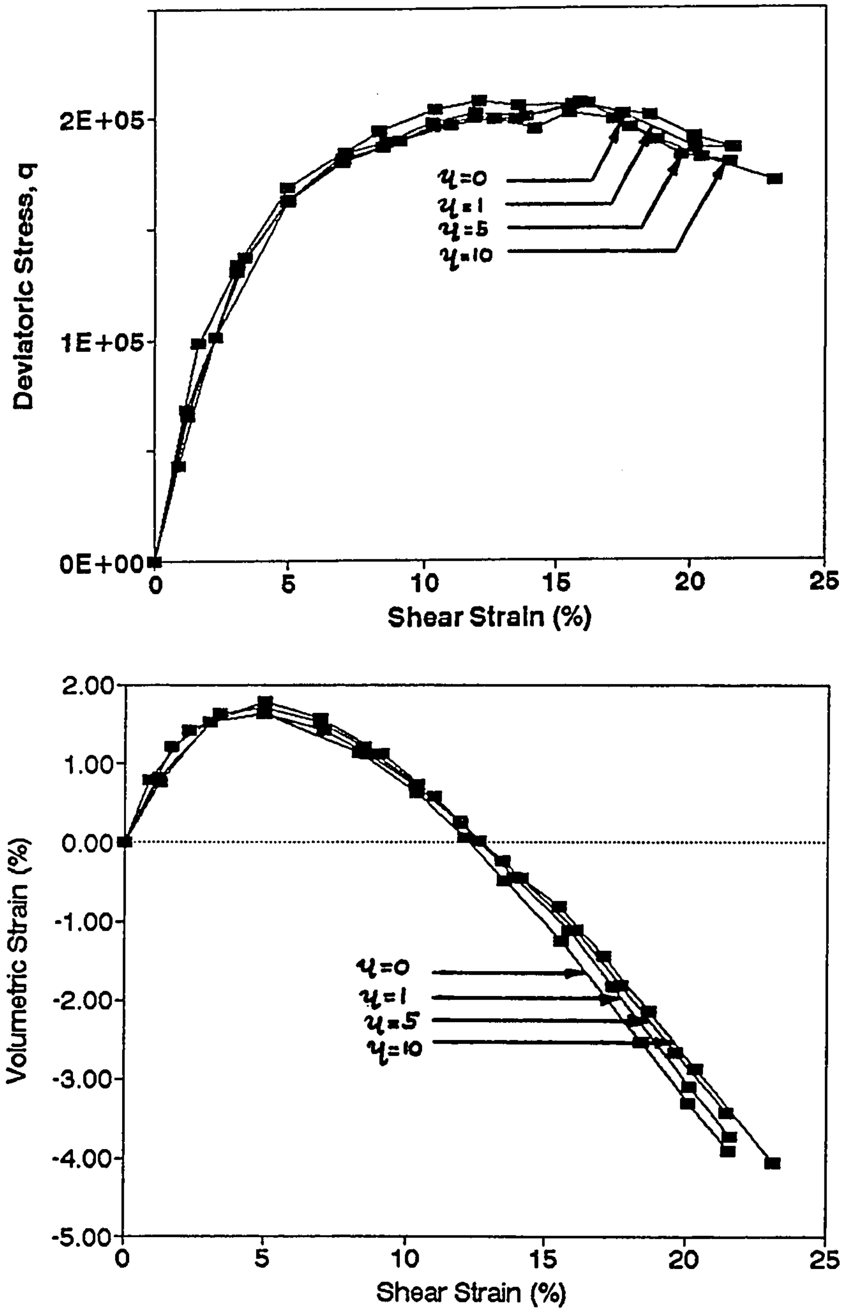

Figure D.8 Drained Stress-Strain Behavior of a Medium-Dense Sand with Different Pore Fluid Viscosities Simulated at an Effective Consolidation Stress of 75000 Stress Units.

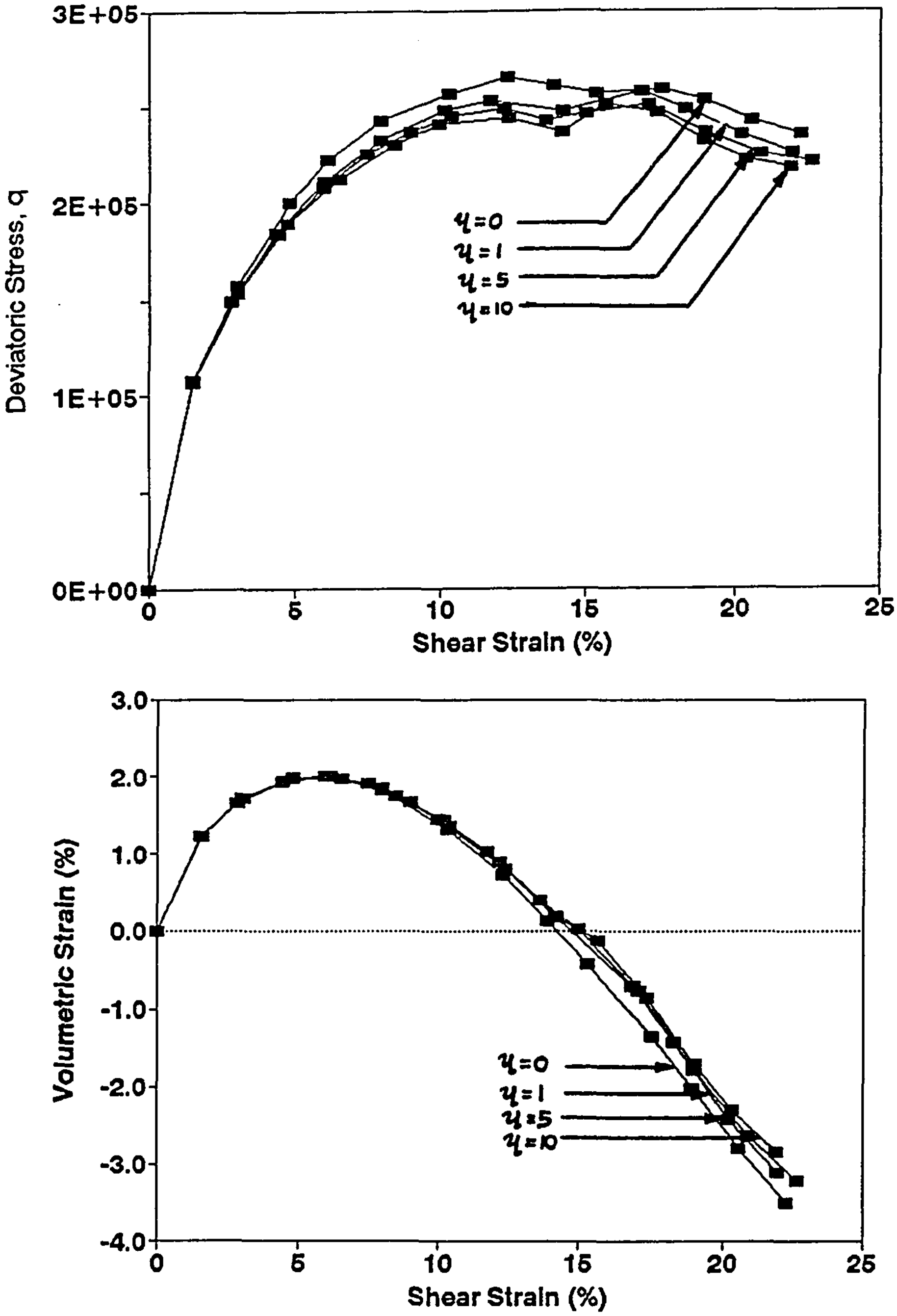

Figure D.9 Drained Stress-Strain Behavior of a Medium-Dense Sand with Different Pore Fluid Viscosities Simulated at an Effective Consolidation Stress of 100000 Stress Units.

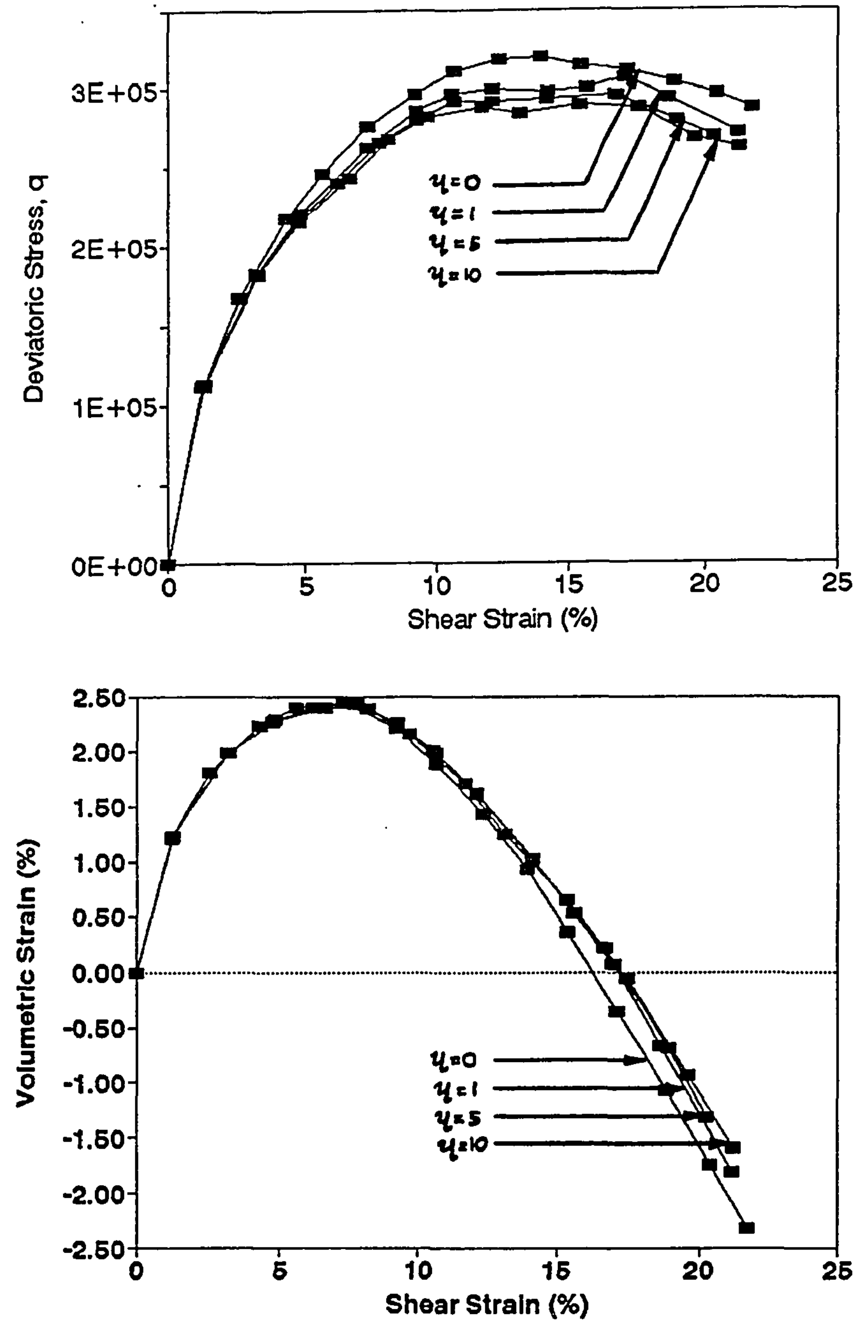

Figure D.10 Drained Stress-Strain Behavior of a Medium-Dense Sand with Different Pore Fluid Viscosities Simulated at an Effective Consolidation Stress of 125000 Stress Units.

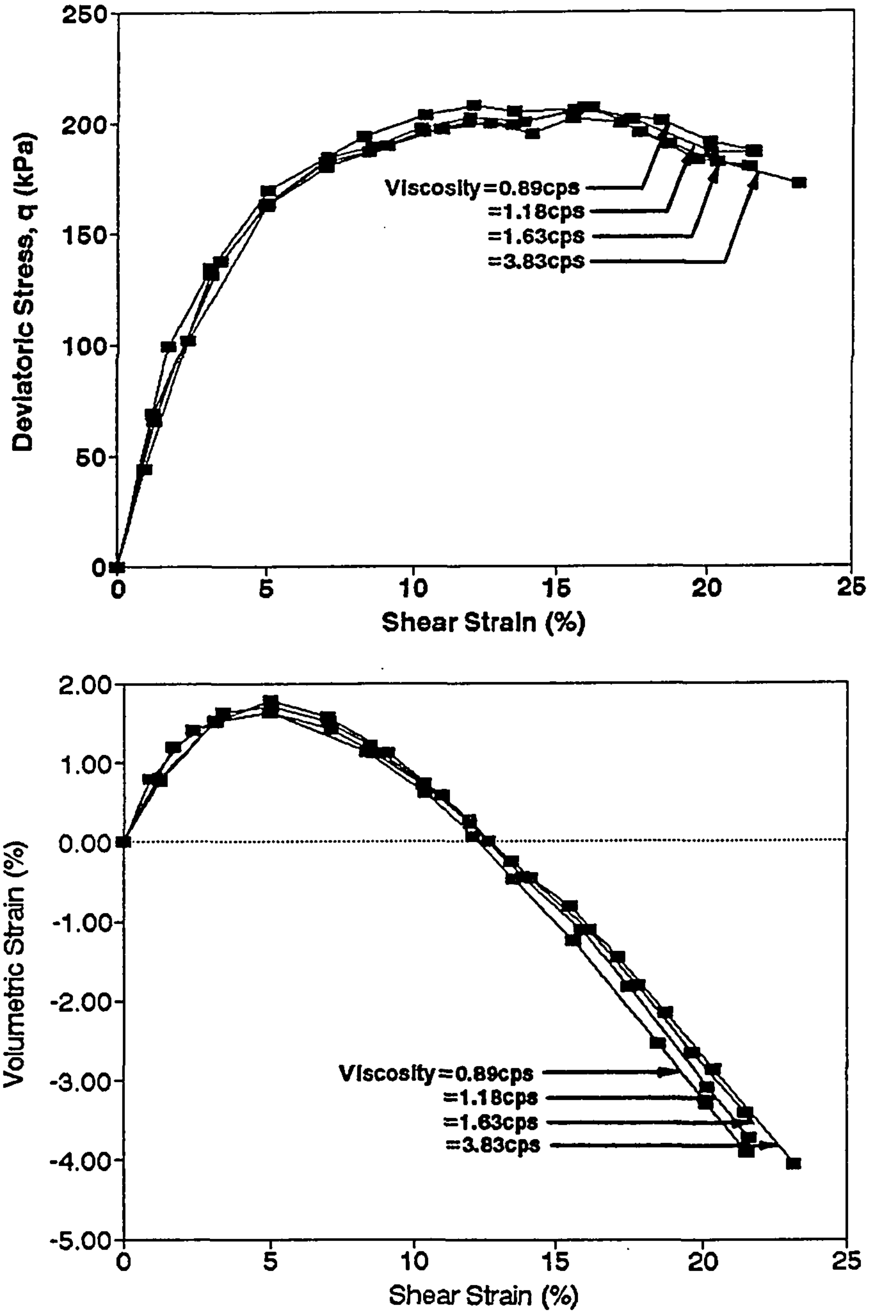

Figure D.11 Drained Stress-Strain Behavior of a Medium-Dense Sand with Different Pore Fluid Viscosities Simulated at an Effective Consolidation Stress of 75kPa.

BIBLIOGRAPHY

Bishop, A. W. (1954) Discussion on A. D. M. Penman (1953), Geotechnique, Lond., 4, No. 1, pg. 43.

Cameron, A. (1976) *Basic Lubrication Theory,* John Wiley & Sons Ltd.

Caquot, A. (1934) *Equilibre des massifs a frottement iterne,* Gauthior-Villars, Paris.

Carnahan, B., H. A. Luther (1969) *Applied Numerical Methods,* John Wiley, New York.

Casagrande, A. (1936) "Classification and Identification of Soils." Trans. ASCE, Vol. 113, pp. 901.

Corkum, B. T., J. M. Ting (1986) "The Discrete Element Method in Geotechnical Engineering." Publication 86-11, Dept. Civil Engineering, University of Toronto, Toronto, Canada.

Cundall, P. A. (1971) "A Computer Model for Simulating Progressive Large Scale Movement in a Blocky Rock System." Symp. ISRM, Nancy, France, Proc., Vol. 2, pp. 129-136.

Cundall, P. A. (1978) "BALL - A Program to Model Granular Media using the Distinct Element Method." Technical Note, Advanced Technology Group, Dames & Moore, London.

Cundall, P. A. (1988) "Computer Simulations of Dense Sphere Assemblies." Micro-mechanics of Granular Materials, Edited by M. Satake & J. T. Jenkins, Elsevier Science Publishers, Amsterdam, pp. 113-123.

Cundall, P. A. (1989) TRUBAL: Fortran Source Code and User Manual, Version 1.51.

Cundall, P. A., R. D. Hart (1989) "Numerical Modeling of Discontinua." Proceedings, 1st U. S. Conference on Discrete Element Methods, Golden, Colorado, Oct., pp. 34 - 54.

Cundall, P. A., O. D. L. Strack (1979a) "The Development of Constitutive Laws for Soil using the Distinct Element Method." Third International Conference on Numerical Methods in Geo-mechanics, Aachen, pp. 289-298.

Cundall, P. A., O. D. L. Strack (1979b) "A Discrete Numerical Model for Granular Assemblies." Geotechnique, Vol. 29, pp. 47-65.

Cundall, P. A., O. D. L. Strack (1983) ''Modeling of Microscopic Mechanisms in Granular material.'' Mechanics of Granular Materials: New Models and Constitutive Relations, ed. J. T. Jenkins and M. Satake, Elsevier Sci. Pub., Amsterdam, pp. 137-149.

Cundall, P. A., O. D. L. Strack (1984) ''Fundamental Studies of Fabric in Granular Materials.'' Interim Report to National Science Foundation concerning Grant CEE-8310729: Dept. of Civil and Mineral Engineering, University of Minnesota.

Dobry, R., T. T. Ng ''Discrete Modeling of Stress-Strain Behavior of Granular Media at Small and Large Strains.'' Proc. 1st US Conf. on Discrete Element Methods, Golden, Colorado, Oct., pp. 128-137.

Evgin, E., B. M. Das (1992) ''Mechanical Behavior of an Oil Contaminated Sand.'' Environmental Geotechnology, Edited by Usman and Acar, Balkema Publishers, pp. 101-108.

Hakuno, M., T. Hirao (1973) ''A Trial Related to Random Packing of Particle Assemblies.'' Proc. of JSCE, No. 219, pp. 55-63 (in Japanese).

Hakuno, M., Y. Tarumi (1988) ''A Granular Assembly Simulation for the Seismic Liquefaction of Sand.'' Structural Eng./ Earthquake Eng., Vol. 5, No. 2, pp. 333s-342s, Japan Society of Civil Engineers (Proc. of JSCE No. 98/I-10)

Hill, R. (1964) ''Elastic Properties of Reinforced Solids: Some Theoretical Principles.'' J. Mech. Phys. Solids, 11, pp. 357 - 372.

Holtz R. D., W. D. Kovacs (1981) *An Introduction to Geotechnical Engineering*, Prentice-Hall, Inc., Englewood Cliffs, New Jersey.

Horn, H. M., D. U. Deere (1962) ''Frictional Characteristics of Minerals.'' Geotechnique, Vol. 12, No. 4, pp. 319-335.

Iwashita, K., M. Hakuno (1988) ''Granular Assembly Simulation for Dynamic Cliff Collapse due to Earthquake.'' Proc. of WCEE, Vol. 3, pp. 175-180.

Izutsu, H., H. Kiyama, H. Fujimura, T. Nishimura (1986) ''DEM Analysis Taking into Account the Behavior of Pore Water.'' Proceedings, 21th annual meeting of the Japanese Society of Soil Mechanics and Foundation Engineering. pp. 1621-1622 (in Japanese).

Kaliakin V. N., L. R. Herrmann (1989) ''Numerical Implementation of the

Elastoplastic-Viscoplastic Bounding Surface Model for Isotropic Cohesive Soils: The EVALVP Computer Program."

Kiyama, H., H. Fujimura (1983) "The Analysis of the Gravity Flow of Rock Granular Assemblies using Cundall's Model." Proc. of Japan Society of Civil Engineers, No. 333, pp. 137-146 (in Japanese).

Kiyama, H., H. Fujimura, T. Nishimura (1982) "On Analyzing Settlement of the Ground Surface Owing to Tunnel Excavation with Cundall's Model." Annual meeting of Japan Society of Civil Engineers, Vol. 3, pp. 309-310 (in Japanese).

Lee, K. L., H. B. Seed, P. Dunlop (1967) "Effect of Moisture on the Strength of a Clean Sand." Journal of SM&FD, SM6, pp. 17-40.

Li, X. S., C. K. Chan, C. K. Shen (1988) "An Automated Triaxial Testing System, STP 977, ASTM, pp. 95-106

Meegoda, N. J., (1989) "The Influence of Chemicals on Shear Strength of Clays." ASTM Symposium on Physico-Chemical Aspects of Soil, Rock and Related Materials, St. Louis, MO.

Mogami, T. (1965) "A Statistical Approach to the Mechanics of Granular Materials." Soil and Foundation, Vol. 5, No. 2, pp. 26-36.

Petrakis, E., R. Dobry, T. T. Ng (1989) "Small Strain Response of Random Arrays of Elastic Spheres using a Non Linear Distinct Element Procedure." Proc. International Symposium on Wave Propagation in Granular Media, eds. D. Karamanlidis, R. B. Stout, pp. 214-217.

Proctor, R. R. (1933) "Fundamental Principles of Soil Compaction." Engineering News-Record, Vol. 111, No. 9, New York, pp. 245-248.

Rajapakse, R. (1989) "The Influence of Chemical Contaminants on the Permeability of Clays." Masters Thesis, New Jersey Institute of Technology.

Ratnaweera, P., N. J. Meegoda (1991a) "Comparison of a Microscopic Model and a Macroscopic Model Predictions on the Stress-Strain Behavior of a Soil." Mechanics Computing in 1990's and Beyond, ASCE Eng. Mech. Specialty Conference Proceedings (Edited by H. Adeli & R. L. Sierakowski), Vol. 2, pp. 1199-1203.

Ratnaweera, P., N. J. Meegoda (1991b) "Microscopic Modeling of Shear Strength of Contaminated Soils." Mechanics Computing in 1990's and Beyond, ASCE Eng. Mech. Specialty Conference Proceedings (Edited by H. Adeli & R. L. Sierakowski), Vol. 2, pp. 1204-1208.

Roscoe, K. H., A. N. Schofield, C. P. Wroth (1958), "On the Yielding of Soils." Geotechnique Vol. 8, No. 1, pp. 22-52.

Rowe, P. W. (1962), "The Stress-Dilatancy Relation for Static Equilibrium of an Assembly of Particles in Contact." Proc. Roy. Soc. London A269, pp. 500-27.

Rowe, P. W. (1971) "Theoretical Meaning and Observed Values of Deformation Parameters for Soil." in Stress-Strain Behavior of Soils, Proc. Roscoe Memorial Symp. Cambridge, Edited by R. H. G. Parry, pp. 143-194.

Scott, R. F., (1963) *Principles of Soil Mechanics,* Addison Wesley Publishing Co., Inc., Reading, Mass.

Schofield, A. N., C. P. Wroth (1968) *Critical State Soil Mechanics,* McGraw-Hill, London.

Sladen, J. A., J. M. Oswell (1989) "The Behavior of Very Loose Sand in the Triaxial Compression Test." Candadian Geotechnical Journal, Vol.26, pp. 103-113.

Strack, O. D. L., P. A. Cundall (1984) "Fundamental Studies of Fabric in Granular Materials." Interim Report to National Science Foundation Concerning Grant CEE-8310729: Dept. of Civil and Mineral Engineering, University of Minnesota.

Taylor, D. W. (1948) *Fundamentals of Soil Mechanics,* New York, J. Wiley and Sons.

Ting, J. M., B. T. Corkum (1987) "Discrete Numerical Modeling of Soil: Validation and Application." Publication 87-03, Dept. of Civil Engineering, Univ. of Toronto, Toronto, Canada.

Ting, J. M., B. T. Corkum, C. R. Kauffman, C. Greco (1989) "Discrete Numerical Model for Soil Mechanics." Journal of Geotechnical Engineering, ASCE, Vol. 115, No. 3, pp. 379-398.

Uemura, D. M. Hakuno (1987) "Granular Assembly Simulation using Cundall's Model for the Dynamic Collapse of the Structural Foundation." Structural

Eng/Earthquake Eng, Vol. 4, No. 1, pp.155s-164s, Japan Society of Civil Engineers (Proc. of JSCE, No 380).

Vesic A. S., G. W. Clough (1968) ''Behavior of Granular Materials Under High Stresses." Proc. ASCE, Journal of the Soil Mechanics and Foundation Division, 94, SM No. 3, pp. 661-688.